

Studies on Joining of Aluminium Alloy and Steel by Fusion Joining Processes

A Thesis

submitted by

KRISHNA PRIYA YAGATI

(09ETPM07)

In partial fulfilment of the requirements for the award of the degree of

**Doctor of Philosophy
in
MATERIALS ENGINEERING**

Under the supervision of

Dr. Koteswararao V. Rajulapati

School of Engineering Sciences and Technology
University of Hyderabad, Hyderabad INDIA

and

Dr. G. Padmanabham

International Advanced Research Centre for Powder Metallurgy
and New Materials (ARCI), Hyderabad INDIA



**School of Engineering Sciences and Technology
University of Hyderabad, India**

March 2016

DECLARATION

I, Krishna Priya Yagati declare that this thesis work entitled “**Studies on Joining of Aluminium Alloy and Steel by Fusion Joining Processes**” submitted in partial fulfilment of the requirements for the award of Doctor of Philosophy (in Materials Engineering) in the School of Engineering Sciences and Technology (SEST), University of Hyderabad is completely my own work except for those referenced. This work was done under the supervision of Dr G. Padmanabham (ARCI) and Dr Koteswararao V. Rajulapati (SEST). This report is a record of bonafide work carried out by me and the results incorporated in it have not been reproduced /copied from any source. This work has not been submitted to any other university or institute for the award of any other degree or equivalent.

Krishna Priya Yagati
Reg. No. 09ETPM07
School of Engineering Sciences and Technology
University of Hyderabad
Hyderabad

CERTIFICATE

This is to certify that the thesis work entitled “**Studies on Joining of Aluminium Alloy and Steel by Fusion Joining Processes**” submitted by Krishna Priya Yagati (Re. No. 09ETPM07) in partial fulfilment of the requirements for the award of the degree of Doctor of Philosophy in Materials Engineering is a bonafide work carried out by her under our guidance. This work has not been submitted previously in part or in full to this or any other university or institute for the award of any degree or equivalent.

Thesis supervisor

Dr. Koteswararao V Rajulapati

Assistant Professor
School of Engineering Sciences and Technology
University of Hyderabad
Hyderabad

Approved by

Prof. M. Ghanashyam Krishna

Dean
School of Engineering Sciences and Technology
University of Hyderabad
Hyderabad

ACKNOWLEDGEMENTS

I would like to express my special thanks to my project supervisor **Dr. G. Padmanabham (Director (I/C), ARCI, Hyderabad)** for giving me an opportunity to work with him. I appreciate his encouragement, guidance and the constant support he has provided throughout the course of my research work. I have learned a lot from his suggestions, comments and discussions.

I would like to express my special thanks to my project supervisor **Dr. Koteswararao V Rajulapati (Assistant Professor, SEST, UOH)** for giving me an opportunity to work with him. I appreciate his encouragement, guidance and the constant support he has provided throughout the course of my research work. I have learned a lot from his suggestions, comments and discussions. I express my sincere gratitude to **Prof. K. Bhanu Sankara Rao (former Dean)** who has been my supervisor during his tenure at School of Engineering Sciences and Technology for his wonderful suggestions and discussions.

I would like to express my special thanks to my project supervisor **Dr. Ravi N Bathe (Scientist'E', Centre for Laser Processing of Materials, ARCI, Hyderabad)** for helping me throughout my research work. I appreciate his encouragement, guidance and the constant support he has provided throughout the course of my research work. I have learned a lot from his suggestions, comments and discussions.

I would like to express my special thanks to my project supervisor **Dr. Joydip Joardar (Scientist'E', Centre for Nano Science, ARCI, Hyderabad)** for helping mein Micro area X-Ray Diffraction (Micro XRD) studies. I am grateful to express my gratitude for his valuable suggestions. I have learned a lot from his suggestions, comments and discussions.

I would like to thank the doctoral research committee members **Dr.-Ing. V. V. S. S Srikanth** and **Dr. J. P. Gautham** for their valuable suggestions provided during the review meetings. I am grateful to **Prof Ghanashyam Krishna** (Dean) and all the faculty members of SEST for their support during the course of my work. I am thankful to Prof. R. Singh (former Dean) and **Prof. Sundararaman** (former Dean) for their encouragement and support.

LIST OF PUBLICATIONS/CONFERENCE **PROCEEDINGS**

Publications:

1. Y. Krishna Priya, Ravi N Bathe, Koteswararao V Rajulapati, , K. Bhanu Sankara Rao, G. Padmanabham, “Fluxless Arc Weld-Brazing of Aluminium alloy to Steel”, Journal of Materials Processing Technology, 214, 2014:2949-2959
2. G. Padmanabham, Y Krishna Priya, K.V. Phani Prabhakar and Ravi N. Bathe, K. Bhanu Sankara Rao, “A comparison of interface characteristics and mechanical properties of Aluminium-Steel Joints made by P-MIG and Cold Metal Transfer (CMT) Processes”, Trends in Welding Research, Proceedings of the 9th international conference, June4-8, 2012, Chicago, USA, 227-234
3. Krishna Priya .Y, Ravi Bathe, K. V. Phani Prabhakar, J. Joardar, K. V. Rajulapati, Bhanu Sankara Rao. K, Padmanabham. G “Influence of pulsing and filler wire composition on the interface morphology and strength of cold metal transfer brazed aluminium-steel joint” (To be communicated)

Conference proceedings

1. Y. Krishna Priya, K. V. Phani Prabhakar, K. Bhanu Sankara Rao, G. Padmanabham, “Effect of Si content on macro and microstructural features of cold metal transfer brazed aluminium steel joints”, International Welding Symposium 2k12 (IWS 2k12),volume 1: 133-139.
2. Y. Krishna Priya, Ravi Bathe, K. Bhanu Sankara Rao, G. Padmanabham, “Effect of torch orientation on Pulsed-MIG brazed aluminium-steel joints”, SOJOM 2012, volume 1:ICA 089:1-6.

3. Y. Krishna Priya, Ravi Bathe, K. Bhanu Sankara Rao, G. Padmanabham, “Joining of Aluminium alloy to Steel using Pulsed MIG Welding”, International conference Global trends in joining, cutting and surface technology, 355-351.

Poster Presentation:

Y. Krishna Priya, Ravi Bathe, K. Bhanu Sankara Rao, G. Padmanabham, “Characterization of MIG-brazed Aluminium Steel interface “, Workshop of Electron Microscopy-2011(WEM-2011), Institute of Physics, Bhubaneswar, Odisha, India organized by Institute of Physics, Bhubaneswar

CONTENTS

LIST OF FIGURES	I
LIST OF TABLES	VI
ABSTRACT	IX
CHAPTER 1 INTRODUCTION	1
1.1 Background	1
1.2 Applications of dissimilar aluminium-steel joints.....	2
1.3 Problems involved in aluminium-steel fusion joining	4
1.4 Intermetallic compounds (IMC) and formation	6
1.4.1 Binary Fe-Al phases	6
1.4.2 Ternary Al-Fe-Si phases	7
1.5 Objectives.....	10
1.6 Overview of the thesis	11
CHAPTER 2 LITERATURE REVIEW	16
2.1 Thermal joining techniques.....	18
2.2 Brazing	18
2.3 Arc brazing	19
2.3.1 Gas metal arc welding (GMAW)	20
2.3.2 Pulsed-GMAW.....	21
2.3.3 Cold metal transfer (CMT) welding.....	21
2.4 Effect of parameters of arc brazing process	23
2.4.1 Effect of surface chemistry of steel.....	23
2.4.2 Effect of filler wire composition.....	24
2.4.3 Effect of pre-heating of the filler wire.....	26
2.4.4 Effect of pre-heating of the base materials	26
2.4.5 Effect of wire feed rate (WFR)	27
2.4.6 Effect of processing speed	28
2.4.7 Effect of shielding gas and flow rate.....	28
2.5 Laser brazing	30
2.6 Effect of processing parameters of laser brazing	32
2.6.1 Wavelength (Nd:YAG, diode, fiber, CO2 lasers).....	32
2.6.2 Laser power.....	33

2.6.3 Spot size	34
2.6.4 Laser beam tailoring	35
2.6.5 Effect of roll pressure	38
2.6.6 Effect of processing speed	39
2.6.7 Effect of filler wire composition.....	40
2.6.8 Effect of pre-heating the filler wire.....	41
2.6.9 Effect of surface chemistry of Steel	42
2.6.10 Effect of flux	43
2.7 Mechanical properties of laser brazed aluminium-steel joints.....	43
2.8 Summary of literature review.....	45
2.8.1 Pulsed-GMAW.....	45
2.8.2 Cold metal transfer (CMT) brazing process	45
2.8.3 Laser brazing.....	46
2.9 Problem identification and approach.....	46
CHAPTER 3 EXPERIMENTAL WORK.....	49
3.1 Materials used.....	49
3.2 Joint configuration.....	49
3.3 Processes chosen.....	51
3.4 Pulsed-gas metal arc welding (P-GMAW)	51
3.4.1Bead on plate (BOP) experiments for identification of usable parametric window	53
3.4.2 Dissimilar material Al-steel joint experiments	55
3.5 Cold metal transfer welding	58
3.6 Laser brazing	61
3.7 Thermal transient measurements.....	63
3.8 Characterization of joints	64
3.8.1 Metallography	66
3.8.2 Stereo microscopy.....	66
3.8.3 Optical microscopy.....	66
3.8.4 Scanning electron microscopy (SEM).....	67
3.8.5 Micro area x-ray diffraction.....	67
3.8.6 Lap shear test	68
3.9 Enthalpy of formation	69
CHAPTER 4.....	73

4.1 Introduction	73
4.2 Base material characterization.....	73
4.3 Thermal transient measurements	76
4.4 Study of effect of various parameters	76
4.4.1 Angle of tilt	77
4.4.2 Torch orientation	82
4.4.3 Surface chemistry of steel.....	83
4.4.3.1.1 Effect of gap on wetting and porosity.....	86
4.4.4 Effect of filler wire composition	99
4.4.5 Effect of heat input	103
4.5 Phase analysis	106
4.5.1 Summary	120
CHAPTER 5	124
5.1 Introduction	124
5.2 Effect of pulsing and filler wire composition.....	125
5.2.1 Thermal transient measurements.....	125
5.2.2 Macrostructure	125
5.2.3 Microstructure.....	127
5.2.4 Lap shear test	132
5.3 Effect of heat input	133
5.3.1 Macrostructure	133
5.3.2 Microstructure.....	134
5.3.3 Lap shear test	136
5.4 Phase analysis	137
5.5 Effect of interfacial morphology on failure.....	151
5.6 Summary.....	155
5.7 Conclusions.....	155
CHAPTER 6 LASER BRAZING	159
6.1 Introduction	159
6.2 Macrostructure.....	159
6.3 Microstructure	161
6.4 Lap shear test	163

6.5 Conclusions.....	163
CHAPTER 7 SUMMARY AND CONCLUSIONS	164
CHAPTER 8 SCOPE FOR FUTURE WORK	169

LIST OF FIGURES

CHAPTER 1

Figure 1.1 Adhesive bonding technology adopted in Honda Acura for joining aluminium and steel	3
Figure 1.2 Friction stir welding technology adopted in Honda Accord for joining aluminium and steel in front sub frame	3
Figure 1.3 Rivet bonding in Audi TT	4
Figure 1.4 Fe-Al binary equilibrium phase diagram.....	6
Figure 1.5 Isothermal section of ternary Al-Fe-Si system at 550°C	8
Figure 1.6 IMC layer at Al/steel interface	9
Figure 1.7 Relationship between IMC layer thickness and joint strength of dissimilar Al/steel joints	10

CHAPTER 2

Figure 2.1 Schematic of metal transfer in cold metal transfer proces.....	21
Figure 2.2 Flow sheet of various variables effecting the joint formation.....	22
Figure 2.3 Variation in wetting length and angle with surface chemistry of steel and filler wire	23
Figure 2.4 Effect of laser power and defocusing distance on wetting and strength of joint a) laser power vs wetting b) defocusing distance vs wetting c) laser power vs joint strength d) defocusing distance vs joint strength	25
Figure 2.5 Effect of heat input on wetting behaviour a) low heat input b) high heat input	26
Figure 2.6 Macrostructure of Zn coated steel over aluminium weld showing porosity.....	31
Figure 2.7 Strength of A5052/IF steel and A5052/SUS304 brazed joints	32
Figure 2.8 Effect of twin laser spot on joint strength	35
Figure 2.9: Energy distribution in single and twin spot system	36
Figure 2.10 Schematic of laser roll welding of aluminium alloy and steel	37
Figure 2.11 Effect of processing speed on joint thickness of IMC layer	38

CHAPTER 3

Figure 3.1 Schematic of lap fillet joint configuration.....	49
---	----

Figure 3.2 Experimental methodology adopted for brazing process and characterisation.....	49
Figure 3.3 Pulsed-GMAW wave forms a) sinusoidal b) rectangular	51
Figure 3.4 Bead appearance of dissimilar Al/steel joints a) uniform bead b) non-uniform bead.....	54
Figure 3.5 Schematic of P-GMAW brazing assembly.....	55
Figure 3.6 Schematic of metal transfer in CMT process.....	57
Figure 3.7 Schematic of CMT brazing assembly.....	58
Figure 3.8 Schematic of laser brazing set up.....	61
Figure 3.9 Schematic of thermal transient measurement setup.....	62
Figure 3.10 Flow chart of used characterization techniques and their consequences.....	64
Figure 3.11 Schematic of micro area x-ray diffraction unit.....	67
Figure 3.12 Schematic of lap-shear test specimen.....	67
CHAPTER 4	
Figure 4.1 Optical microstructures of base materials at 500X magnification a) 6061-T6 aluminium alloy b) Interstitial Free steel.....	73
Figure 4.2 Base material microstructures a) galvanized (GI) steel b) galvanealed (GA) steel.....	74
Figure 4.3 DSC curves of IF steel in two surface conditions of steel a) galvanealed b) galvanized.....	74
Figure 4.4 Thermal transient recorded in P-MIG brazing of aluminium and steel with 4043 filler wire.....	75
Figure 4.5 Schematic of brazing assembly a) 0° tilt b) 12° tilt.....	76
Figure 4.6 Transverse cross sectional SEM macrostructures of aluminium/GA steel joints.....	76
Figure 4.7 Optical images of microstructure at various locations of aluminium/GA IF steel joint at 500X magnification a) aluminium/bead interface b) braze bead c) bead/steel interface.....	78
Figure 4.8 Schematic indicating various locations of bead/steel interface.....	78
Figure 4.9 SEM microstructures of bead/steel interface at 1000X magnification.....	79

Figure 4.10 Schematic of brazing assembly with variation in torch orientation.....	81
Figure 4.11 SEM macrographs of aluminium/steel joints under different surface conditions of steel a) Al/GA steel, b) Al/GI steel, c) Al/uncoated steel.....	83
Figure 4.12 Optical micrographs of crevice and Zn rich zone at head and foot regions a) head region b) foot region.....	85
Figure 4.13 Transverse cross-section SEM macrographs of Al/GI steel joints at different interfacial gaps a) < 50 μm b) 200 μm c) 300 μm d) 500 μm	86
Figure 4.14 Optical micrographs of crevice formation and Zn rich zones in joints made with increased gap (300 μm).....	87
Figure 4.15 SEM micrographs at different locations of bead/steel interface at 5.5 kX magnification a) head region (Al/GI steel interface) b) central region (Al/GI steel interface) c) foot region (Al/GI steel interface) d) head region (Al/GA steel interface) e) central region (Al/GA steel interface) f) foot region (Al/GA Steel interface) g) head region (Al/uncoated steel interface) h) central region (Al/uncoated steel interface) I) foot Region (Al/uncoated steel interface).....	88
Figure 4.16 Schematic of different modes of failure a) reduced region failure b) Interfacial failure.....	91
Figure 4.17 Variation in fracture load with gap between the plate.....	92
Figure 4.18 SEM macrographs of fractured surfaces a) under cut region failure (Al/GI steel) b) interfacial failure (Al/GI, Al/GA steel, Al/uncoated steel.....	93
Figure 4.19 Elemental mapping at central region of interfacial failure (Al/GI & Al/GA steel) a) image indicating location of elemental mapping b)Al distribution c) Fe distribution d) Si distribution.....	95
Figure 4.20 Elemental mapping at central region of interfacial failure (Al/uncoated steel) a) image indicating location of elemental mapping b)Al distribution c) Fe distribution d) Si distribution.....	96
Figure 4.21 Transverse cross-section SEM macrographs of Al/steel brazed joints made with Al-12%Si filler.....	98
Figure 4.22 SEM micrographs at different locations of bead/steel interface at 5.5 kX magnification a) head region b) center region c) foot region.....	99
Figure 4.23 EPMA plots across the joint interface for joints made with two different filler wires a) 4043 b) 4047.....	101
Figure 4.24 Transverse cross-section SEM macrographs of Al/steel brazed joints made with Al-5%Si filler at a wire feed rate of 4m/min and speed of 1.2m/min.....	102

Figure 4.25 SEM micrographs of Al/steel joints at different regions of the steel/bead interface made with Al-5%Si filler wire at wire feed rate of 4 m/min a) head b) center c) foot.....	103
Figure 4.26 Schematic indicating locations of x-ray diffraction A) head B) center C) foot.....	107
Figure 4.27 Micro area XRD patterns of head region of bead/steel interface made with two filler wires a) Al-5%Si filler b) Al-12%Si filler.....	108
Figure 4.28 Micro area XRD patterns of central region of bead/steel interface made with two filler wires a) Al-5%Si filler b) Al-12%Si filler.....	109
Figure 4.29 Micro areas XRD patterns of foot region of bead/steel interface made with two filler wires a) Al-5%Si filler b) Al-12%Si filler.....	110
Figure 4.30 Isothermal section of Al-Fe-Si system at 550°C.....	115
Figure 4.31 Schematic of interfacial morphology of P-GMAW brazed specimen with two different filler wires a) Al-5%Si (head) b) Al-12%Si (head) c) Al-5%Si (center) d) Al-12%Si (center) e) Al-5%Si (foot) f) Al-12%Si (foot).....	118

CHAPTER 5

Figure 5.1 Thermal history measurement a) CMT process b) P-CMT process.....	124
Figure 5.2 Transverse cross-section SEM micrographs of aluminium/steel joints a) CMT (Al-5%Si filler) b) P-CMT (Al-5%Si filler) c) CMT (Al-12%Si filler) d) P-CMT (Al-12%Si filler).....	125
Figure 5.3 SEM micrographs of the aluminium-steel joint a) schematic indicating different regions of microstructural observation b) braze bead c) aluminium/bead interface d) bead/steel interface.....	128
Figure 5.4 Schematic of different regions of bead/steel interface.....	128
Figure 5.5 SEM micrographs of various locations of bead/steel interface at 2k magnification a) head (CMT Al-5%Si filler) b) center (CMT Al-5%Si filler) c) foot (CMT Al-5%Si filler) d) head (P-CMT Al-5%Si filler) e) center (P-CMT Al-5%Si filler) f) foot (P-CMT Al-5%Si filler) g) head (CMT Al-12%Si filler) h) center (CMT Al-12%Si filler) i) foot (CMT Al-12%Si filler) j) head (P-CMT Al-12%Si filler) k) center (P-CMT Al-12%Si filler) l) foot (P-CMT Al-12%Si filler).....	129
Figure 5.6 Transverse cross-section SEM micrographs of CMT brazed aluminium/steel joints made with Al-5%Si filler wire.....	132
Figure 5.7 SEM micrographs of various locations of bead/steel interface of CMT brazed joints made with 4043 filler wire with variation in heat input at 5.5k magnification a) head (WFR : 4m/min) b) center (WFR : 4m/min) c) foot (WFR : 4m/min) d) head (WFR : 4.5m/min) e) center (WFR: 4.5 m/min) f) foot (WFR: 4.5 m/min).....	134

Figure 5.8 Schematic indicating various locations of x-ray diffraction A) head B) center C) foot.....	136
Figure 5.9 Micro area XRD patterns of head region of bead/steel interface made with Al-5%Si filler wire a) CMT b)P-CMT.....	138
Figure 5.10 Micro area XRD patterns of central region of bead/steel interface made with Al-5%Si filler wire a) CMT b) P-CMT.....	139
Figure 5.11 Micro area XRD patterns of foot region of bead/steel interface made with Al-5%Si filler wire a) CMT b) P-CMT.....	140
Figure 5.12 Micro area XRD patterns of head region of bead/steel interface made with Al-12%Si filler wire a) CMT b) P-CMT.....	141
Figure 5.13 Micro area XRD patterns of central region of bead/steel interface made with Al-12%Si filler wire a) CMT b) P-CMT.....	142
Figure 5.14 Micro area XRD patterns of foot region of bead/steel interface made with Al-12%Si filler wire a) CMT b) P-CMT.....	143
Figure 5.15 Al-Fe-Si isothermal section at 600°C	150
Figure 5.16 Schematic of bead/steel interface indicated with probable IMC compounds, fracture load and failure location a) head (CMT (Al-5%Si)) b) center (CMT (Al-5%Si)) c) foot (CMT(Al-5%Si)) d) head (P-CMT(Al-5%Si)) e) center (P-CMT(Al-5%Si)) f) foot (P-CMT(Al-5%Si)) g) head (CMT(Al-12%Si)) h) center (CMT(Al-12%Si)) i) foot (CMT(Al-12%Si)) j) head (P-CMT(Al-12%Si)) k) center (P-CMT(Al-12%Si)) l) foot (P-CMT(Al-12%Si)).....	151
Figure 5.17 Various interfacial morphology I) wavy and curved type II) rectangular block type III) irregular blocks with flat surface.....	152
CHAPTER 6	
Figure 6.1 SEM transverse cross-section macrostructures of laser brazed specimens.....	158
Figure 6.2 SEM micrographs of various braze bead of laser brazed specimen.....	161
Figure 6.3 Bead/steel interface of laser brazed joints under various processing conditions.....	161

LIST OF TABLES

CHAPTER 1

Table 1.1 Thermo-physical properties of aluminium and steel.....	5
Table.1.2 Problems involved in joining aluminium to steel.....	6
Table 1.3 List of binary Fe-Al IMC phases.....	6
Table 1.4 List of Al-Fe-Si ternary IMC phases.....	8

CHAPTER 2

Table 2.1 Variation in IMC layer thickness, joint strength and failure location with filler wire composition.....	24
Table 2.2 Joint strengths of arc brazed Aluminium alloy and Steel.....	29
Table 2.2 Joint strengths of various Aluminium-Steel dissimilar combination.....	43

CHAPTER 3

Table 3.1 Power source characteristics of KEMPPI ProMig 4500R.....	52
Table 3.2 P-GMAW parameters for dissimilar material combination (BOP experiments).....	53
Table 3.3 P-GMAW parameters for dissimilar material combination (dissimilar material joining experiments).....	55
Table 3.4 Material combinations tried in P-GMAW process.....	56
Table 3.5 Power source characteristics of Fronius Trans Pulse Synergic 3200/5000 CMT machine.....	58
Table 3.6 Parametric window for aluminium-steel joining for CMT process.....	59
Table 3.7 Material combinations tried in CMT process.....	60
Table 3.8 Characteristics of laser brazing set up.....	61
Table 3.9 Laser brazing processing parameters.....	61
Table 3.10 Material combinations used in laser brazing process.....	62

CHAPTER 4

Table 4.1 Chemical composition of the base materials.....	72
---	----

Table 4.2 Mechanical properties of the base materials.....	73
Table 4.3 Bead geometry measurements of aluminium/GA IF Steel joints.....	77
Table 4.4 IMC layer thickness at various locations of bead/steel interface.....	80
Table 4.5 Lap shear test result	81
Table 4.6 Bead geometry measurements.....	83
Table 4.7 Bead geometry measurements with variation in interfacial gap.....	86
Table 4.8 IMC layer thickness at different locations of bead/steel interface.....	89
Table 4.9 Lap shear properties with gap < 50 μm	90
Table.4.10 Variation in tensile properties with gap between the plates.....	92
Table 4.11 EDS spot analysis at central region (Al/GI & Al/GA steel).....	95
Table 4.12 EDS spot analysis at central region of interfacial failure (Al/uncoated steel).....	96
Table 4.13 Bead geometry measurements.....	98
Table 4.14 Lap shear test results.....	102
Table 4.15 Bead geometry measurements.....	103
Table 4.16 IMC layer thickness at various locations of bead/steel interface at wire feed rate of 4m/min.....	104
Table 4.17 Tensile test results at varied heat input.....	105
Table 4.18: Details of intermetallic phases formed.....	112
CHAPTER 5	
Table 5.1 Bead geometry measurements.....	125
Table 5.2 IMC layer thickness under various conditions.....	131
Table 5.3 Lap shear test results.....	131
Table 5.4: Bead geometry measurements of CMT brazed joints made with Al-5%Si filler wire.....	133
Table 5.5 IMC layer thickness under various heat input conditions.....	135
Table 5.6 Lap shear test results under various heat input conditions.....	135
Table 5.7 Phase data (composition, crystal structure & enthalpy of formation.....	144

Table 5.8: XRD analysis of the IMC layer.....	145
---	-----

CHAPTER 6

Table 6.1: Bead geometry measurements of laser brazed specimens.....	159
--	-----

Table 6.2 Lap shear test results.....	162
---------------------------------------	-----

ABSTRACT

Light-weighting is one of the main areas of interest to automotive industry in order to reduce fuel consumption and environmental pollution. Selective substitution of steel with aluminium & its alloys is one such strategy being pursued in order to reduce the weight at a reasonable cost. Development of suitable joining technique (s) for the aluminium alloy-steel dissimilar material combination is a pre-requisite to realise this strategy in automotive industry. However, the wide variation in thermo-physical properties of aluminium and steel and low solubility in each other pose problems in joining. The main problem is the formation of the brittle intermetallic compound (IMC) layer at the joint interface, distortion and galvanic corrosion. Therefore, an in-depth investigation on suitable joining process is needed. A variety of joining techniques like solid state techniques, fusion joining techniques, and mechanical joining techniques have been reported in the literature. The automotive industry is more familiar with fusion joining techniques. Accordingly, the present work is undertaken to investigate the fusion joining techniques such as pulsed-GMAW, cold metal transfer (CMT) and laser brazing. The main driver for choosing these processes is that they are all low heat input processes, which are expected to minimise intermetallic formation at the interface.

Aluminium alloy AA6061-T6 sheet of 2 mm thickness and Interstitial Free (IF) steel with three different surface conditions that is uncoated, galvanized and galvanealed were used as base metals and Al-Si alloys (4043 & 4047) as filler wires. Joints were made in lap configuration in weld-brazing mode wherein only the aluminium base metal and the filler wire are melted and made to wet the steel surface to form a braze-like joint. In arc processes, the aluminium sheet is placed over the steel sheet and the arc is run along the edge of the aluminium sheet. In laser brazing, the focussed laser beam melts the tip of the filler wire and the droplets wet the base material to form a joint. The joints were characterised for their

macro/microstructure and mechanical performance. The microstructural features of the joint are analysed using scanning electron microscope (SEM) with an energy dispersive spectroscopy (EDS) attachment. The mechanical performance of the joints was evaluated using lap shear test. An in-depth investigation of the interfacial IMC layer has been carried out using micro area diffraction techniques based on x-rays.

Both arc brazing and laser brazing techniques are successful in joining aluminium alloy to steel. The wetting behaviour is found to be effected by torch position, surface chemistry of steel and filler wire composition. The joints made using galvanized steel showed better performance under lap shear conditions. Increase in interface gap between the base material sheets to 300 μm has increased the strength of the joint as it allows for easy escape of Zn vapors formed during the process. Al-12%Si filler wire is found to perform better compared to Al-5%Si filler wire due to higher fluidity and lower melting temperature. Interface IMC layer thickness could be controlled to less than 8, 4 and 1.2 μm with P-GMAW, CMT and LB techniques respectively. The joints made with Al-5%Si filler wire recorded interfacial failure in all the cases whereas joints made using Al-12%Si filler wire have recorded bead failure.

The interfacial IMC layer varied in thickness, morphology and type with filler wire composition and the joining process adopted. The joint interface of arc brazed specimens using Al-5%Si filler wire showed the presence of Fe-Al based binary IMC phases whereas joints made with Al-12%Si filler wire showed Al-Fe-Si base ternary IMC phases. The laser brazed specimen showed Al, Fe, Si, Zn based quaternary phases at the interface. The increase in heat input favoured Al rich IMC phases at the interface. The formation of Al rich IMC phases are found detrimental to mechanical performance of the joint.

Among arc brazing techniques, CMT brazing techniques showed better performance than P-GMAW process. Laser brazed joints showed better joint strength than arc brazed joints. The joint's load bearing capacity was found to be around 236, 280 and 303 N/mm of bead length made using P-GMAW, CMT and LB techniques respectively.

In summary, a comprehensive investigation of Al-steel joining with three fusion joining techniques has been carried out. Process related, microstructural and performance aspects have been evaluated and process-microstructure-property relations have been established.

CHAPTER 1 INTRODUCTION

1.1 Background

The focus of the entire world is on energy saving and environmental protection. During the years 1950-2000, in 5 decades, there has been a tenfold increase in the number of vehicles and further increase is estimated to be about double by 2025. Consequently, there is a tremendous increase in demand for fuel and simultaneously increasing concern over environmental degradation. Depleting oil reserves and forests are forcing the entire world to minimize the fuel consumption. Simultaneously, polluting emission control is gaining high prominence. The CO₂ levels from vehicles need to be brought down substantially, which demands low fuel consumption models. Improvement in fuel economy can be addressed by developing energy efficient technologies. Vehicle weight accounts for 30% of total fuel consumption. A 30 % reduction in vehicle mass results in 6-7% reduction in fuel consumption [1].

In early days material selection is dictated by cost, as the demand for mass production grows [2]. The draining effect of two world wars on the supply of materials led the automotive engineers to concentrate on automotive body design based on aspects like emissions control, recyclability and safety. In 1920s, the cars were made from wood and fabric, subsequently replaced by deep drawing steel sheets with good formability in 1950s, followed by anti-corrosive steel sheets in 1960s. Low cost, ease of forming, consistency of supply, and corrosion resistance by zinc coating, ease of joining, recyclability, and good crash energy absorption made steel a candidate automotive body-in-white material. There is a reduction in thickness of the steel sheets used from 0.9-2 mm to 0.8 mm which is now further reduced to 0.7 mm in view of cost and weight reduction. In 1970s and 1980s, the high strength steels in thinner gauges found its way as automotive material. Later in 1990s major

concern for fuel economy, safety and environmental protection resulted in further investigation in developing light weight technologies. Hence, the light weight and low dense materials like aluminium, magnesium and their alloys gained prominence as automotive materials. In 1980s, micro alloyed steels were developed and applied to crank shafts and connecting rods. Sinter forged connecting rods were also developed. Aluminium alloys were used for cylinder heads and stainless steels for exhaust manifolds. In 1990s, cylinder blocks and cylinder head covers were made from aluminium and magnesium alloys, respectively. Stiffness and rigidity are crucial for shape stability which is determined by the elastic modulus of the material. The choice of metallic materials needs to be widened and the use of plastics in automotive design also needs attention, where 20 different types of plastics can be used in motor vehicles. 50% weight reduction is possible by substituting steel with aluminium and its alloys in outer panels. 100% substitution of steel with aluminium is not possible in view of strength, crash resistance and toughness requirements. Automotive materials undergo a severe forming, stretching and joining operations which affects the energy absorption and impact resistance. Hence, the drawing ability, work hardening and joining ability should be considered for effective utilization of different material combinations. Hence, the effective utilization of different material combinations require an in depth investigation into the technical issues like forming and joining techniques and environmental performance.

1.2 Applications of dissimilar aluminium-steel joints

Aluminium-steel dissimilar material combination can substitute heavier steel structures in the outer panel [2]. Recently in 2013, Honda implemented adhesive bonding technology for joining aluminium and steel for inner and outer door trims in Acura RLX as shown in Fig 1.1 [3]. Friction stir welding technology is employed in front sub-frame of

Honda Accord as shown in Fig 1.2 [4]. In BMW 5 series, aluminium front section is joined to pillars made of steel using punch rivets and glue. Rivet bonding is adopted in Audi TT for joining aluminium assemblies to steel in rear end parts in sheet form as shown in Fig 1.3 [5].

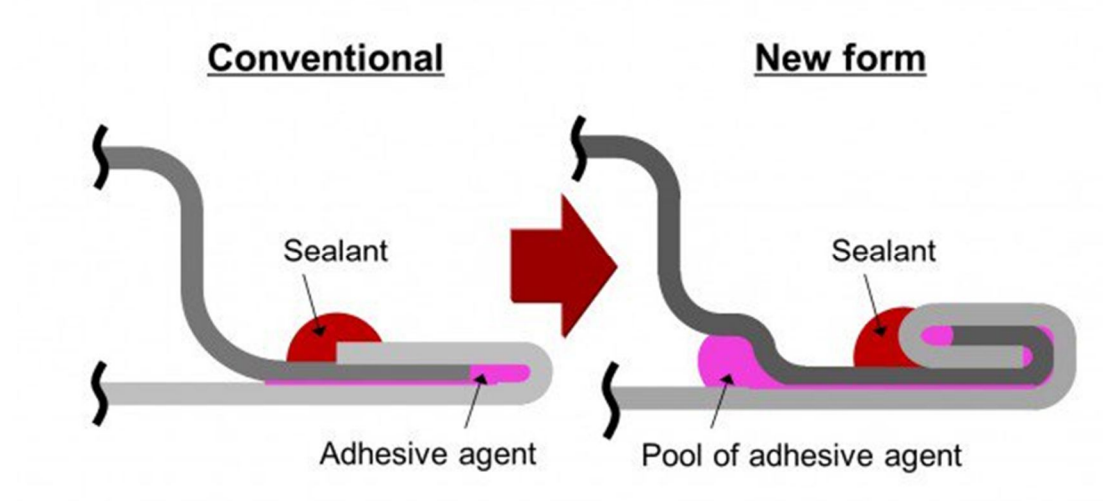


Figure 1.1 Adhesive bonding technology adopted in Honda Acura for joining aluminium and steel [3].

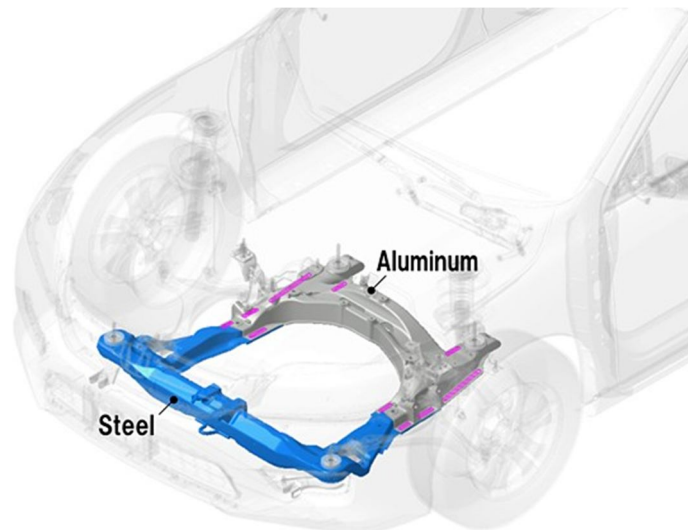


Figure 1.2 Friction stir welding technology adopted in Honda Accord for joining aluminium and steel in front sub frame [4].



Figure 1.3 Rivet bonding in Audi TT (Tourist Trophy) [5].

Depending on the joint configuration and feasibility, riveting, friction stir welding and adhesive bonding are adopted for joining Aluminium to Steel in actual applications.

1.3 Problems involved in aluminium-steel fusion joining

Table 1.1 Thermo-physical properties of aluminium and steel

Property	Material	
	Aluminium	Steel
Melting Point (K)	933.47	1809
Density (kg.m⁻³)	2710	7870
Thermal Conductivity, K (W.m⁻¹.K⁻¹)	231	80
Coefficient of thermal expansion (20-100°C), α (1/k)	23.6×10^{-6}	11.8×10^{-6}
Standard Potential, E°, (V)	-1.66	-0.44
Specific Heat, C_p (kJ/kg.K)	0.91	0.49

Properties of aluminium and steel are listed in Table 1.1. A wide disparity in physical and thermal properties like density, melting point, thermal conductivity, electrical conductivity, coefficient of thermal expansion etc. between Al and Fe (Table 2.1) renders fusion joining

difficult to be accomplished. Mutual solubility among Al and Fe is less. Hence, the formation of Fe-Al solid solution is not thermodynamically feasible. They form intermetallic compounds (IMC) at the interface rather than a solid solution.

An in-depth literature survey on aluminium to steel fusion joining revealed the following issues:

- poor wettability of iron by aluminium
- formation of brittle intermetallic phases due to partial solid solubility affecting joint strength
- formation of weld cracks & distortion of specimen due to variation in thermal expansion coefficients
- galvanic corrosion
- porosity and poor bead surface - process related problems [5-10].

Material properties differences their effects above are summarised in Table 1.2

Table 1.2 Problems involved in fusion joining aluminium to steel

Material dissimilarities/properties	Problems
Different melting points and heat conductivities	Overheating of the aluminium part, spatter formation
Mixing of steel and aluminium when one member is in liquid state	Formation of brittle intermetallic phases, insufficient mechanical properties
Different thermal expansion coefficients	Contraction stresses and resulting cracks in the weld
Formation of an oxide layer on the aluminium	Problems when brazing

1.4 Intermetallic compounds (IMC) and formation

1.4.1 Binary Fe-Al phases

It is important to understand the Fe-Al system in order to accomplish fusion joints between aluminium alloys and steels. Fig 1.4 shows the binary Fe-Al phase diagram. The IMCs are phases with different crystal structures than the constituting elements. These form in various combinations of metals and non-metals. The IMC phases possess a complex crystal structure which in turn increases the hardness and limit formability.

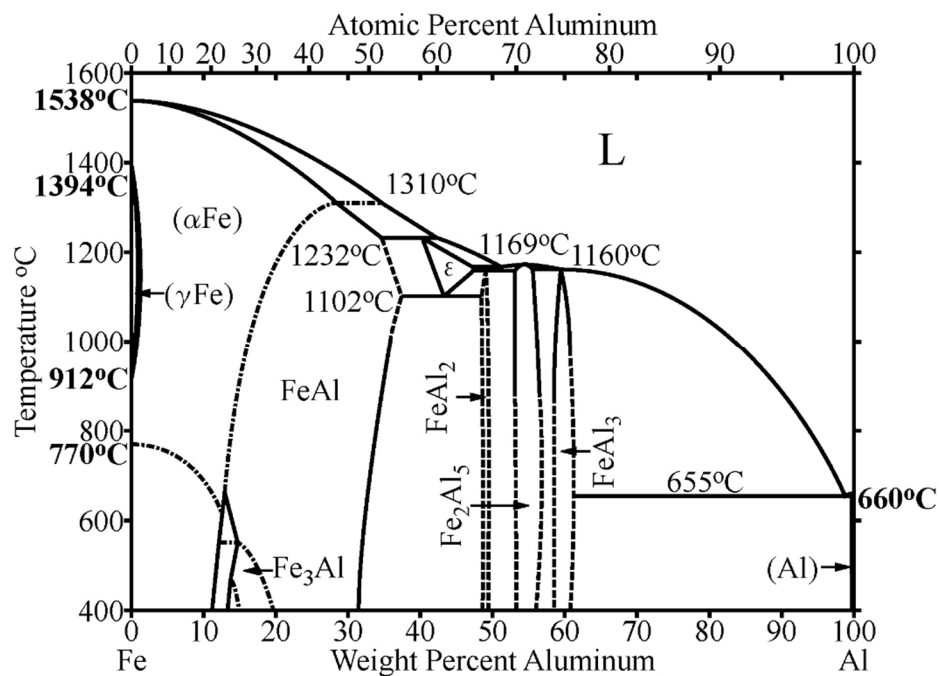


Figure 1.4: Fe-Al binary equilibrium phase diagram[11].

Table 1.3 List of binary Fe-Al IMC phases.

Symbol	Stoichiometry	Crystal Structure
β'	Fe ₃ Al	Cubic
E	Fe ₅ Al ₈	Cubic
B	FeAl	Cubic
Z	FeAl ₂	Triclinic
η	Fe ₂ Al ₅	Orthorhombic
θ	Fe ₄ Al ₁₃	Monoclinic

The low mutual solubility of Fe and Al results in formation of brittle intermetallic compounds (IMC). Fe_3Al , FeAl , Fe_5Al_8 , Fe_2Al_5 , FeAl_3 are the intermetallic phases observed in equilibrium phase diagram as listed in Table 1.3. Among the above mentioned phases Fe_3Al and FeAl are the two ordered phases present on the Fe rich side and FeAl_2 , Fe_2Al_5 and $\text{Fe}_4\text{Al}_{13}$ are found on Al rich side of the equilibrium diagram. Among these IMC phases the Aluminium rich phases namely Fe_2Al_5 and FeAl_3 are most commonly seen in fusion joining of aluminium and steel [11-13]. These two compounds normally form only above 1090°C . Apart from these equilibrium phases, rapid solidification results in Fe_2Al_9 , FeAl_p and FeAl_x type metastable phase formation [14]. The orthorhombic Fe_2Al_5 phase is observed in most of the Al/Fe interfaces and is known to grow rapidly by diffusion of Al atoms in vacant sites along the c-axis of the structure.

1.4.2 Ternary Al-Fe-Si phases

The addition of Si in the aluminium melt is known to decrease the viscosity and increase the fluidity of the molten metal pool. Therefore Al-Si based filler wires are mostly chosen for fusion joining of aluminium and steel. Hence, the ternary Al-Fe-Si based IMC phases may form at the Al/steel interface. Fig 1.5 shows the isothermal section of Al-Fe-Si system at 550°C . The list of ternary phases along with the stoichiometry and crystal structure is given in Table 1.4. The ternary system is found to be much more complex than the binary system and is comprised of complex crystal structures. The complexity of the system is due to the following reasons 1) coexistence of several IMC phases in a narrow range of chemical composition; 2) the ternary IMC phases possess complex crystal structures and planar defects; 3) the order disorder transformations towards the Fe-corner; 4) high number of unending invariant reactions; and 5) the dependence of phase formation on heterogeneous

nucleation during solidification. This ternary system is comprised of nine ternary phases (T_1 - T_{10}) and nineteen invariant reactions.

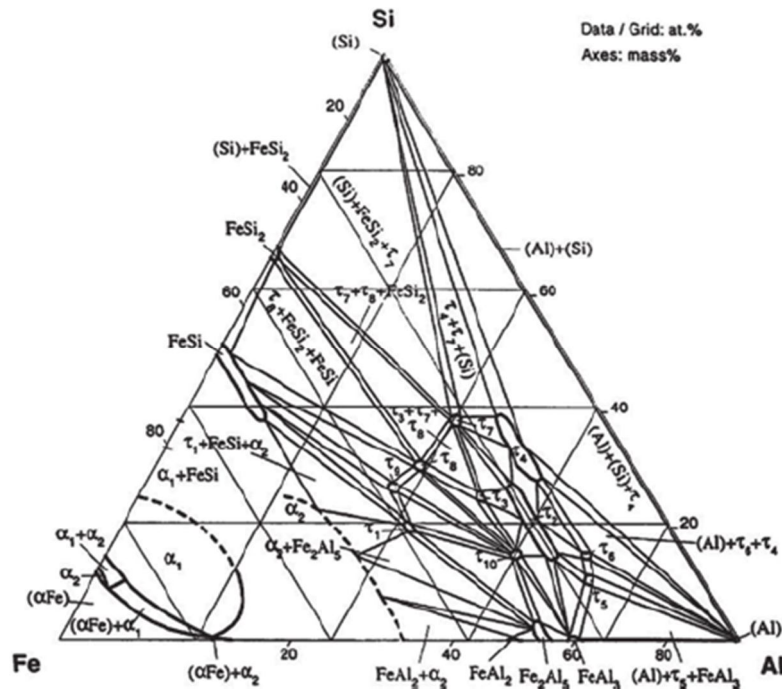


Figure 1.5: Isothermal section of ternary Al-Fe-Si system at 550 °C [15].

Table 1.4 List of Al-Fe-Si ternary IMC phases.

Symbol	Stoichiometric formula	Crystal structure	Reference
T_1	$Al_2Fe_3Si_3$	Triclinic	[16]
T_{23}	Al_2FeSi	Orthorhombic	[17]
T_4	Al_3FeSi_2	Orthorhombic	[18]
T_5	Al_8Fe_2Si	Hexagonal	[19]
T_6	$Al_{4.5}FeSi$	Monoclinic	[20]
T_7	$Al_3Fe_2Si_3$	Monoclinic	[21]
T_8	$Al_2Fe_3Si_4$	Orthorhombic	[16]
T_{10}	$Al_4Fe_{1.8}Si$	Hexagonal	[22]

The major contribution to this system is by Takeda et al., where 6 ternary compounds [15, 23-25] are reported, out of which four phases (τ_2 , τ_4 , τ_5 & τ_6) can be detected easily. The compound τ_2 and τ_3 are reported to be the same compounds with small variation in homogeneity ranges and designated as τ_{23} . Similarly, the compounds τ_1 and τ_9 possess small variation in homogeneity ranges and hence designated as same phases. At 550 °C, the phase τ_1/τ_9 coexist with FeAl, $\text{Fe}_4\text{Al}_{13}$, Fe_2Al_5 , FeSi, τ_2 , τ_3 , τ_7 , τ_{10} , τ_8 [14] . At 550 °C, τ_2 coexists with $\text{Fe}_4\text{Al}_{13}$, τ_4 , τ_1/τ_9 , τ_5 , τ_6 and τ_7 . At 550°C τ_4 coexists with Si, τ_2 , τ_6 and τ_7 . τ_5 , τ_2 $\text{Fe}_4\text{Al}_{13}$ and τ_6 exist together at 550 °C. The phase τ_6 at 550°C exists along with Al, Si, τ_2 , τ_4 and τ_5 . At 550 °C, the ternary phase τ_7 exists along with Si, τ_1/τ_9 , τ_2 , τ_4 and τ_8 . At 550 °C, the phase τ_{10} coexists with τ_1/τ_9 , τ_3 and $\text{Fe}_4\text{Al}_{13}$. Therefore all the ternary phases are found to coexist with each other which in turn increase the difficulty in phase identification.

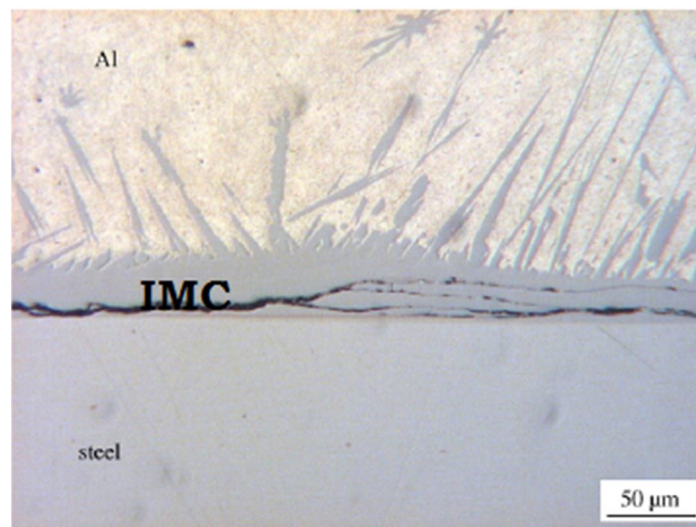


Figure 1.6 IMC layer at Al/steel interface [26].

A variety of processes like solid state, fusion and mechanical joining techniques are reported in the literature. The solid Fe/solid Al, solid Fe/semi solid Al, solid Fe/liquid Al reactions take place in mechanical, solid state and fusion joining processes, respectively. Hence, due to

these reactions, IMC phases form at the aluminium/steel interface as shown in Fig 1.6. The thickness of the interface IMC layer affects the joint strength. There are reports that the joint strength is varied with IMC layer as shown in Fig 1.8. There are reports that if the IMC layer thickness is restricted to less than 10 μm , it shows negligible effect on joint strength. Hence, the candidate joining process should be able to restrict the growth of IMC layer.

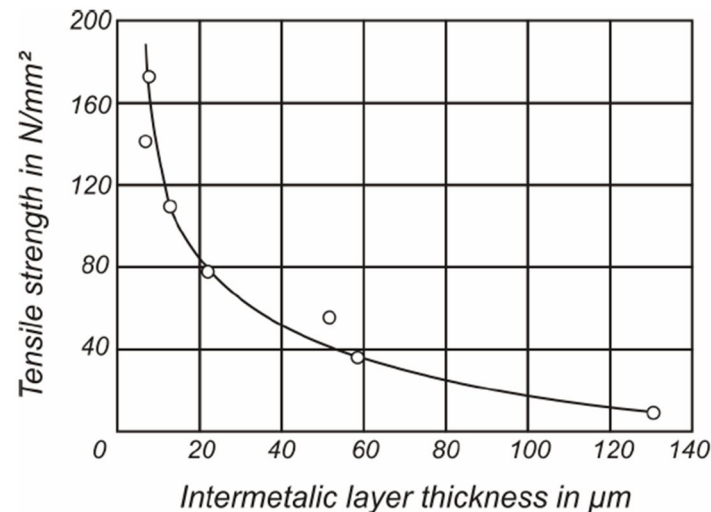


Figure 1.7 Relationship between IMC layer thickness and joint strength of dissimilar Al/steel joints [27].

Based on above important phenomena reported in the literature about Al-Steel fusion joining and the need for developing fusion joining techniques for applications such as automotive light weighting, this investigation on fusion joining techniques to understand the joint formation and its effect on performance is felt to be very expedient.

1.5 Objectives

Based on the literature survey, above mentioned background and motivation, following are the objectives to be accomplished in developing a fusion joining technology for joining aluminium alloy and steel.

- evaluating the applicability of fusion joining processes like Pulsed-Gas Metal Arc Welding (P-GMAW), Cold Metal Transfer Welding (CMT) and Laser Braze Welding (LBW) processes to aluminium-steel dissimilar material joining.
- attaining a flawless and leak proof aluminium-steel brazed joint.
- study on the effect of process and material related variables on joint forming capability and efficiency.
- study on the effect of heat input, filler wire composition and type of process on the thermodynamics of layer formation at braze bead/steel interface.
- in depth characterization of the reaction layer at braze bead/steel interface using micro X-Ray Diffractometer (micro XRD) for phase identification.

1.6 Overview of the thesis

The thesis comprises of eight chapters.

Chapter 1 covers the motivation, the problems related to Al-steel joining and objectives of the present thesis.

Chapter 2 discusses the related work reported in the literature.

Chapter 3 deals with the detailed experimentation (Pulsed-GMAW, CMT and LBW processes) and characterization (microstructural and mechanical characterization) techniques that have been used to achieve the objectives of the present study.

Chapter 4 discusses pulsed-GMAW process optimization and identifying the parametric window, effect of process related variants like angle of tilt, torch orientation, heat input, gap between the plates and material related variants like chemical composition of the steel surface

and filler wire (wettability studies) on mechanical performance of the joint. It also talks about interfacial characterization using micro diffraction techniques like micro XRD and correlating to joint efficiency. A part of this chapter has already been published in Journal of Materials Processing Technology, 214 (2014) 2949.

Chapter 5 comprises of CMT brazing process optimization and identifying the parametric window, effect of variants like heat input and chemical composition of filler wire on joint efficiency. It also discusses on phase formation at braze bead/steel interface and its effect on mechanical performance of the joint.

Chapter 6 is on applicability of laser braze welding technique to aluminium-steel dissimilar material combination. Chapter 7 summarizes the outcomes of the current work. Chapter 8 outlines the directions for future investigations.

References

- [1] Automotive Engineering Lightweight, Functional, and Novel Materials, Taylor & Francis, New York, London, 2008.
- [2] G. Davies, Materials for /automotive Bodies, Butterworth-Heinemann, 2012.
- [3] A. Lim, 2013. <http://www.autoindustryinsider.com/?p=5397>
- [4] A. Marsh, 2012. <http://paultan.org/2013/02/22/honda-develops-new-tech-to-join-steel-and-aluminium/>.
- [5] H. Zhang, J. Liu, Materials Science and Engineering a-Structural Materials Properties Microstructure and Processing, 528 (2011) 6179-6185.
- [6] J. Tsujino, K. Hidai, A. Hasegawa, R. Kanai, H. Matsuura, K. Matsushima, T. Ueoka, UltraThereforenics, 40 (2002) 371-374.
- [7] E. Taban, J.E. Gould, J.C. Lippold, Materials & Design, 31 (2010) 2305-2311.
- [8] R. Qiu, H. Shi, H. Yu, K. Zhang, International Journal of Materials & Product Technology, 49 (2014) 285-293.
- [9] M.J. Rathod, M. Kutsuna, Welding Journal, 83 (2004) 16S-26S.
- [10] H. Ozaki, M. Kutsuna, S. Nakagawa, K. Miyamoto, Journal of Laser Applications, 22 (2010) 1-6.
- [11] L. Agudo, N. Jank, J. Wagner, S. Weber, C. Schmaranzer, E. Arenholz, J. Bruckner, H. Hackl, A. Pyzalla, Steel Research International, 79 (2008) 530-535.

- [12] J. Liu, S. Jiang, Y. Shi, Y. Kuang, G. Huang, H. Zhang, *Optics and Laser Technology*, 66 (2015) 1-8.
- [13] H. Ma, G. Qin, L. Wang, X. Meng, L. Chen, *Materials & Design*, 90 (2016) 330-339.
- [14] G. Ghosh, Ternary Alloys, *A Comprehensive Compendium of Evalu-* 52. B. Sundman, B. JansThereforen, and J.-O. AndersThereforen: CALPHAD, 1985, vol.nated Constitutional Data and Phase Diagrams, VCH Publishers, New York, 1992.
- [15] V. Raghavan, *Journal of Phase Equilibria and Diffusion*, 33 (2012) 322-326.
- [16] T.I. YanThereforen, M.B. Manyako, O.I. Bodak, N.V. German, O.S. Zarechnyuk, R. Cerny, J.V. Pacheco, K. Yvon, *Acta Crystallographica Section C-Crystal Structure Communications*, 52 (1996) 2964-2967.
- [17] N.V. German, V.E. Zavodnik, T.I. YanThereforen, O.S. Zarechnyuk, *Kristallografiya*, 34 (1989) 738-739.
- [18] P.K. Panday, Schubert, K, J. *Less-Common Met*, 18 (1969) 175-202.
- [19] C. Gueneau, C. Servant, F. Dyvoire, N. Rodier, *Acta Crystallographica Section C-Crystal Structure Communications*, 51 (1995) 177-179.
- [20] C. Romming, V. Hansen, J. Gjønnes, *Acta Crystallographica Section B-Structural Science*, 50 (1994) 307-312.
- [21] D. MunThereforen, *J. Inst. Met*, 95 (1967) 217-219.
- [22] V.K.B.s. N.V. German, T.I. YanThereforen, and O.S. Zarechnyuk, *Kristallografia*, 34(3) (1989) 735-737.

- [23] K.M. H. P. Takeda, Tetsu to Hagane-Journal of the Iron and Steel Institute of Japan, 26 (1940) 335-361.
- [24] V.G. Rivlin, Raynor, G.V, Int. Met. Rev, 26 (1981) 133-152.
- [25] Y. Li, B. Legendre, Journal of Alloys and Compounds, 302 (2000) 187-191.
- [26] G. Sierra, P. Peyre, F.D. Beaume, D. Stuart, G. Fras, Materials Characterization, 59 (2008) 1705-1715.
- [27] J.R. D. R. G. Achar, S. Sundaresam, Aluminium, 56 (1980) 220-228.

CHAPTER 2 LITERATURE REVIEW

In view of the aspects explained in chapter-1 viz., the thermo physical and metallurgical differences between aluminium and steel, following directions are important:

- Type of joint: It should be a braze-like joint wherein the materials to be joined are not melted. In this case it could be a welding-brazing kind of joint wherein Al having a lower melting point than steel could melt and wet the steel surface and forms a joint.
- Heat input: Temperature, pressure and composition are the major influencing factors for the formation of intermetallic phases. These intermetallic phases are deleterious to mechanical performance of the joint. These can be minimized by controlling the temperature that inhibits the reaction between iron and aluminium. Hence, by controlling the heat input, formation of brittle intermetallic phases can be minimized.
- Chemical composition: By altering the chemistry at the joint interface intermetallic formation can be minimized. Selection of a suitable filler metal or application of an interlayer which is compatible with both Fe and Al aids in minimizing the diffusion between Fe and Al which in turn reduces intermetallic formation.
- Surface modification: Efficiency of a brazed joint is highly dependent on wetting and capillary action. Wetting and capillary action depends on surface phenomenon of the materials to be joined. Therefore by activating the surface by modification techniques like laser texturing, plasma treatment or interlayer, aids in improvement in wetting behaviour.

Hence, the chosen processes and materials should satisfy the following criteria:

Process

- low heat input

- suitable to thin sheet joining and
- easy adaptability to automotive industry

Aluminium base material

- alloy and its thickness suitable to automotive component
- weldable alloy with good mechanical properties and
- anti-corrosion

Steel base material

- alloy and its thickness suitable to automotive components
- weldable alloy with good mechanical properties
- anti-corrosion; and
- should possess a wetting friendly surface to molten filler

Filler wire

- low melting point
- high fluidity
- compatible with both Al and Fe
- ability to wet Steel surface and
- minimising the IMC formation or restricting the diffusion between Al and Fe

In view of the above mentioned concept the processes and materials satisfying the above mentioned conditions are as follows

Processes

- Pulsed-gas metal arc welding (P-GMAW)

- Cold metal transfer welding (CMT) and
- Laser brazing (LB)

Materials:

- 2 mm thick 6061-T6 condition aluminium alloy
- 1.2 mm thick interstitial free steel with galvanized and galvannealed coating
- 1.2 mm diameter Al-5%Si and Al-2%Si filler wire

Several works have been reported in the literature with respect to application of fusion joining techniques for Al-steel joining. A detailed literature survey on the processes and joint formation behaviour reported is enumerated as follows:

2.1 Thermal joining techniques

In these techniques, the metallurgical bond between the base materials is formed by melting the base materials or externally added filler wire or both and forms a leak proof joint. Welding, brazing and soldering are three joining techniques. Both base materials melt in welding, externally added filler wire melts in brazing and externally added filler melts at less than 450 °C in soldering. Brazing qualifies as a suitable joining technique for dissimilar aluminium-steel joining.

2.2 Brazing

Brazing is a process of coalescence of materials by heating them to the brazing temperature in the presence of a low melting filler wire. Exclusively, in brazing the metallurgical bond is established by melting only filler material but not the parts to be joined. The filler material melts, flows, distributes by means of capillary action between the tightly fitted base materials and solidifies to form a leak-tight seal, a strong structural bond. The ability to join dissimilar

material combinations like metals to ceramics, made brazing a familiar technique in the industry. The flexibility in manual operation and automation made it popular in various industries. Based on the heat source, brazing processes are categorized as furnace brazing, torch brazing, induction brazing, dip brazing, resistance brazing, infrared brazing, laser brazing, weld brazing, exothermic brazing and microwave brazing. The cleaning of the base materials and protecting them from excessive oxidation by fluxing or by the use of controlled atmosphere is critical in obtaining a good braze joint. The aspects like filler metal flow, base material characteristics, filler material characteristics, surface preparation, joint design and clearance, temperature and time, rate and Source of heating are important for obtaining a satisfactory braze joint. In a brazing operation, the temperature of the brazement is raised till it becomes molten, wets, spreads and fills the gaps between the base materials. The strength of a braze joint is guided by wetting and spreading of molten metal on base materials. The driving forces for wetting can be explained by the thermodynamic aspects like surface free energy and free energy of formation of phases which may form due to reactions occurring during brazing operation, followed by spreading or distribution of molten metal into gaps through capillary action. The wetting and spreading phenomenon is highly influenced by the chemical reactions occurring at the interface and in the filler material. Wetting phenomenon is also governed by the temperature differential between the liquid and the substrate, viscosity of the liquid, temperature of the liquid [1-3].

2.3 Arc brazing

Arc brazing is a process in which an electric arc generated between the base materials serves as a heat Source for melting and joining of the base materials. The following are the different arc brazing processes reported in the literature.

2.3.1 Gas metal arc welding (GMAW)

GMAW is one among the fusion joining techniques in which an arc is generated between the base materials and consumable electrode serves as a heat source causing fusion and coalescence of base materials in the presence of an inert or active gas. Usage of inert gases like Argon (Ar), Helium (He) and their mixtures provides necessary shielding to the arc and the molten weld pool. Active gases like CO₂ and O₂ are also used in welding of steel up to 0.4%C and low alloy grades. The molten pool generated at the electrode tip is transferred to the work piece through three basic metal transfer modes namely globular, spray and short circuiting. Globular transfer occurs at relatively low welding currents, in which the molten droplets close to or larger than the diameter of the electrode is transferred to the work piece through the arc under the influence of gravity. The spray mode of metal transfer demands welding currents above a critical limit. In this, due to high welding currents, small discrete droplets of metal reach the work piece through the arc gap under the influence of electromagnetic force at higher frequency than globular transfer. The critical current limit depends upon the material and size of the electrode and the composition of the shielding gas used. In short circuiting mode, the short circuiting between the electrode and work piece raises the current locally, melting the electrode tip leading to deposition. Hence, the mode of metal transfer is dependent on the factors such as magnitude and type of welding current, electrode diameter, electrode composition, electrode extension and shielding gas used. Spray transfer mode is desirable as it enables smooth and spatter free metal transfer. But, requirement for high welding currents resulting in high heat input disables the use of this mode for thin sheet and dissimilar material welding that demands less dilution. Hence, altered current-voltage cycles may aid in minimizing energy input. Based on this view the following modified GMAW processes have emerged in the field of low heat input welding suitable for thin sheet and dissimilar material welding.

2.3.2 Pulsed-GMAW

Pulsed-GMAW is a modified GMAW process in which controlled spray transfer at low heat input condition is possible. In this process, controlled melting off of the filler occurs by pulsing at regular frequency between background current which keeps the gap ionized and maintains the arc, the pulse current which melts the wire tip and propels the molten droplets across the arc. Thus, lower heat output than pure spray transfer but higher than the dip transfer, allows thin section welding with spray transfer avoiding poor fusion that sometimes occurs with dip transfer. All positional welding is performed much more easily. This process enables good root fusion, even penetration, minimal distortion and good filling up of joint and it gives efficient results at fully automated conditions. The first generation pulsed-GMAW units consist of half or full wave rectified sine wave with the pulse frequency fixed by that of the main supply at either 50 or 1000 Hz. The pulse parameters like peak current, background current and pulse width for particular transfer are determined by the electrode diameter and composition. Complexity of parametric adjustment and skill needed by the operator hence limited its applicability. Possibility of generation of rectangular waveform (synergic pulse) instead of sine wave using electronically controlled and transistorized power Source enhanced the applicability of this process to a wide range of materials [3].

2.3.3 Cold metal transfer (CMT) welding

CMT stands for cold metal transfer and it is basically intended for thin sheets and dissimilar material joining which demands low energy input. CMT is a modified GMAW process operating at lower heat input in which the movement of the wire is integrated as a process controlling parameter. Method of droplet detachment adds innovation to this process. CMT in its basic form is a short circuit welding process. As soon as the power Source detects a short circuit, the filler wire is retracted mechanically and welding current drops to zero, enabling

zero current droplet detachment as shown in Fig 2.1. The backward movement of the wire facilitates smooth droplet detachment during short circuit. The filler wire is moved forward again and the cycle is repeated. The filler wire is retracted at every short circuit at regular intervals. The arcing time is only 1/3 of total cycle time. The thermal input is reduced after the arc is extinguished, creating an oscillating hot/cold weld pool. This type of metal transfer produces small and fast freezing weld pool. There is no significant metal transfer occurring across the arc gap. In conventional GMAW process the short circuiting between the electrode tip and work piece rises the current locally causing melting of the wire tip and pinches off the molten droplet. The action of violent separation of the molten droplet results in spatter during welding. Smooth droplet detachment at nearly zero currents allows spatter free metal transfer in CMT process. Reduced spatter, low thermal input, arc stability, high precision, gap bridging ability, high speed welding, high quality welds, ability to weld light gauge materials (nearly 0.3 mm) and dissimilar materials are the major advantages of CMT over conventional GMAW process. The major parameters affecting the weld geometry and quality are welding current (wire feed rate), polarity, electrode diameter, arc voltage, electrode extension, travel speed, torch angle and shielding gas [4, 5].

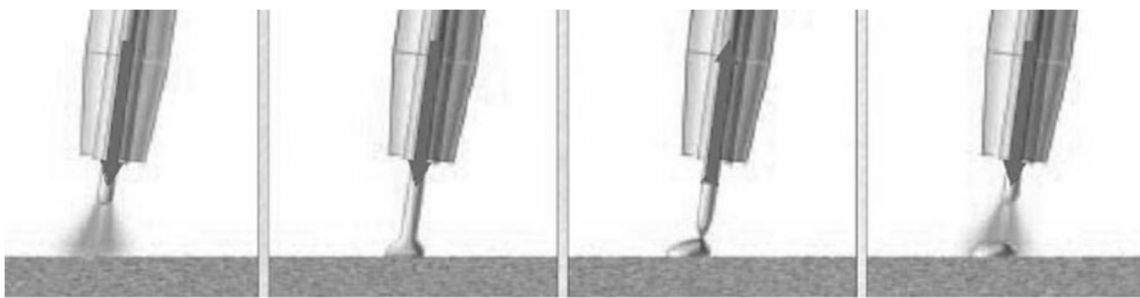


Figure 2.1 Schematic of metal transfer in Cold Metal Transfer process [4].

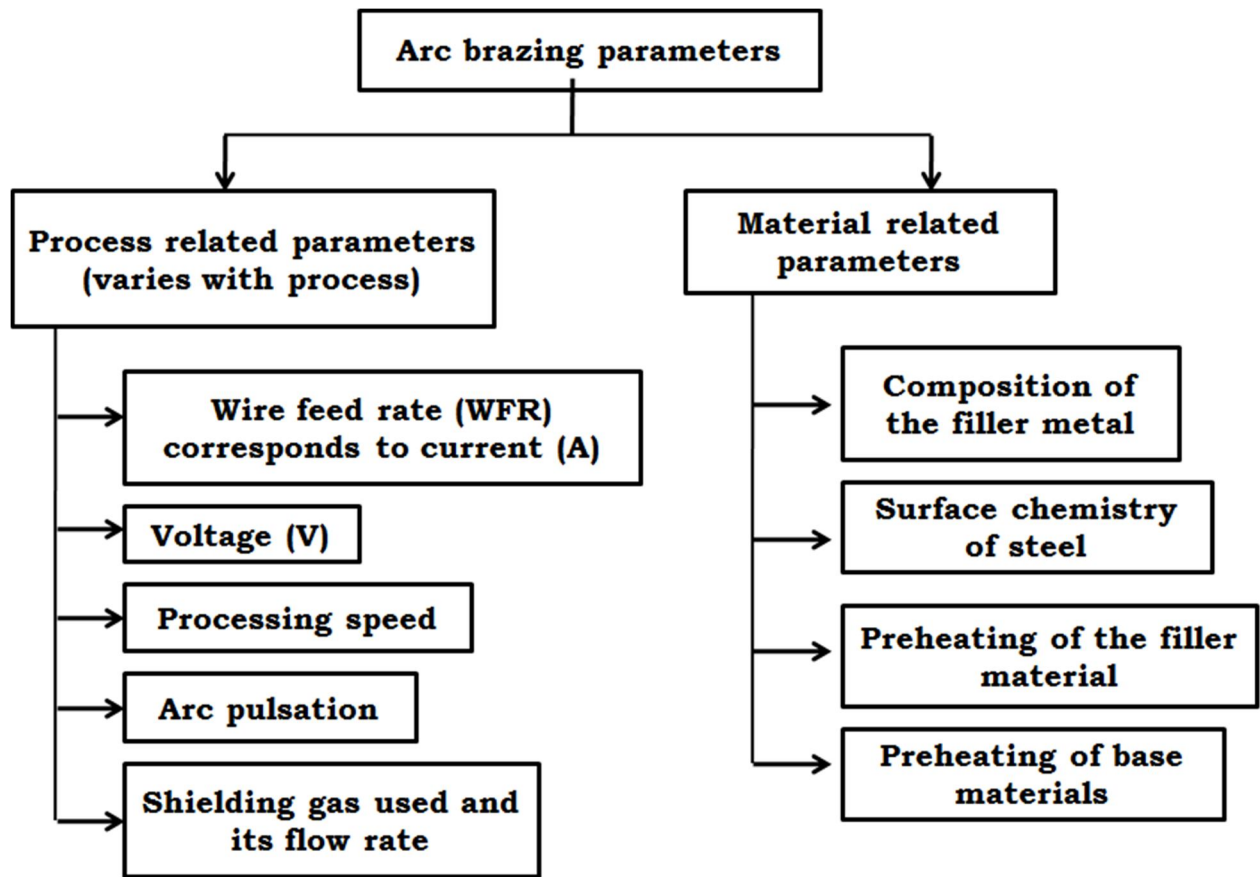


Figure 2.2 Flow sheet of various variables effecting the joint formation.

There are different variables that effect the arc brazing process and its efficiency. Fig 2.2 shows variables that affect the joint formation in an arc brazing process. The effect of each variable is explained in detail in the following section.

2.4 Effect of parameters of arc brazing process

2.4.1 Effect of surface chemistry of steel

There is limited literature available in arc brazing with respect to surface chemistry of the Steel. There are a few reports that galvanized surface showed better response to wetting, spreading and recorded better mechanical properties. Kang et al.[6] studied the effect of aluminium and zinc coating on steel on joint properties. It has been reported that the joints

made with galvanized steel showed better wetting and spreading than joints made with aluminized steel as shown in Fig 2.3 [6] [7].

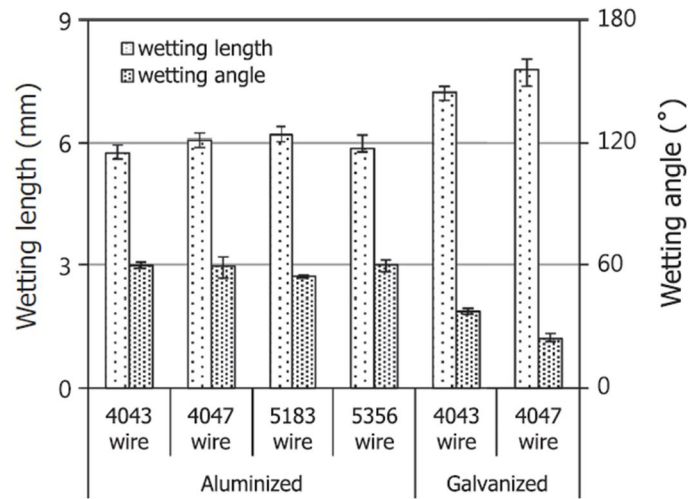


Figure 2.3 Variation in wetting length and angle with surface chemistry of steel and filler wire [6].

2.4.2 Effect of filler wire composition

Agudo, et al. [8] studied the effect of Al99.5, 4043 (AlSi₅), AlMn₁ and AlSi₃Mn₁ type filler wires on interfacial characteristics and mechanical performance of CMT brazed butt joints of DX54D steel and AW5182-H111 aluminium alloy. Zhang, et al [5] reported the joint characteristics of hot dip galvanized cold rolled Q235 low carbon steel and 6061 aluminium alloy using 4043 (AlSi₅) filler wire made using cold metal transfer process. The variation in IMC layer thickness, joint strength and failure location with filler wire composition are listed in Table 2.1. The addition of 3 wt. % Si to the aluminium filler wire showed a reduction in intermetallic layer thickness by nearly 40%. CMT welding using any filler wire restricts the intermetallic layer growth to less than 5 µm as given in Table 2.1. The addition of Mn in aluminium filler adds to the strength of the joint but has negligible effect on restricting the intermetallic growth. The joints made with Al99.5 and AlMn₁ showed the presence of Fe₄Al₁₃ and Fe₂Al₅ type of intermetallic compounds at the filler/steel interface. Among all the

possible intermetallic phases, Fe_2Al_5 occupies the major fraction. It grows as cuboidal grains with the larger grain axis perpendicular to the interface. It grows mostly on the steel side of the interface. $\text{Fe}_4\text{Al}_{13}$ compound is most favourable to form towards the filler side of the interface with some grains embedded in the aluminium filler matrix. With Si based filler wires, along with the above mentioned intermetallic compounds Al-Fe-Si ternary phase is also observed at aluminium filler side of the interface. In case of Si based filler wire, the length of the larger grain axis of Fe_2Al_5 is 5 times less compared to non-Si based filler wire. The $\text{Fe}_4\text{Al}_{13}$ grains in Si containing fillers are always found in contact with Fe_2Al_5 grains or overlapping with Al-Fe-Si grains. Hence, the nature of interface formation in terms of morphology and sequential arrangement alters with the type of filler wire. Joints made with filler wires containing Mn reported slightly high fracture loads and failure in the steel base material that is approximately about 3 mm away from the weld bead. Joints made with pure Al-Si based filler wires showed failure in the filler region. Hence, presence of Mn helps in improving the joint strength and shifts the failure to base materials. Joints made with pure aluminium filler showed rupture along the intermetallic phase region [8] [9].

Table 2.1 Variation in IMC layer thickness, joint strength and failure location with filler wire composition

Filler wire	IMC layer thickness (μm)	Joint strength (MPa)	Failure location
Al99.5	3.5	296	bead, bead/steel interface
AlSi ₅	2	293	bead
AlMn ₁	4	291	bead, steel base material
AlSi ₃ Mn ₁	2.2	304	steel base material

2.4.3 Effect of pre-heating of the filler wire

The increased fluidity and reduced viscosity of the molten pool generated caused by pre-heating of the filler wire may probably help in improved wetting and spreading action. But there is no literature available with respect to arc brazing processes.

2.4.4 Effect of pre-heating of the base materials

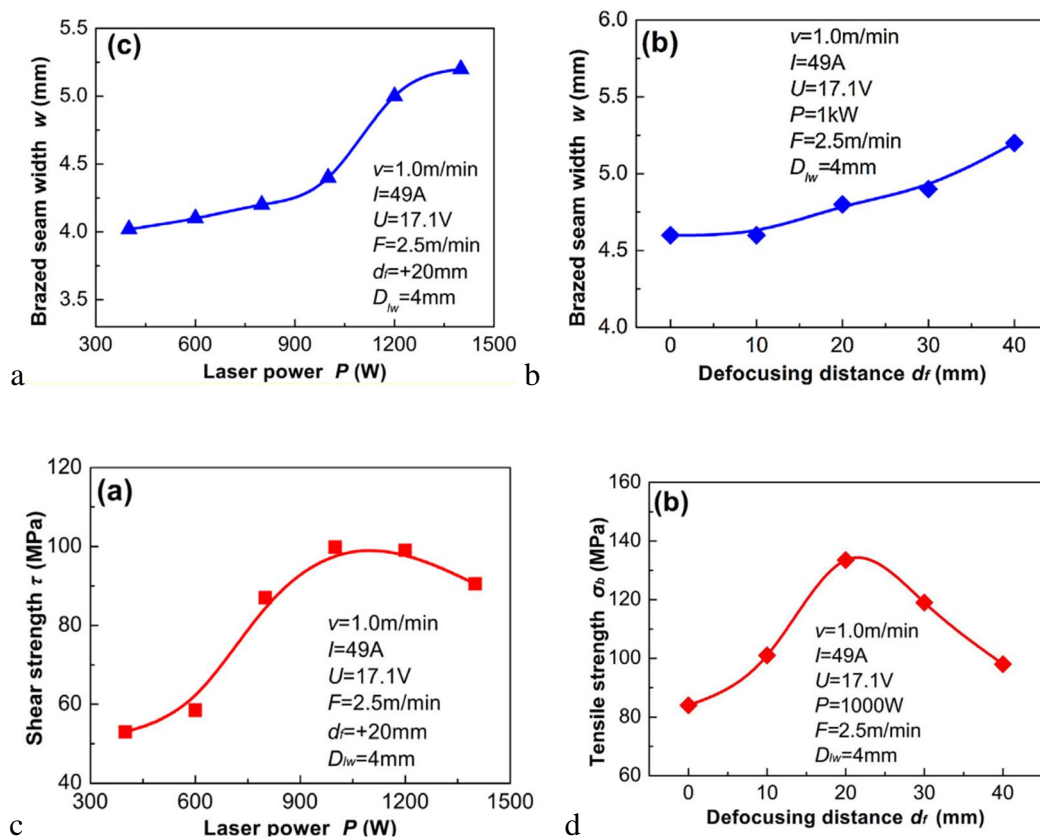


Figure 2.4 Effect of laser power and defocusing distance on wetting and strength of joint
a) laser power vs wetting b) defocusing distance vs wetting c) laser power vs joint strength d) defocusing distance vs joint strength [10].

The wetting and spreading behaviour is governed by the thermal gradient between the base material and the molten pool. Pre-heating of the base materials helps in minimizing the thermal gradient which in turn aids in better wetting. The wide variation in coefficient of thermal expansion between Fe and Al results in distortion. Hence, pre-heating also helps in minimizing the distortion. There is a limited literature available on this concept. Qin et al.[10]

studied the effect of laser beam pre-heating at varied laser power, defocusing distance on wetting behaviour and joint performance. Fig 2.4 shows the effect of laser power, defocusing distance on wetting width and joint strength. It is observed that increase in laser power resulted in improved wetting. This is reflected in the increase in braze bead width with increase in laser power as shown in Fig 2.4a. It is also observed that increase in defocusing distance of laser also resulted in improved wetting as shown in Fig 2.4b. Increasing the laser pre-heating power up to 900 W showed a positive effect on joint strength whereas beyond 900W the joint strength is decreased as shown in Fig 2.4c. Defocusing distance up to 20 mm showed a positive effect on joint strength whereas further increase in distance reduced the joint strength as shown in Fig 2.4d.

2.4.5 Effect of wire feed rate (WFR)

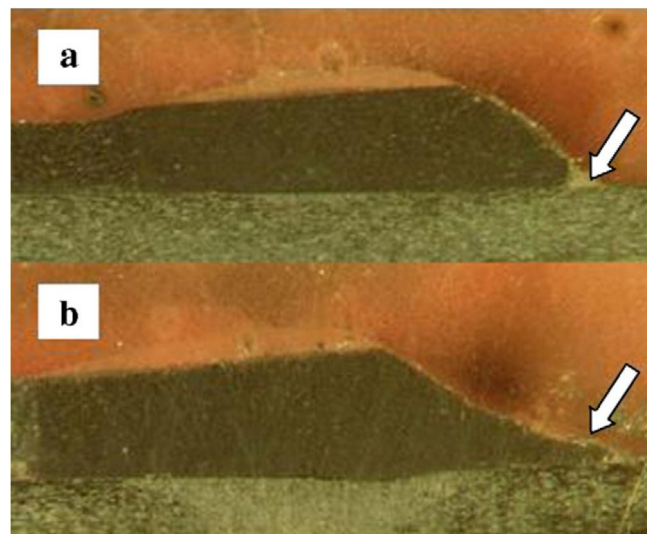


Figure 2.5 Effect of heat input on wetting behaviour a) low heat input b) high heat input [7].

In an arc welding process, the wire feed rate corresponds to welding current. Higher the wire feed rate, higher the welding current and higher the heat input into the work piece. In the present context, dilution between aluminium and iron should be as less as possible to minimize the growth of brittle intermetallic compounds at the interface. The heat input should

be sufficient enough to generate minimal molten pool to wet the steel surface. Pulsing helps in minimizing the heat input, enabling low current or zero current metal transfer to the work piece. In pulsed GMAW process, pulsing between higher and lower levels of current occurs allowing low average current spray transfer whereas in CMT welding it is zero current droplet detachment. Welding currents in the range of 65-70 A are adopted for aluminium-steel joining in the thickness range of 1-2 mm [7]. The variation in wire feed rate alters the heat input, in turn changing the wetting behaviour, which is observed from the toe angle of the bead as shown in Fig 2.5.

2.4.6 Effect of processing speed

In an arc welding process, welding speed effects the uniformity of the bead. Too high or low travel speed results in wavy or humpy bead formation. The welding speed has to be optimized to obtain a uniform bead with no waviness. At higher travel speeds the molten pool is thrown with high pressure resulting in non-uniform bead, whereas low travel speeds deposits lumps of molten metal resulting in more dilution and non-uniform bead. The travel speed combined with welding current accounts to overall heat input of the process. Hence, the welding speed has to be optimized for obtaining a uniform bead with minimum dilution, in aluminium and steel joining. Welding speeds in the range of 0.8-1.2 m/min are adopted depending upon the type and thickness of the material.

2.4.7 Effect of shielding gas and flow rate

Shielding gas is responsible for maintaining the arc, shielding the molten pool from outside atmosphere and transfer of heat to the weld. The shielding gas during arcing forms plasma and maintains the arc. The shielding gas with less ionization potential is suitable for generation of plasma and maintenance of stable arc. For aluminium-steel dissimilar material

joining the heat input should be less with maximum possible shielding of the molten pool. Helium (He) is lighter, possessing high ionization potential and thermal conductivity, hence results in more heat conducted to the weld pool. The reaction between molten aluminium and nascent nitrogen results in formation of AlN phases in N₂ shielding. Argon (Ar) is slightly heavier and possesses low ionization potential and thermal conductivity. The low thermal conductivity of the Ar plasma aids in minimizing the heat transfer to the weld pool therefore minimizes the intermetallic compound growth. Hence Ar shielding is preferable in aluminium-steel dissimilar material joining. The viscosity of the molten aluminium is less and can be easily carried away by the gas. The gas flow rate effects the molten pool flow and direction. High gas flow rates results in non-uniform bead formation due to aggressive pushing of the molten pool. Low flow rates results in insufficient shielding of the molten pool. Hence, the gas flow rate should be optimized for proper shielding with uniform bead [11].

For a lap fillet configuration under tension, shear testing conditions prevail rather than a tensile condition. Therefore, some of the mechanical properties reported in the Table 2.2 shows the joint strength of arc brazed aluminium alloy and steel joints [5, 6, 8, 12-14] in terms of load bearing per unit bead length (N/mm), rather than MPa. Hence, most of the reported strength values of lap-fillet welds of aluminium alloy and steel are in N/mm and for butt joints they are expressed in MPa.

Table 2.2 Joint strengths of arc brazed aluminium alloy and steel

S.No	Base materials (thickness in mm)			Joint strength		Failure location	Ref
	Al alloy	Steel	Filler	N/mm	MPa		
1	6061-T6 (2)	Galvanized low carbon steel (1.2)	Al-5%Si (1.2)	337		weld metal	[12]
2	6061(2)	Low carbon steel (0.7)	Al-5%Si(1.2)	166		interface	[13]
4	5052(1)	Aluminised steel (1.2)	Al-12%Si(1.2)	175		weld metal	[6]
5	5052(1)	Aluminised steel (1.2)	5183 (1.2)	250		HAZ of Al	[6]
6	5052(1)	Galvanized steel (1.2)	Al-12%Si	170		weld metal	[6]
7	6061(1)	Zn coated Q235 steel (1)	Al-12%Si	200		weld metal	15
8	6061 (1)	Zn coated Q235 steel (1)	Al-5%Si (1.2)		96	interface	[5]
9	AW5182-H11 (1.4)	Galvanized DX54D steel (1)	Al99.5		296	interface	[8]
10	AW5182-H11 (1.4)	Galvanized DX54D steel (1)	AlSi ₅		293	weld metal	[8]
11	AW5182-H11 (1.4)	Galvanized DX54D steel (1)	AlSi ₃ Mn ₁		304	HAZ of Al	[8]
12	AW5182-H11 (1.4)	Galvanized DX54D steel (1)	AlMn ₁		291	weld metal & HAZ of Al	[8]

2.5 Laser brazing

Laser brazing is a specialized technique applied for specific applications that demand localized area heating like thin walled critical braze joints, for example, brazing of thin

sections, heat sensitive parts, parts that are sensitive to distortion caused by conventional brazing techniques, joints inside transparent solids such as sealed glasses and quartz tubes. Laser offers the advantage of local and precise heating of base materials enabling minimal distortion, greater accuracy, diminished heat affected areas enhancing joint efficiency, high productivity and simple joint design, good process flexibility and reliability and applicability to a wide range of materials. Laser beams are insensible to magnetic field enabling magnetic material processing. In this process the molten pool generated by melting of the filler wire by laser beam irradiation wets the base material to form leak proof joint. Precise heating of the brazing filler restricts the flow of the molten filler to the area heated by the laser beam. Laser melting occurs in two modes mainly keyhole mode and conduction mode. Power density (power/area of spot, W/cm^2) is critical in laser processing of materials in determining the parametric window for a particular. The melting efficiency of a material depends on its absorptivity to laser wavelengths. Materials like aluminium, copper and their alloys are highly reflective to laser radiation, demanding high energy densities for coupling. Based on absorptivity to various materials and availability in different beam modes, Nd: YAG, diode and fiber lasers have emerged as better options for laser brazing. The controlled heat input into the base materials aids in obtaining a quality joint. High energy input supplied, results in redundant melting of base materials leading to reduced joint efficiency. The processing parameters like laser power, wavelength, spot size, beam mode, position of focal plane, beam modifications, processing speed influences the joint appearance and performance. The effect of these parameters is discussed in detail in the following section.

2.6 Effect of processing parameters of laser brazing

2.6.1 Wavelength (Nd:YAG, diode, fiber, CO₂ lasers)

Laser material interaction results in phenomena such as absorption, heating, melting, evaporation, recoil pressure, piston effect, plasma formation, and laser supported absorption waves, marangoni convection and kelvin-helmholtz instabilities which are the leading aspects in laser material processing. Laser is an electromagnetic radiation operating in a wide wavelength range from far IR to deep UV or soft x-rays depending on the lasing medium. The optical properties of the material determine the absorption capacity of the material to laser. High absorptivity to reflective materials, less power requirement, minimal plasma effects, fibre delivery system qualifies Nd:YAG and diode lasers for brazing operation. The use of Nd:YAG, CO₂, diode and fiber lasers has been reported in the literature [14-16]. Demand for high power densities for coupling and resulting in higher dilution between the base materials restricts the use of CO₂ laser in the field of aluminium-steel brazing. Chen, et al [15] studied the fiber laser welding of Zn coated steel over the aluminium alloy. It is observed that, spatter is the main problem in this type of welding, resulting in unstable melt pool and porosity as shown in Fig 2.6. Kazuyoshi Saida, et al [14] studied the diode laser brazing of A5052/IF Steel and A5052/SUS304 steel using 4047 filler wire. It has been reported that the strength of base A5052 alloy can be attained as shown in Fig 2.7. It is also reported that use of fibre laser enables the stronger joint formation at high processing speeds or low heat input conditions than CO₂ laser [16-18].

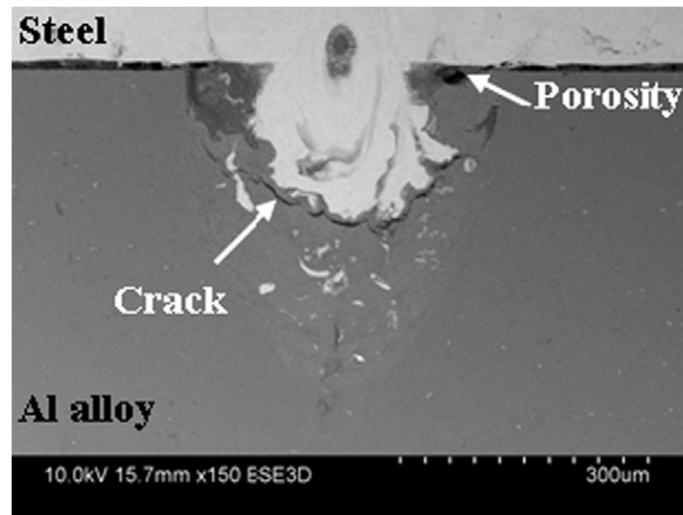


Figure 2.6 Macrostructure of Zn coated Steel over aluminium weld showing porosity [19].

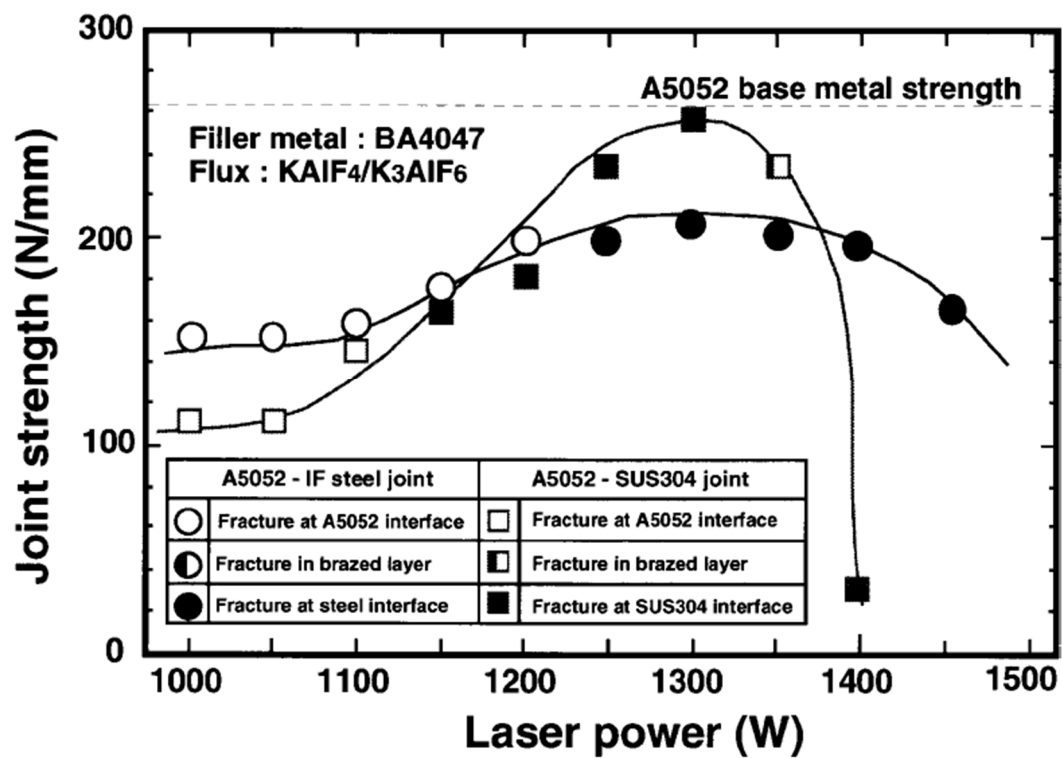


Figure 2.7 Strength of A5052/IF Steel and A5052/SUS304 brazed joints [14].

2.6.2 Laser power

The thermal history underwent by base materials during brazing operation affects the final properties of a braze joint. In laser brazing of aluminium-steel combination both keyhole and

conduction mode of melting are reported. High energy demand for keyhole generation makes conduction mode of melting suitable to aluminium-steel brazing. Two joint assemblies steel on aluminium and aluminium on steel are tried [16-18]. For steel on aluminium assemblies, partial penetration welding in keyhole mode and melting of aluminium edge through conduction from steel by heating it below its melting temperature are tried. In aluminium on steel joining mostly the direct laser irradiation melts the filler material or the edge of base aluminium, the molten pool generated wets the steel surface to form the joint. aluminium possessing high reflectivity and high thermal conductivity conducts away heat resulting in unnecessary heating of high volume of the material, hence, demands high power densities for melting. Higher power densities may sometimes deteriorate the joint efficiency due to more dilution and elevated growth of IMC layer. Melting the filler wire is less energy intense than base materials. Hence, using a filler based joining is advisable in this context. The penetration depth should be restricted to less than 200 μm for obtaining a sound joint with minimal IMC layer [17, 18]. Laser power in the range of 1100-1300W was reported to yield the best joint properties [20].

2.6.3 Spot size

The spot size is crucial in a laser based process. The ratio of laser power to area of spot is power density which determines the mode of laser processing. For a given power, as the spot size decreases, the physical phenomenon changes from heating to melting to vaporization. In aluminium-steel dissimilar joining the laser source should melt the aluminium base material along with filler and should heat the steel surface prior to wetting. Too small spot sizes may probably result in unnecessary melting of the steel. Too big spots may result in just heating of the aluminium base material. Hence, the spot size should be appropriately chosen for melting the aluminium and heating the steel simultaneously.

2.6.4 Laser beam tailoring

In any brazing operation wetting and spreading of the molten pool on the base materials determines the mechanical strength of the joint. The wetting and spreading phenomenon can be improved by altering the thermal profile experienced by the base materials by beam defocusing, beam tilting, twin beam spots, and beam splitting which are discussed in detail in the following section.

2.6.4.1 Defocusing

Laser beam defocusing alters the spot size and in turn power density. Defocusing increases the area under the laser beam, reducing the power density. Increase in spot size and reduction in power density helps in heating of the steel surface hence improving wetting ability. In some cases defocusing may probably result in no melting of aluminium base material as well. Hence, defocusing limit should be appropriately chosen. In general defocused beam is usually used as a pre-heating beam to heat the steel side enabling better wetting.

2.6.4.2 Laser beam tilting

Laser beam tilting also alters the spot size and shape and hence power density. The elliptical shape of the spot obtained by tilting helps in heating the steel surface and melting of the aluminium simultaneously.

2.6.4.3 Twin laser beam spots

Temperature differential between the base material and the molten metal is crucial aspect in wetting phenomenon. Pre-heating of Steel is likely to reduce the temperature differential between the solid steel surface and the aluminium melt, aiding in better wetting. Pre-heating can be done using various techniques like infrared heating, induction heating, and resistance heating. In the present context a laser beam is used for pre-heating. In this, two laser beam spots from two laser sources are used, spot with lower energy preheats the steel surface and

spot with high energy melts the aluminium edge to form the joint. Saida, et al.[21, 22] explained the effect of pre-heating on the wetting behaviour. The effect of variation in pre-heating location and power on wetting behaviour is also reported. It is observed that with increase in pre-heating beam power shows negligible effect on wetting behaviour of “galvanized” steel, because the driving force for wetting is the formation of Al-Zn alloy at the triple point which exerts pulling action on the molten pool. The effect of pre-heating the steel side on wetting is negligible for Zn coated steel. Increase in pre-heating power up to 150 W showed positive effect on wetting behaviour and further increase resulted in deterioration of wetting behaviour. More dilution coming from the steel side getting alloyed with molten zinc due to excessive pre-heating may be the probable reason for poor wetting properties.

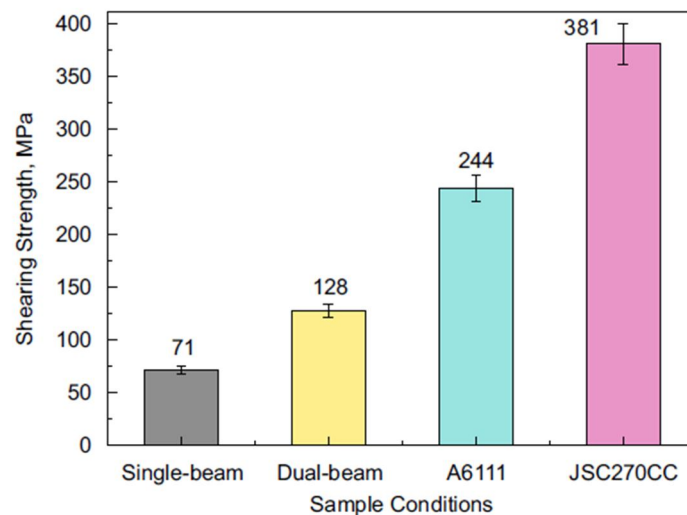


Figure 2.8 Effect of twin laser spot on joint strength[22].

Hence, pre-heating the steel is efficient in improving the joint properties for non-wettable steels [23]. A combination of continuous and pulsed laser can also be used for improving wetting phenomenon, accordingly enhancing joint efficiency as shown in Fig 2.8. The continuous wave laser spot serves the purpose of melting and the pulsed laser as stirring and penetration source. The continuous wave heats the base material and generates the weld pool whereas pulsed wave creates a root shape at the weld interface through penetration and stirs

the molten pool and levitates the gas bubbles generated in the molten pool. The thickness of the IMC layer can be restricted to less than 10 μm through this process [22].

2.6.4.4 Laser beam splitting

More dilution due to high energy intense laser beam spots is detrimental to aluminium-steel brazing. Two spots of less energy yields superior properties than a single high energy intense spot. A. Matheu, et al.[24] studied the effect of beam splitting on the joint formation and its mechanical performance using an aluminium-zinc based filler wire [25]. In laser beam splitting the energy of the single laser spot is distributed to two spots. For this, laser beam shaping prism is inserted between the collimating and focusing lenses. The resulting beam consists of two half spots separated from each other. Fig 2.9 illustrates the energy distribution of the laser spots. Among the two spots the spot with lower energy acts as a pre-heating spot and the high energy spot is utilized for melting of the filler material. In this the maximum energy density is less and the total surface irradiation is bigger, hence leading to softer and longer heating of the weld zone. The volume of base material getting melted is less and therefore the intermetallic compound formation is also minimized aiding in improved mechanical strength of the joint. The beam splitting made the weld bead stronger and weaker HAZ of aluminium failed during tensile test. Restricting the IMC layer thickness to less than 5 μm , fracture load of 230 N/mm and failure in the steel base material are attained by optimizing the processing parameters. Hence, by beam splitting the wetting behaviour and mechanical behaviour of aluminium-steel braze joints can be altered [24].

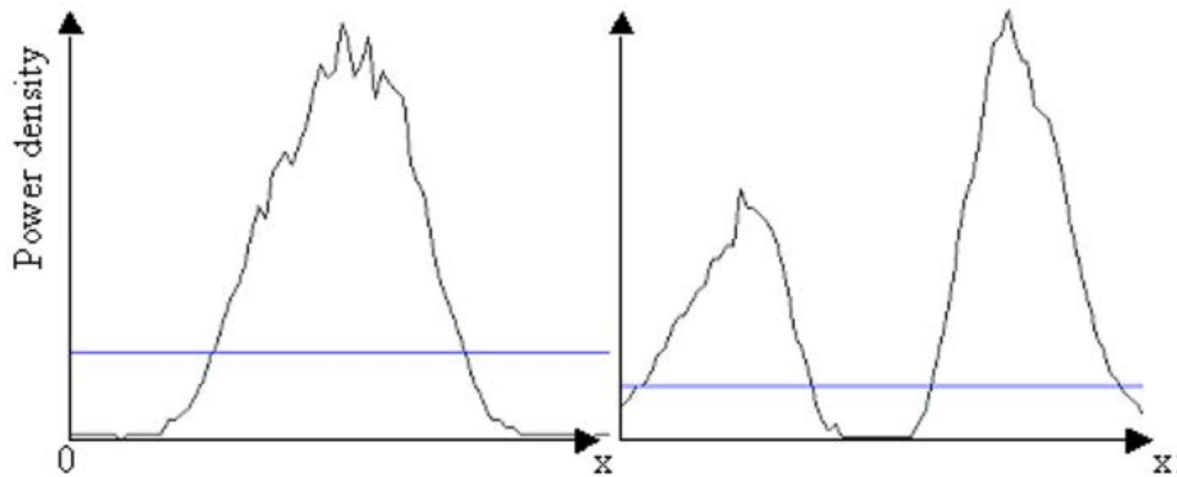


Figure 2.9: Energy distribution in single and twin spot system [25].

2.6.5 Effect of roll pressure

Ozaki, et al.[19] carried the laser roll welding of low carbon steel (SPCC steel) and 5052 aluminium alloy in overlap joint configuration. The combined effect of fibre laser heating followed by pressing using a roller on the tendency of intermetallic compound formation and mechanical performance of the joint has been reported. The laser as a heat source heats the steel side and the roller presses the steel at high temperature against the base aluminium, aluminium melts by conduction and wets the steel to form a joint under the action of roll pressure. The application of roll pressure enables better adherence of aluminium to steel. The high temperature plastic deformation caused due to laser heating and application of roll pressure resulted in slightly curved weld surface. The joints suitable for tensile specimen cutting are obtained in the heat input range of 375-800 J/cm. Exceeding this heat input melts the steel sheet leading to failure due to intermetallic compound formation. Joints with failure on steel side could be made using laser roll welding.

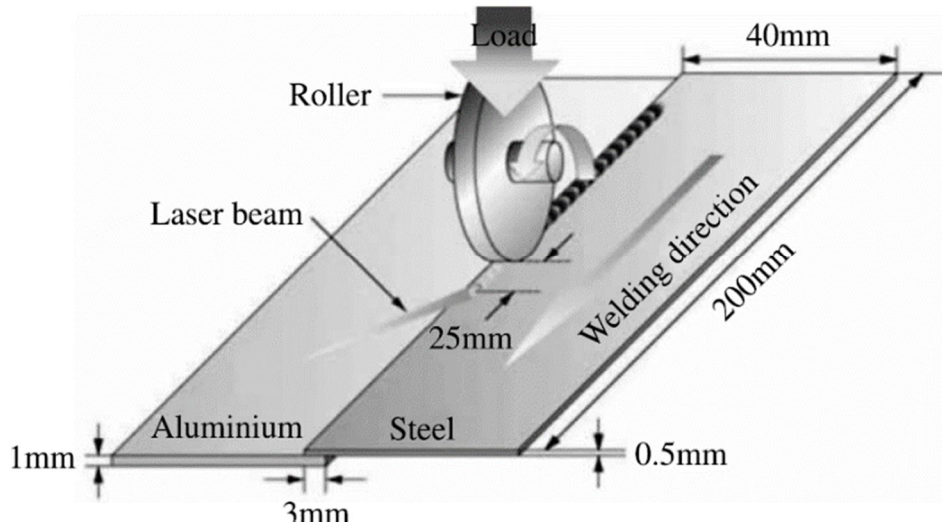


Figure 2.10 Schematic of laser roll welding of aluminium alloy and steel [19].

2.6.6 Effect of processing speed

Processing speed combined with power is termed as heat input, one of the influencing parameter in any brazing process. Formation of a uniform bead without undulations is the basic requirement for a successful braze joint. The undulated bead results in a weak braze joint. Uniformity of the bead is dependent on the processing speed. Increase in processing speed results in humps and valleys in the bead due to uneven deposition resulting from fast travel speed. Decrease in processing speed leads to lumps of molten metal getting deposited at a single point. Hence, the processing speed should be optimized for obtaining a uniform bead. Especially, laser brazing process facilitates high processing speeds. In aluminium-steel brazing by varying the processing speed and laser power, the overall heat input into the materials should be kept as minimum as possible to avoid the formation of brittle intermetallic phases. The effect of processing speed on interfacial IMC layer thickness is shown in Fig 2.11. It is observed that for a given brazing condition the increase in processing speed results in decrease in heat input and decrease in heat input aids in minimizing the dilution between aluminium and steel thus improving the joint strength.

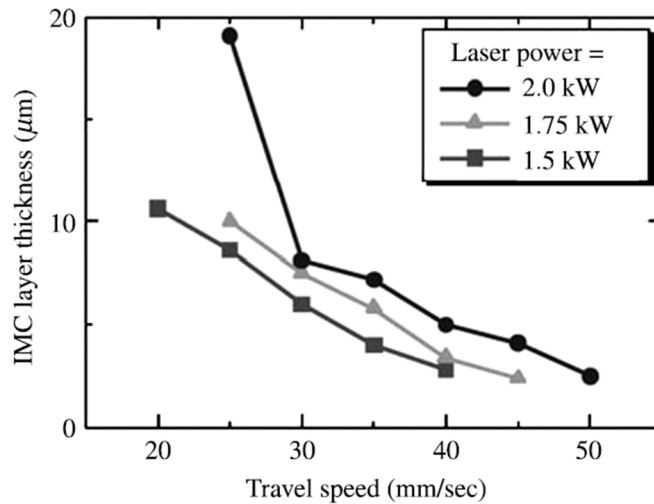


Figure 2.11: Effect of processing speed on joint thickness of IMC layer [19].

2.6.7 Effect of filler wire composition

Filler material is one of the major variants in any brazing operation that ultimately affects the phase formation at the interface and joint efficiency. In any brazing operation filler wire should possess low melting temperature, high fluidity. Additionally, in this particular context the filler material should minimize or restrict the formation and growth of brittle intermetallic compounds. In the present application the materials to be joined are aluminium and steel, based on the low melting base material, aluminium based fillers are preferable especially of eutectic composition. In aluminium-steel brazing operation pure Al, aluminium-silicon based filler materials (Al-12%Si, Al-5%Si) and aluminium-zinc based filler wires like Zn-15%Al, Zn-2%Al are used. The addition of Si in filler material have beneficial effects such as enhanced fluidity, forms an impermeable Al-Fe-Si based complex intermetallic compound that hinders further diffusion and restricts the IMC layer growth. Using increased Si content filler wire that is filler wire, with 12%Si content which is a eutectic composition possessing low melting point and low viscosity than Al-5%Si alloy allows more spreading of the molten filler on the steel surface leading to increase in bead width, consequently improves the joint efficiency. The molten state time of Al-12%Si is high compared to Al-5%Si resulting in high

diffusion rates, slightly high intermetallic compound thickness. But this increased intermetallic thickness is compensated by improved braze bead width. With Al-Si based filler wire, the intermetallic compound layer thickness can be restricted to less than 5 μm based on the optimized processing parameters. A mixture of intermetallic compounds like FeAl_3 , Fe_2Al_5 , FeAl , Fe_3Al , $\text{Fe}_3\text{Al}_3\text{Si}_2$, $\text{Fe}_2\text{Al}_{7.4}\text{Si}$, $\text{Fe}_2\text{Al}_8\text{Si}_2$ and $\text{FeAl}_{4.5}\text{Si}$ are reported in the literature when Al-Si based filler wires are used [16-18, 20, 22]. Zinc aluminium based filler wires having low melting temperature and high fluidity are also suitable for aluminium-steel brazing. The presence of zinc in the filler wire compensates for the loss of zinc through vaporization and aids in minimizing the vaporization porosity. The presence of zinc in filler wire also aids in improving corrosion resistance of the braze joint. The joints with IMC layer thickness less than 8 μm can be formed. The variation in joint strength with filler wire composition is listed in Table 2.3.

2.6.8 Effect of pre-heating the filler wire

High molten metal fluidity and temperature aids in better wetting of steel by aluminium melt. The fluidity can be enhanced by pre-heating the filler material. Matheu et al.[26] explained the effect of pre-heating of the filler wire on wetting behaviour and interfacial characteristics in laser brazing of aluminium to steel using Al-12%Si filler wire [25]. The filler wire is heated by Joule effect. Pre-heating the filler wire enhances the melting efficiency which results in better wetting of the steel surface than cold wire. This also helps in reducing the laser power needed for melting the filler wire. Pre-heating of the filler wire augments the temperature of the droplet formed, hence diminishes the viscosity of the molten pool aiding in enhanced wetting properties which can be observed from the macrostructures. Pre-heating helps in better adhesion and the filling of the braze bead is better than cold wire. The increased bead width due to pre-heating effect enhances the joint strength.

2.6.9 Effect of surface chemistry of Steel

In aluminium-steel brazing the molten aluminium should wet the steel surface to form the joint. The nature of the surface of steel in terms of roughness and chemistry effects the wetting behaviour. Increase in roughness enhances the wettability of wettable fluids and makes non-wettable fluids much more non-wettable. Hence, the surface roughness should be kept minimum. Aluminium-steel dissimilar joints are mostly used in automotive industry. Galvanized and galvannealed low carbon steel sheets are well known automotive steels in which the steel surfaces are coated with Zn and annealed, resulting in elemental Zn and iron zinc alloy on the surface, respectively. These days' aluminized steels that are steels coated with aluminium are developed. This changed surface chemistry of the steel alters the wetting behaviour to a large extent. Among the three different coated steels, galvanized steel showed better wetting than aluminized and galvanealed steels. In case of aluminized steel the joining is between aluminium to aluminium. In galvanized steel it is between zinc and aluminium and in galvannealed steel it is between aluminium and iron zinc alloy. Aluminium possessing high cohesive energy hinders the spreading of molten aluminium on aluminium. The wettability of iron zinc alloy by molten aluminium is also poor. The molten aluminium-zinc alloy formed at triple line (solid/liquid/vapour interface) due to reaction between aluminium filler or base material and zinc coating in case of galvanized steel, exerts pulling action on the molten pool leading to more spreading of the molten aluminium on the steel surface. Hence, zinc coating on steel showed improvement in wetting behaviour than aluminized or galvannealed steel [23]. Nearly 20-25% improvement in wetting is observed in case of galvanized steel than galvannealed and aluminized steel. This improved wetting enhances the load bearing capacity of the braze joint.

2.6.10 Effect of flux

Aluminium is always adhered with tenacious oxide layer that poses problem during brazing operation. Therefore, use of flux dissolves the oxide layer through chemical reaction, exposing fresh aluminium for brazing action. In laser brazing the nocolock brazing flux ($\text{KAlF}_4 + \text{K}_3\text{AlF}_6$) is used. The powdered flux is mixed with ethanol to make it into paste and is applied on the aluminium side of the joint interface. In any joining operation the thermal cycles undergone by the base materials determines the macrostructure and microstructure of the joints. Presence of flux alters the thermal history experienced by the base materials and in turn alters the wetting behaviour. Use of flux results in less wetting and spreading of the aluminium melt on the steel surface. It acts as a thermal barrier minimizing the temperature of the melt pool and steel surface, generating higher wetting angles than without flux. The wetting angle increased to 31° from 21° when flux is used. Acting as thermal barrier and diffusion barrier it restricts the growth of brittle intermetallic compounds that deteriorates the joint performance. Under similar processing conditions the use of flux reduced the IMC layer thickness by nearly 50-60%, highlighting the role of flux. In spite of less wetting, use of flux has improved the mechanical performance of the braze joint due to minimum intermetallic compound formation [26, 27].

2.7 Mechanical properties of laser brazed aluminium-steel joints

Table 2.3 lists the mechanical properties of Al-steel joints obtained by laser brazing as reported in the above sections. A load bearing capacity of 260 N/mm of bead length can be achieved using this laser brazing process. As described above various factors contribute to the strength of the joints

Table 2.3 Joint strengths of various aluminium-steel dissimilar combination

S.No	Base Materials (thickness in mm)			Joint strength		Failure Location	Ref
	Al alloy	Steel	Filler	N/mm	MPa		
1	6016 T4 (1)	Galvanized GXES low carbon (0.77)	Zn-15%Al (1.2)	220		HAZ of Al	[24]
2	6016 T6 (1.1)	DC04 GI : (0.9)	Zn-2%Al (1.2)		220	HAZ of Al	[21]
3	5052 (1.2)	IF (1.2)	Al-12%Si (1.2)	260		HAZ of Al	[14]
4	5052 (1.2)	304SS (1.2)	Al-12%Si (1.2)	200		HAZ of Al	[14]
5	6016 T4 (1)	DC04 (1.2)	No filler	230		HAZ of Al	[28]
6	6016 T4 (1)	GXES (0.77)	Zn-15%Al (1.2)	225		Steel	[24]
7	6016-T4 (1)	DC04 (1)	No filler	250		HAZ of Al	[27]
8	5052 (0.5)	SPCC (0.5)	No filler	168.4		Steel	[19]
9	1050 (1)	GASPPC (1)	No filler	180		Fusion zone	
10	6061-T6 (1)	Galvanized IF (1)	Zn-5%Al in foil form (0.2)	120		Fusion zone	[25]
11	5754 (2)	Low carbon st15 Steel (0.8)	No filler		300	Al base material	[18]
12	6016-T4 (1.2)	DP600 (0.7)	Zn-15%Al (1.2)	250		Al base material	[29]
12	5754 (1)	Galvanized DX54 (1)		230		HAZ of Al	

2.8 Summary of literature review

Joining of aluminium to steel by fusion joining is possible by both arc brazing and laser brazing techniques. The strength of the joints is largely dependent on the wetting behaviour, interface characteristics and bead formation which are dependent on the base metal surface characteristics, filler wire, heat input and the profile of the bead. Precise control of the heat input is possible using lasers. But lasers are very expensive and the industry being familiar with arc brazing processes, it is expedient to consider these for detailed investigation in order to understand in-depth the process behaviour vis-à-vis resulting properties. Especially, the wetting behaviour and interface morphology which effect the joint formation and strength are the key phenomena to be investigated and optimised for. In this context both Pulsed-GMAW and CMT processes are good candidates.

Following are the major gaps of the already reported work in these directions:

2.8.1 Pulsed-GMAW

- Limited work on brazing aluminium alloy and steel. The effect of only few parameters has been reported
- No reports on IMC phase determination of joint interface made by P-GMAW process.

2.8.2 Cold metal transfer (CMT) brazing process

- Limited work on aluminium-steel joining in terms of effect of processing parameters
- Only one report is available on interfacial IMC phase determination.
- In almost all the cases the interfacial IMC phases are confirmed only through EDS analysis which is not the best option.
- Limited work reported on corrosion studies of arc brazed aluminium/steel joints

2.8.3 Laser brazing

- The applicability of laser brazing to aluminium and steel is explored in different ways that is a variety of laser sources are used, the effect of laser related parameters on joint properties is studied.
- Limited literature is available on effect of laser related parameters on joint properties. Especially, the possibility of beam scanning to tailor the thermal gradients in the brazing zone is not reported.
- The interfacial IMC phase determination is not complete and only a very few papers are available.
- Corrosion studies on laser brazed aluminium/steel joints are just initiated.

2.9 Problem identification and approach

Therefore, in view of the above mentioned literature and background the objectives of the present work (as already mentioned in chapter 1) are:

- Understanding of P-GMAW and CMT brazing of aluminium and steel, study of effect of various process related parameters, and material related parameters on joint formation and its mechanical performance.
 - Interfacial IMC layer determination using micro diffraction techniques like EBSD, TEM, micro area x-ray diffraction techniques of both P-GMAW and CMT brazed specimens.
 - Effect of filler wire composition on interfacial characteristics and joint strength
 - Correlating the interfacial characteristics to joint strength.
- Laser brazing, effect of beam scanning, flux and heat input on interface and joint strength.

References

- [1] AWS committee of brazing and soldering, Brazing Handbook, 5 ed., AMERICAN WELDING SOCIETY (AWS), UNITED STATES OF AMERICA, 2007.
- [2] M.M. Schwartz, Brazing, Brazing, ASM International, Ohio, 2003, pp. 52-54.
- [3] A.C. Davies, The Practice of Welding, 10 ed., Cambridge University Press, New York, 1993.
- [4] H.T. Zhang, J.C. Feng, P. He, B.B. Zhang, J.M. Chen, L. Wang, Materials Science and Engineering a-Structural Materials Properties Microstructure and Processing, 499 (2009) 111-113.
- [5] H.T. Zhang, J.C. Feng, P. He, Materials Science and Technology, 24 (2008) 1346-1349.
- [6] M. Kang, C. Kim, Materials & Design, 81 (2015) 95-103.
- [7] H. Zhang, J. Liu, Materials Science and Engineering a-Structural Materials Properties Microstructure and Processing, 528 (2011) 6179-6185.
- [8] L. Agudo, N. Jank, J. Wagner, S. Weber, C. Schmaranzer, E. Arenholz, J. Bruckner, H. Hackl, A. Pyzalla, Steel Research International, 79 (2008) 530-535.
- [9] T. Murakami, K. Nakata, H.J. Tong, M. Ushio, Isij International, 43 (2003) 1596-1602.
- [10] G. Qin, Z. Lei, Y. Su, B. Fu, X. Meng, S. Lin, Journal of Materials Processing Technology, 214 (2014) 2684-2692.
- [11] S. Kou, Welding Metallurgy, 2 ed., Wiley-Blackwell, Canada, 2002.
- [12] Y. Liu, Q. Sun, J. Liu, S. Wang, J. Feng, Materials Letters, 152 (2015) 29-31.
- [13] S. Yang, J. Zhang, J. Lian, Y. Lei, Materials & Design, 49 (2013) 602-612.
- [14] K. Saida, W. Song, K. Nishimoto, Science and Technology of Welding and Joining, 10 (2005) 227-235.
- [15] H. Ozaki, M. Kutsuna, Welding International, 23 (2009) 345-352.
- [16] G. Sierra, P. Peyre, F. Deschaux-Beaume, D. Stuart, G. Fras, Materials Science and Engineering a-Structural Materials Properties Microstructure and Processing, 447 (2007) 197-208.
- [17] M.J. Zhang, G.Y. Chen, Y. Zhang, K.R. Wu, Materials & Design, 45 (2013) 24-30.
- [18] M.J. Torkamany, S. Tahamtan, J. Sabbaghzadeh, Materials & Design, 31 (2010) 458-465.
- [19] H. Ozaki, M. Kutsuna, S. Nakagawa, K. Miyamoto, Journal of Laser Applications, 22 (2010) 1-6.

- [20] J. Ma, M. Harooni, B. Carlson, R. Kovacevic, *Materials & Design*, 58 (2014) 390-401.
- [21] H. Laukant, C. Wallmann, M. Muller, M. Korte, B. Stirn, H.G. Haldenwanger, U. Glatzel, *Science and Technology of Welding and Joining*, 10 (2005) 219-226.
- [22] S. Yan, Z. Hong, T. Watanabe, J. Tang, *Optics and Lasers in Engineering*, 48 (2010) 732-736.
- [23] K. Saida, H. Ohnishi, K. Nishimoto, *Welding International*, 24 (2010) 161-168.
- [24] A. Mathieu, R. Shabadi, A. Deschamps, M. Suery, S. Mattei, D. Grevey, E. Cicala, *Optics and Laser Technology*, 39 (2007) 652-661.
- [25] T. Takemoto, S. Kimura, Y. Kawahito, H. Nishikawa, S. Katayama, *Welding International*, 23 (2009) 316-322.
- [26] A. Mathieu, S. Pontevicci, J.-c. Viala, E. Cicala, S. Mattei, D. Grevey, *Materials Science and Engineering a-Structural Materials Properties Microstructure and Processing*, 435 (2006) 19-28.
- [27] G. Sierra, P. Peyre, F.D. Beaume, D. Stuart, G. Fras, *Materials Characterization*, 59 (2008) 1705-1715.
- [28] P. Peyre, G. Sierra, F. Deschaux-Beaume, D. Stuart, G. Fras, *Materials Science and Engineering a-Structural Materials Properties Microstructure and Processing*, 444 (2007) 327-338.
- [29] C. Dharmendra, K.P. Rao, J. Wilden, S. Reich, *Materials Science and Engineering a-Structural Materials Properties Microstructure and Processing*, 528 (2011) 1497-1503.

CHAPTER 3 EXPERIMENTAL WORK

3.1 Materials used

The aluminium-steel dissimilar material joints have good potential for light weighting applications in automotive industry. Keeping in view the above requirements the following materials have been chosen for experimental investigations.

- Aluminium alloy: 6061 (Al-Mg-Si)-T6 condition alloy (2 mm thick sheet)
- Steel: Galvanized, galvanealed and uncoated interstitial free (IF) steel (1.2 mm thick sheet)
- Filler: 4043 (Al-5%Si) and 4047 (Al-12%Si) alloy (1.2 mm diameter wire)

The sheets of both 6061-T6 aluminium alloy and IF steel were sheared to a size of 150 mm X 100 mm and the edges of aluminium are ground prior to brazing operation. The adherent oxide layer on the surface of the aluminium sheet is removed using a steel wire brush and both steel and aluminium sheets are thoroughly cleaned using ethanol.

3.2 Joint configuration

Fig 3.1 shows the selected joint configuration. It is a lap fillet configuration wherein aluminium sheet is placed over the steel sheet and an arc or laser beam is run along the aluminium edge to form a braze-like joint. The methodology adopted in aluminium-steel joining and subsequent characterisation is shown in Fig 3.2. The methodology followed was common for all the three selected fusion joining processes presented in this thesis.

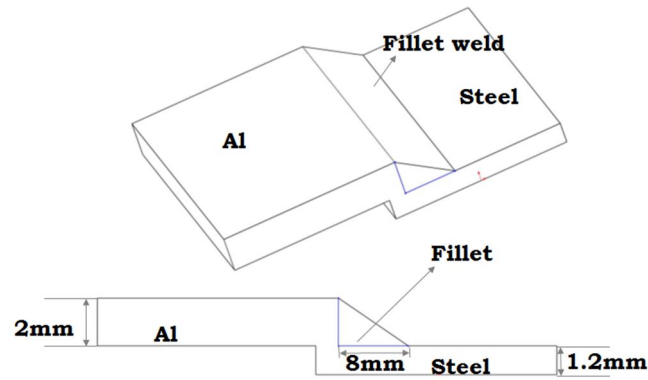


Figure 3.1: Schematic of lap fillet joint configuration.

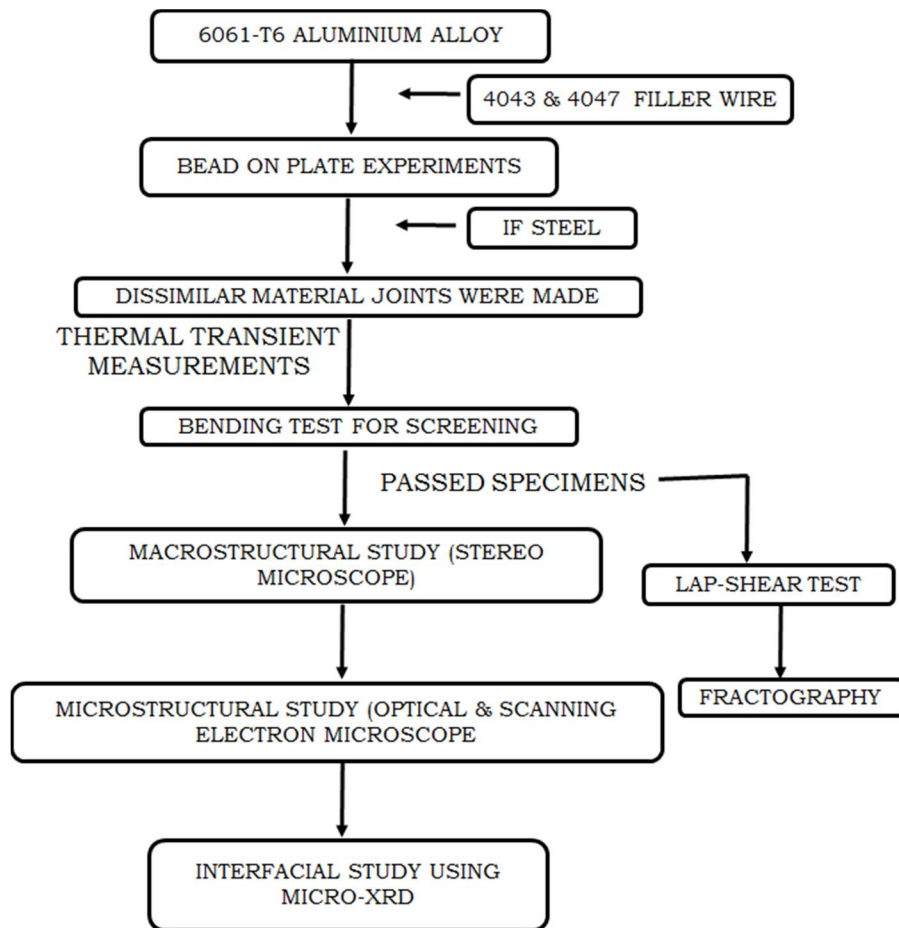


Figure 3.2: Experimental methodology adapted for brazing process and subsequent characterization.

3.3 Processes chosen

Based on the detailed literature survey the following processes have been chosen for the present work.

- Pulsed-gas metal arc welding (P-GMAW)
- Cold metal transfer welding (CMT)
- Laser brazing

3.4 Pulsed-gas metal arc welding (P-GMAW)

It is an arc welding process with modified form of spray transfer that allows control over the melting of the droplet. In this the welding current/voltage is periodically switched between higher and low limit thus facilitating low heat output than pure spray transfer and higher than dip transfer. The metal transfer is independent of gravity as a strong electromagnetic force acts on droplet aiding in droplet detachment. Therefore welding in all positions is feasible at low average currents. This process is mainly applicable in cases where high heat input (DC mode) leads to weak joining. In this process there are two currents i) background current that maintains the arc and ii) pulse current for melting the wire and droplet detachment. Initially, a P-GMAW unit used to generate a half or full wave rectified sine waveform with a fixed pulse frequency similar to supply frequency as shown in Fig 3.3a. Hence, four variables namely peak current or voltage, wire feed rate, pulse frequency and background current has to be set. The high skill required for getting correct welding conditions, variation in transfer mode with stick out and narrow operating range limits its use in the field of welding. However, with the rectangular waveforms (Fig 3.3b) instead of sinusoidal waveforms can be generated with the advent of transistorised and electronically controlled power sources and the process could be

used with a wide operating range. This process has now developed to a stage that if one parameter is changed then the other parameters will set to their respective values automatically and hence is easy to operate. This is called synergic mode. The details of the KEMPPI power source used in the present work are shown in Table 3.1.

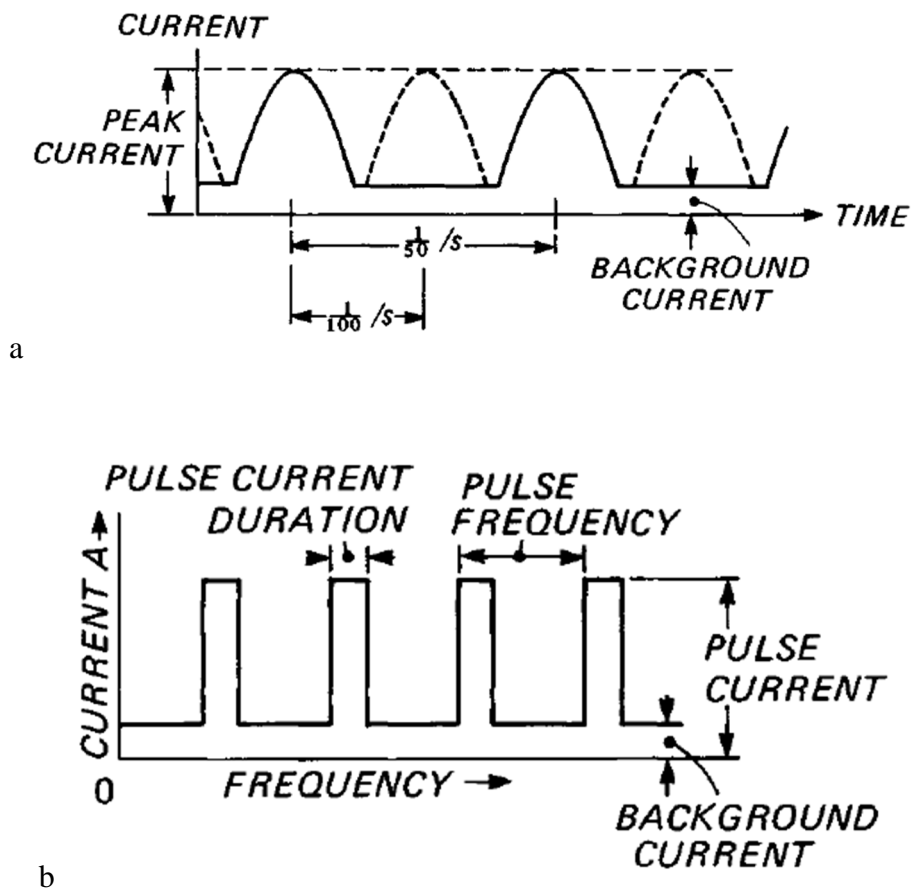


Figure 3.3 Pulsed-GMAW wave forms a) sinusoidal and b) rectangular [1].


The following are the advantages relevant to Al-steel joining process

- it is a low heat input process as it enables spray transfer at low average currents.
- it enables spatter free, good weld bead formation.
- it can be applied to a wide range of materials.
- suitable to thin sheet welding and possesses good gap bridging ability;

- popular, cost effective and easy for automation.
- all-position welding.

Hence, it is one of the low heat input processes suitable for joining aluminium and steel.

Table 3.1 Power source characteristics of KEMPPI ProMig 4500R

Characteristics	Model image
<p>Open circuit voltage: 75 V</p> <p>Open circuit power: < 55 W</p> <p>Maximum welding voltage: 40 V/400 A</p> <p>Efficiency: 0.85 (400 A/36 V)</p> <p>Power factor: 0.95 (400 A/36 V)</p>	

3.4.1 Bead on plate (BOP) experiments for identification of usable parametric window

Aluminium-steel dissimilar material joining is a braze-like joint wherein the molten pool generated by melting of filler wire and melting of aluminium base material should wet the steel surface to form a joint. Sufficient volume of molten pool should be present to ensure wetting. Initial bead-on-plate screening experiments on aluminium sheet have been carried out to understand the bead formation. Following conditions were set to identify the right parameters:

- visually smooth, uniform and defect free bead
- full penetration bead;
- minimal heat affected zone width
- no undercut

Various parameters tried and optimized based on the above BOP experiments are given in Table 3.2.

Table 3.2 P-GMAW parameters for bead-on-plate experiments (BOP experiments)

Processing parameter	Experimental range	Working range
Operation mode	Synergic	Synergic
Nozzle to plate distance from Al edge (mm)	4-14	6-10
Wire feed rate (WFR, m min ⁻¹)	2-6	3-5.5
Welding speed (S, m min ⁻¹)	0.5-1.8	0.8-1.4
Shielding gas flow rate, Argon (nozzle diameter: 12 mm) (l.min ⁻¹)	16-22	20
Current (A)	64-140	64-77
Voltage (V)	12-19.8	16.1-16.3

3.4.2 Dissimilar material Al-steel joint experiments

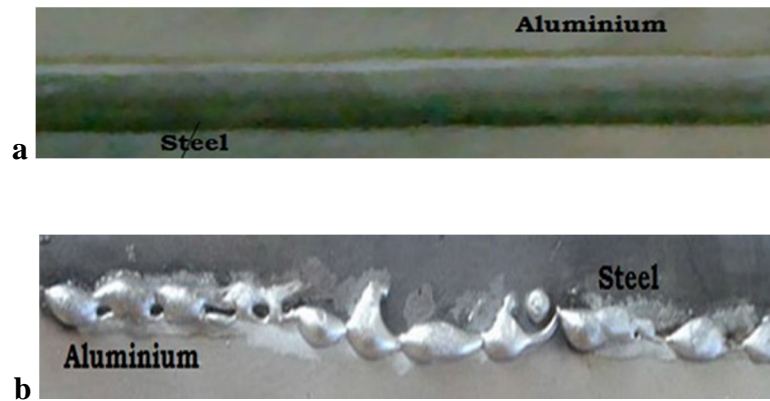


Figure 3.4 Bead appearance of dissimilar Al/steel joints a) uniform bead b) non-uniform bead.

Fig 3.5 shows the P-GMAW brazing assembly. In this the Al sheet is placed over the steel sheet with 8 mm overlap and an arc is run along the edge of the ground Al sheet, Fig 3.4 shows the bead appearance. Fig 3.4a shows the acceptable bead appearance and fig 3.4b shows the non-uniform bead. The screening conditions applied for dissimilar aluminium-steel braze are as follows:

- visually smooth, uniform, shiny and defect free bead formation
- a convex bead with wetting angle less than 90°
- no melting of the steel
- joint with acceptable strength

The parametric working range of bead on plate experiments were further fine-tuned based on these preliminary experiments and tabulated in Table 3.3.

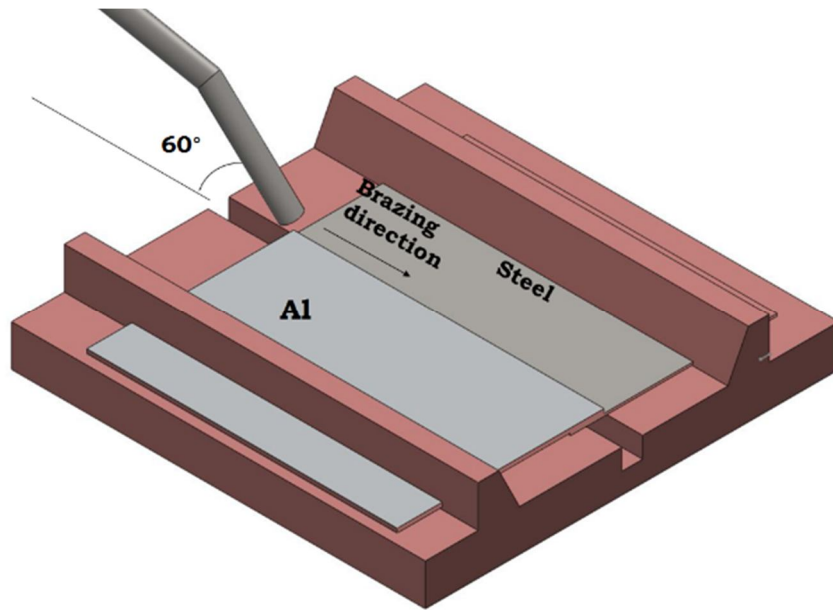


Figure 3.4 Schematic of P-GMAW brazing assembly.

Table 3.3 P-GMAW parameters for dissimilar material combination (Dissimilar material joining experiments)

Processing parameter	Experimental range	Optimized range
Nozzle to plate distance from Al edge (mm)	4-10	6
Wire feed rate (WFR, m min^{-1})	3-5.2	3.5 – 4
Welding speed (S, m min^{-1})	0.9-1.4	1.2
Shielding gas flow rate, Argon (nozzle diameter: 12 mm) (l.min^{-1})	16-22	20
Arc position	-2 to +2 (-ve side towards Al & +ve side towards steel)	Edge of aluminium sheet
Current (A)	64-108	64-77
Voltage (V)	16.1-19.8	16.1-16.3

During the process of optimization the following parameters are found influencing the joint formation ability and efficiency and has been given attention during all further studies

Process related parameters

- a. angle of tilt of the joint interface
- b. torch orientation
- c. wire feed rate
- d. processing speed

Material related parameters

- a. surface chemistry of steel
- b. filler wire composition

Therefore based on the above mentioned criteria the material combinations used in P-GMAW process investigations are given in Table 3.4.

Table 3.4 Material combinations tried in P-GMAW process

S.No	Material combination		
	Aluminium alloy	Steel	Filler
1	6061-T6	Galvanized IF	4043
2	6061-T6	Galvannealed IF	4043
3	6061-T6	Uncoated IF	4043
4	6061-T6	Galvanized IF	4047

3.5 Cold metal transfer welding

It is a reduced energy modified arc welding process in which the wire movement is directly integrated into process control. The wire is moved forward and when short circuit occurs the wire is retracted, facilitating droplet detachment as shown in Fig 3.6. This way it is different from conventional dip transfer processes. The back and forth movement of the wire provides nearly “zero” current metal transfer which makes it different from conventional processes. The “zero” current metal transfer enables spatter free welding. Application of this process lies in areas which require low heat input such as thin sheets and dissimilar metal joining. The Fronius CMT welding system used in the present study is shown in Table 3.5

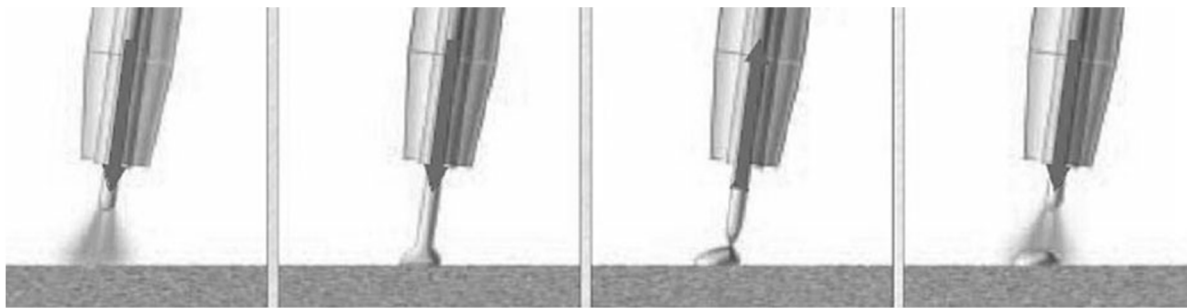


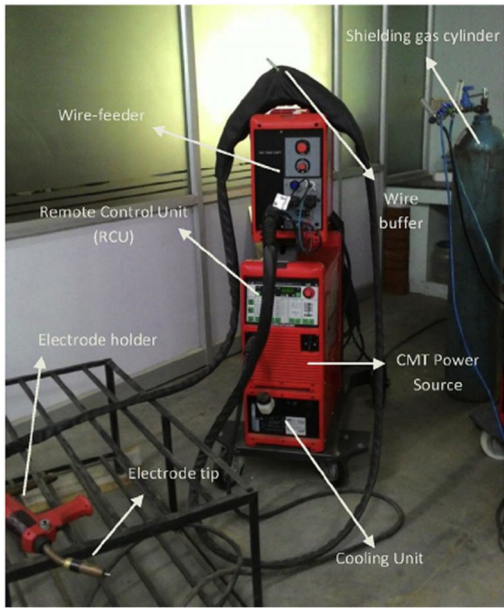
Figure 3.6 Schematic of metal transfer in CMT process [2].

Advantages

- a low heat input process compared to other arc welding processes
- enables very low penetration/dilution welding
- suitable for ultra-high thin sheet brazing in the thickness as low as 0.3 mm
- applicable to wide range of materials
- forms a spatter free, uniform bead with good appearance;
- easy to operate
- cost effective and easy for automation

In this process also the Al sheet is placed over the steel sheet and an arc is run along the edge of the aluminium sheet to form a leak proof joint and the schematic of brazing assembly is shown in Fig 3.7. In this process the torch is placed in almost perpendicular to the plane of base materials at around 80-85° angle. This enables spatter free smooth metal transfer.

Table 3.5 Power source characteristics of Fronius Trans Pulse Synergic 3200/5000 CMT machine

Characteristics	Model image
<p>Open Circuit Voltage: 65 V</p> <p>Maximum welding current: 320 A</p> <p>Welding current minimum: 3 A</p> <p>Operating voltage: 14, 2-30 V</p> <p>Mains fuse: 35 A</p> <p>Mains frequency: 50-60 Hz</p> <p>Mains voltage (+/- 10%): 3 x 400 V</p>	

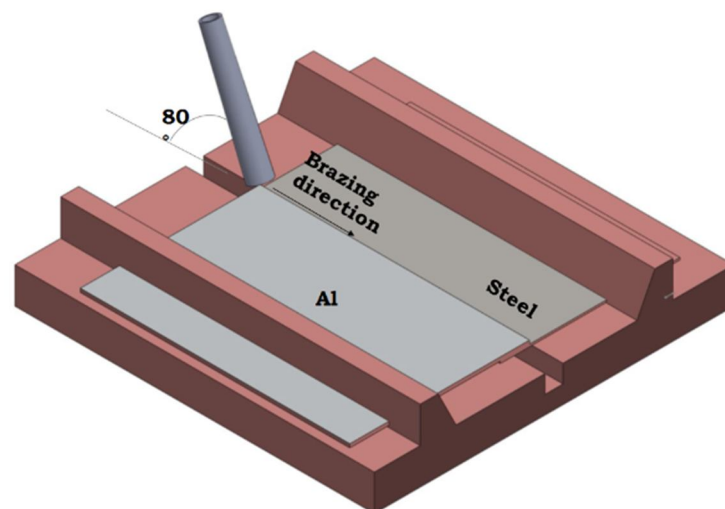


Figure 3.7 Schematic of CMT brazing assembly.

Based on the knowledge obtained from P-GMAW process, the effect of the following parameters is only studied in the CMT process and the list of processing parameters are given in Table 3.6. They are as follows:

Process related parameters

- a. wire feed rate
- b. processing speed
- c. pulsing

Material related parameters

- d. filler wire composition

The material combinations used in the present CMT work is given in Table 3.7.

Table 3.6 Parametric window for aluminium-steel joining for CMT process

Parameter	Experimental range	Optimized range
Standoff distance (mm)	4-10	6
Torch angle (°)	60-90	80-85
Gas flow rate (nozzle diameter: 16mm) (GFR, l/min)	15-20	18-20
Wire position	40-70% on Al side	60% on Al side
Wire feed rate (WFR, m/min)	3.5, 5	3.5, 4
Processing speed (S, m/min)	1, 1.2	1, 1.2
Current (A)	55-102	69-75
Voltage (V)	9-13	10-12.2

Table 3.7 Material combinations tried in CMT process

S.No	Material combination		
	Aluminium	Steel	Filler
1	6061-T6	Galvanized IF	4043
2	6061-T6	Galvanized IF	4047

3.6 Laser brazing


Laser brazing is a technique in which laser is used as a heat Source for brazing operation. In this process laser offers the advantage of localised heating of the brazing filler and the detached droplets of molten metal are directed to the joint location. In this the laser Source is focused only on the filler wire, hence the base materials remain unaffected. In these process different types of laser Sources can be used. But among all, diode laser offers advantages in terms of large spots suitable for brazing. The advantages of the process are as follows.

- it is a low heat input process
- localised heating is involved which results in low dilution of the base materials
- suitable for thin sheet welding
- suitable for dissimilar material joining
- high processing speeds enabling high productivity.

The characteristic of laser brazing set up is shown in Table 3.8 and processing parameters are given in Table 3.9. The material combination used in laser brazing process is given in Table 3.10. The laser brazing set up used in the present context is shown in Fig 3.8. In the present experimentation a Lassy dynamic beam shaping technique is used. In this beam shaping technique the beam is scanned at a particular amplitude and at a particular

frequency. The use of this canning helps in increasing the beam spot size, inturn increasing the working area. In case of dissimilar aluminium-steel joining use of this beam shaping increases the spot size of the laser beam, therefore results in heating of the surrounding base material, which in turn improves the wetting and spreading behaviour.

Table 3.8 Characteristics of laser brazing set up

Diode laser 400 μm fiber Lassy optics 100 mm focal length	
--	--

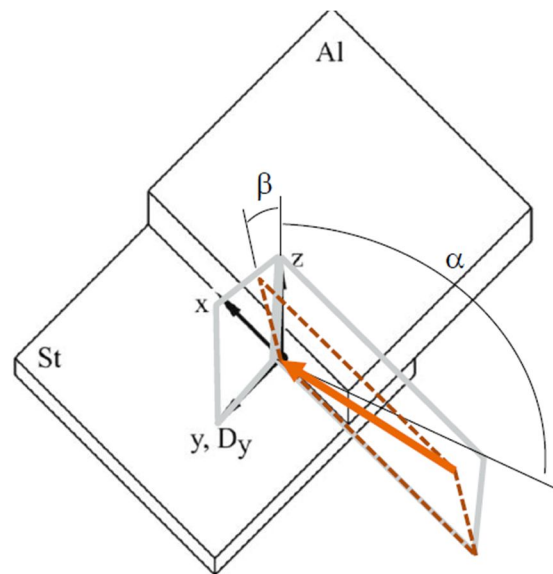


Figure 3.8 Schematic of laser brazing set up.

Table 3.9 Laser brazing processing parameters

Sample id	Variable processing parameters			
	Laser power (kW)	Processing speed (m/min)	Wire feed rate (m/min)	Scanner
S1	4.7	4	4.8	No
S2	4.7	4	4.8	Yes
S3	5	4	4.8	No

Table 3.10 Material combinations used in laser brazing process

Material combinations		
Al alloy	Steel	Filler
6081-T6 (1 mm)	DX56 (0.8 mm)	Al-12%Si (1.2 mm dia)

3.7 Thermal transient measurements

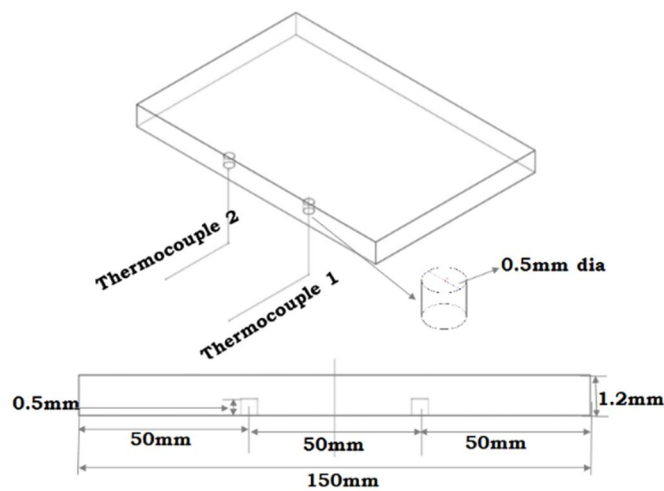


Figure 3.9 Schematic of thermal transient measurement setup.

The thermal cycles experienced by the materials during a joining process effects the macrostructure, microstructure and mechanical performance of the joint. Knowing the thermal history aids in explaining the structure and properties of the joint. In the present context it is the lap fillet configuration where an arc melts the filler wire and the molten metal pool wets the steel surface to form a joint. The temperature cycle at the molten pool/steel interface has to be measured. In this case a k-type thermocouple with a 100 μm tip is used to measure the thermal cycles. The thermocouple is initially calibrated prior to the actual temperature measurement. The schematic of thermal transient setup is shown in Fig 3.9. A hole of 0.5 mm depth from bottom of steel is drilled at an interval of 50 mm, therefore that

thermal transients could be measured at two locations. The thermocouples are inserted in the holes and are filled with a sealant. The holes are coincided with the wire tip such that the molten metal pool generated by arc melting of the filler wire should fall just above the holes and the thermal cycles are recorded using a computer.

3.8 Characterization of joints

Fig 39 shows the flowchart of the different characterisation techniques used to characterize the Al/steel brazed joints. Microstructural and mechanical characterization techniques are involved. The macrostructure and microstructural features of the joint determine the strength. Hence macro, microstructural and mechanical characterizations have been carried out. The very low thickness of the IMC layer formed at bead/steel interface renders the IMC layer characterization difficult. Structural characterization is carried out using SEM, EBSD, XRD, micro area XRD and TEM. X-ray diffraction technique recorded only base material pattern as the percentage of IMC layer is less compared to the remaining material. Unevenness of the polished surface at the interface due to disparity in hardness levels between aluminium and steel, limited the use of EBSD technique. The IMC layer formation at bead/steel interface is location specific. It is highly difficult to obtain a region for electron transmission locally using conventional route of TEM specimen preparation. The high thinning rate of aluminium compared to steel resulted in leaving only the steel in most of the cases. This limited the use of TEM. Micro area x-ray diffraction technique is the only option for interfacial phase analysis in the current interface. Hence, only successful characterization techniques are discussed below.

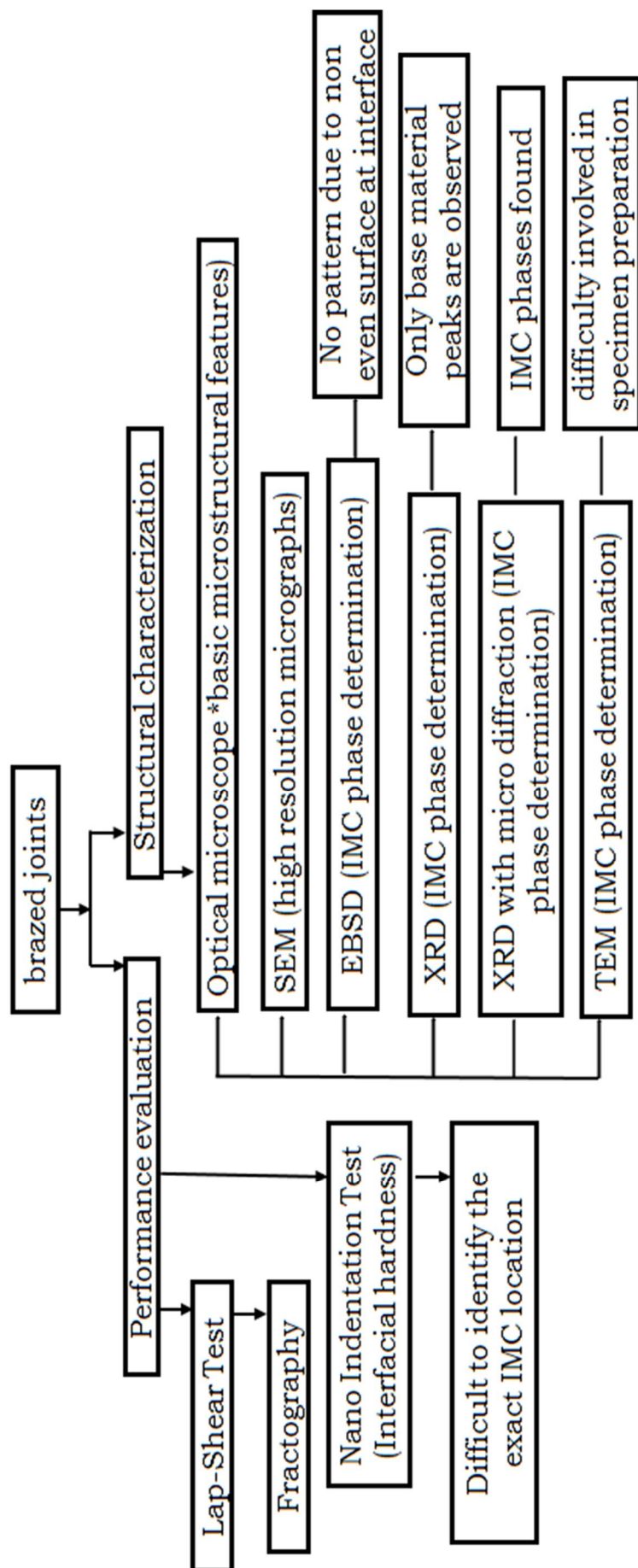


Figure 3.10 Flow chart of used characterization techniques and their consequences.

3.8.1 Metallography

The defect free specimens are cut to a size of 5 mm X 10 mm using abrasive cutting machine and are hot mounted. The specimens are mounted and further polished using 600, 800, 1000, 1200 grit emery papers, followed by 9, 5, 3 & 1 μm diamond suspension. The final polishing is done using 0.05 μm colloidal silica solution. The specimens are then ultrasonically cleaned and etched using Keller's reagent (2.5 ml HNO_3 , 1.5 ml HCl , 1 ml HF in 95 ml H_2O) for further analysis.

3.8.2 Stereo microscopy

It is an optical microscope that works at low magnification. It works with two separate optical parts. Slightly different viewing angles are caused due to two objectives and two eyepieces hence the left and right eye are seeing the same object in two different ways. This different viewing angles of two eyepieces develops a 3D image. This is the uniqueness of this microscope that makes it suitable to many applications. It uses reflected light from the sample surface for viewing. The obtained aluminium-steel dissimilar joints were examined under stereo microscope at a magnification of 6.5X and the bead appearance is recorded. If any flaws or defects present are detected at this stage, the specimens containing defects are discarded.

3.8.3 Optical microscopy

The optical microscope uses visible light and a set of lenses to magnify the minute detail of various materials. The optical microscope creates a magnified image of an object using objectives and eyepiece. The eyepiece magnifies the image to be visible to naked eye. Initially, an inverted real image of the object is captured by the objective lens and this inverted image is followed by eyepiece magnifies the image and shows in the same plane as

magnified image when viewed through eyepiece. In the present work optical microscope is used to observe the basic microstructure at various locations of the Al/steel joint. Various magnifications like 50X, 100X, 200X, 500X are used to analyse the microstructure of the dissimilar aluminium-steel joints [3].

3.8.4 Scanning electron microscopy (SEM)

SEM uses electron beam source to obtain the magnified view of the material. This tool is used to characterize a wide variety of materials and can resolve up to 3 nm. In this the electrons are emitted from the target material. The emitted electrons form a beam and are accelerated towards the surface of the specimen. The electron beam is then focussed down the column using electromagnetic lens. When this electron beam hits the specimen then the loosely bound electrons from the surface of the specimen are emitted as secondary electrons and used to view surface of the specimen. Along with these secondary electrons, back scattered beam, x-rays, auger electrons are also emitted along with some heat. These emitted electrons are used to view various microstructural features of the materials. In the present work microstructures at various locations are collected at various magnifications. Especially, the joint interfaces are studied thoroughly using this tool [4].

3.8.5 Micro area x-ray diffraction

Fig 3.11 shows the micro x-ray diffraction set up used in the present work. X-ray diffraction technique is a widely used tool in the field of materials. X-rays are supposed to reveal the structural features of a material. X-ray diffraction study is used to understand the chemical composition, amount of the elements present, crystallinity, texture, size of crystallites etc. The x-ray beam can be focussed to as small spot size as 100, 50 and 10 μm in diameter. In

the present work an x-ray spot size of $10\ \mu\text{m}$ is used and the scan time of 2 hours is maintained for all the specimens [5].

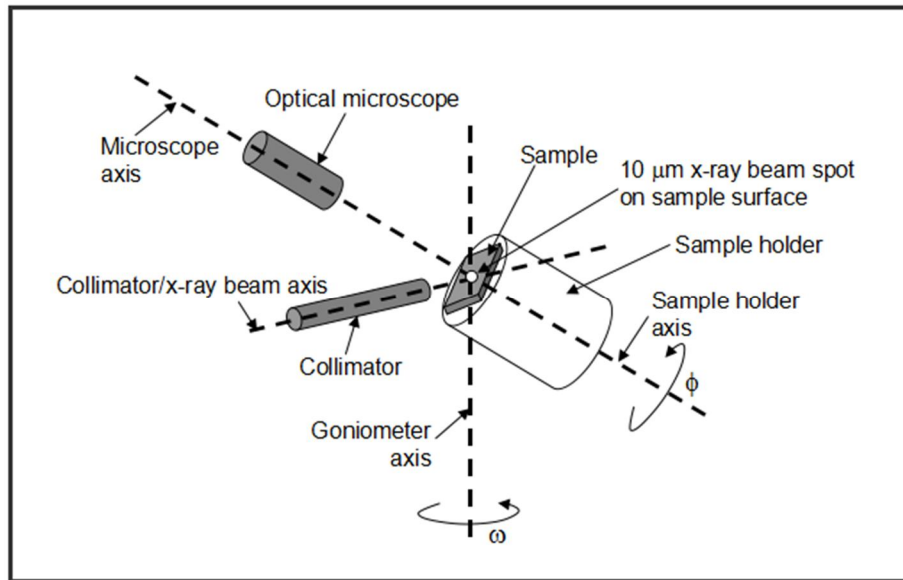


Figure 3.11 Schematic of micro area X-ray diffraction unit.

3.8.6 Lap shear test

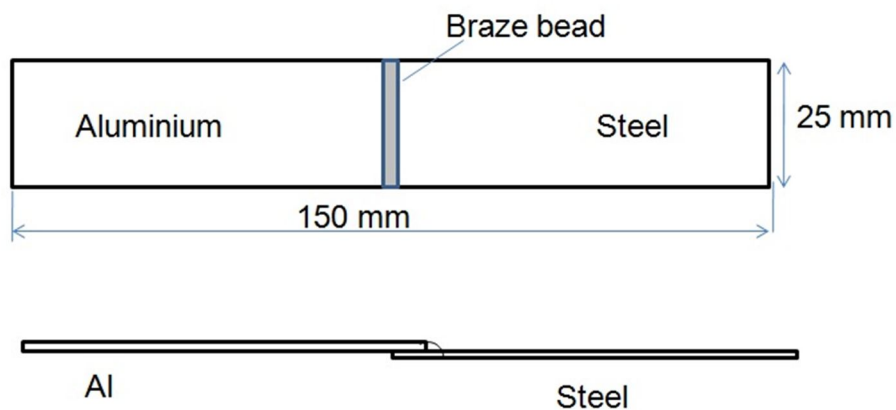


Figure 3.12 Schematic of lap shear test specimen.

Fig.3.12 shows the schematic of the lap shear test specimen. The specimens are cut from 150 mm X 200 mm joints using EDM wire cutting machine. INSTRON is used to carry out the

lap shear test. The specimens are pulled at a cross head speed of 1 mm/min and the load-elongation curve is recorded.

3.9 Enthalpy of formation

Thermodynamics is essential for any phase formation. Thermodynamically the term formation enthalpy ascertains the ability and stability of a given phase formation. Experimental measurements are time intense and cost ineffective. Hence, theoretical approach of enthalpy prediction is significant and efficacious. The four theoretical approaches of enthalpy prediction are first principles calculation using density functional theory, statistical mechanics based methods, extrapolating the experimental data using CALPHAD and other semi empirical models. First principles calculation involves high computing cost and postulates all-out detail of crystal structure. Statistical mechanics based methods need translational, rotational symmetries and atomic vibration details. Thermodynamic variables are expressed as polynomial functions of temperature in CALPHAD and demands panoptic databases. Under these conditions semi empirical approaches can be adapted. Amongst all semi empirical methods, Miedema's model is widely known for ease and fleet calculations. Recent reports confirm its applicability to wide variety of material systems. However, in absence of extensive thermodynamic databases and multi-component systems Miedema's semi empirical model [6, 7] is an idyllic tool. The original Miedema model is designed for a binary system]. Later it has been extended for ternary system. The formation enthalpy of a ternary compound can be calculated using the following equation:

$$\Delta H_{ABC} = x_A f_B^A \Delta h(A \text{ in } B) + x_A f_C^A \Delta h(A \text{ in } C) + x_B f_C^B \Delta h(B \text{ in } C) \quad -(1)[8]$$

Where x_i are ternary atomic fractions and f_i^j is a function accounting to the degree to which atoms of type i are surrounded by atoms of type j in a ternary compound and $\Delta h(i \text{ in } j)$ is the heat of solution of i in j . If the factor f_i^j is not known then the formation enthalpy can be calculated using weighted sum of binaries through following equations.

$$\Delta H_{ABC} = \sum_{i < j} (x_i x_j / x_i' x_j') \Delta H_{ij}(x_i', x_j'), \quad -(2)[8]$$

Where $\Delta H_{ij}(x_i', x_j')$ is the chemical contribution of the heat of formation of binary mixture ij of composition (x_i', x_j') and $(x_i' + x_j' = 1)$. According to Kohler expression x_i' and x_j' can be calculated as follows

$$x_i' = x_i / (x_i + x_j) \quad -(3)[8]$$

$$x_j' = x_j / (x_i + x_j) \quad -(4)[8]$$

$$x_i' + x_j' = 1$$

ΔH_{ij} can be calculated as

$$\Delta H_{ij} = c_i f_j^i v_i^{2/3} / (\eta_{ws}^{-1/3})_{\text{average}} \{ -P(\Delta\phi)^2 + Q(\Delta\eta_{ws}^{1/3})^2 - R \} \quad -(5)[9]$$

$$f_j^i = c_j^s \{ 1 + \gamma(c_i^s c_j^s)^2 \} \quad -(6)[9]$$

$$c_i^s = c_i v_i^{2/3} / (c_i v_i^{2/3} + c_j v_j^{2/3}) \quad -(7)[9]$$

$$c_j^s = c_j v_j^{2/3} / (c_i v_i^{2/3} + c_j v_j^{2/3}) \quad -(8)[9]$$

$$c_i^s + c_j^s = 1$$

Where

c_i , c_j are the atomic concentrations of component i and j respectively in a binary system of i and j ;

c_i^s & c_j^s are the surface fractions of component i and j respectively in a binary system of i and j;

f_j^i is a function of degree to which atoms i are in contact with atoms j in a binary system of i and j;

v_i & v_j are the molar volumes of component i and j;

$\Delta\eta_{ws}$ is the difference in the density at the boundary of the Wigner-Seitz cell of the two components i and j;

$\Delta\phi$ is the difference in work functions of the two components i and j;

P, Q and R are empirical constants for a combination of metals. P, Q are proportionality constants and R is associated with transition and non-transition metal combination.

γ is a constant where $\gamma=0$ for completely disordered alloys, $\gamma=8$ for intermetallic compounds and $\gamma=5$ for amorphous alloys.

In the present work equations 2 to 8 have been used for the calculation of the enthalpy of formation for the various phases formed at the interface.

References

- [1] A.C. Davies, The Practice of Welding, 10 ed., Cambridge University Press, NewYork, 1993.
- [2] H.T. Zhang, J.C. Feng, P. He, B.B. Zhang, J.M. Chen, L. Wang, Materials Science and Engineering a-Structural Materials Properties Microstructure and Processing, 499 (2009) 111-113.
- [3] J. Mertz, Introduction to Optical Microscopy, Roberts and Company Publishers, 2009.
- [4] C.E.L. Joseph I. Goldstein, Dale E. Newbury, Eric Lifshim, sCANNING eLECTRON mICROSCOPY AND x-RAY mICROANALYSIS, Springer, 2007.
- [5] B.D. Cullity, Elements of X-Ray diffraction, 3rd ed., Prentice Hall, 2001.
- [6] A.P. Goncalves, M. Almeida, Physica B, 228 (1996) 289-294.
- [7] B.W. Zhang, W.A. Jesser, Physica B-Condensed Matter, 315 (2002) 123-132.
- [8] L.J. Gallego, J.A. Somoza, J.A. Alonso, Journal of Physics: Condensed Matter, 2 (1990) 6245-6250.
- [9] J.F. Herbst, Journal of Alloys and Compounds, 337 (2002) 99-107.

CHAPTER 4

PULSED GAS METAL ARC WELD-BRAZING OF ALUMINIUM ALLOY TO STEEL

4.1 Introduction

In P-GMAW weld-brazing of aluminium to steel the experimental investigations were carried out on the effect of welding and joint configuration parameters, surface condition of steel, filler wire composition on the joint forming ability, the study of aluminium-steel interface using micro area x-ray diffraction technique. This is for the first time that a detailed investigation of the IMC layer using micro area x-ray diffraction technique has been carried out.

4.2 Base material characterization

In any materials joining, understanding the base materials in terms of microstructure and mechanical properties is important. Hence, the base materials are characterized and reported here. The analysed chemical composition of the base materials are given in Table 4.1 and mechanical properties are given in Table 4.2. The major constituents of 6061 aluminium alloy are Mg and Si. IF steel is a combination of Si, Mn, C, P, S and Fe. Aluminium alloys 4043 and 4047 are Al-Si based alloys with a variation in Si content.

Table 4.1 Chemical composition of the base materials (at. %)

Material	Al	Mg	Si	Mn	C	P	S	Fe
A6061-T6	Bal.	1.0	0.6	-	-	-	-	0.4
IF steel	-	-	0.07	0.21	0.08	0.01	0.02	Bal.
4043 filler	Bal.	-	5.0	0.1	-	-	-	0.35
4047 filler	Bal	-	11.92	0.1	-	-	-	0.35

Table 4.2 Mechanical properties of the base materials

Mechanical property	Material	
	6061-T6	IF Steel
Yield strength (MPa)	207	50
Ultimate tensile strength (MPa)	310	300
% Elongation	12	44

Fig 4.1 shows microstructures of the 6061-T6 aluminium alloy and interstitial free steel. The 6061 alloy used is a precipitation hardened alloy and it is in peak aged condition. The precipitates present in this alloy are in nanometre scale and hence are not revealed in the microstructure shown in Fig 4.1a. The IF steel used is a low carbon steel with a carbon content of 0.08 at. % and hence only ferrite is revealed in the microstructure shown in Fig 4.1b.

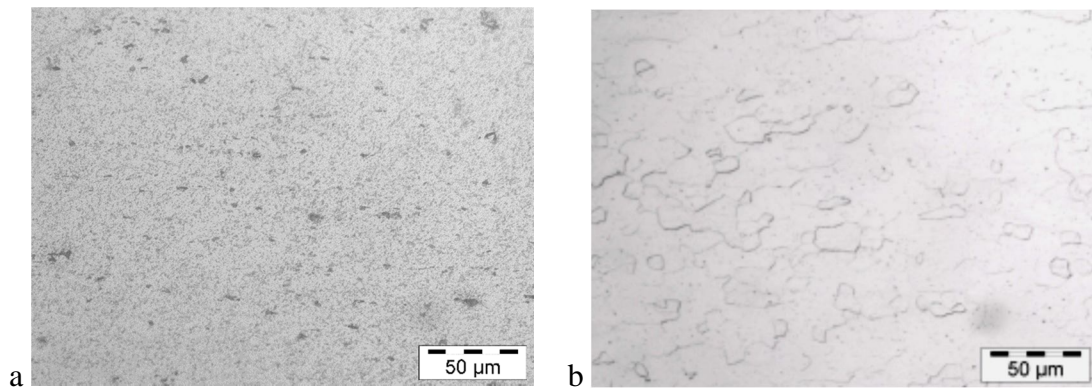


Figure 4.1 Optical microstructures of base materials at 500X magnification a) 6061-T6 aluminium alloy b) interstitial free steel.

Fig 4.2 shows the cross-sectional microstructures of the galvannealed and galvanized IF steel. In galvannealed steel the surface is comprised of 25-28 µm thick Fe-Zn coating as shown in Fig 4.2a. The galvanized steel is comprised of the Zn coating in the thickness range of 14-16 µm as shown in Fig 4.2b.

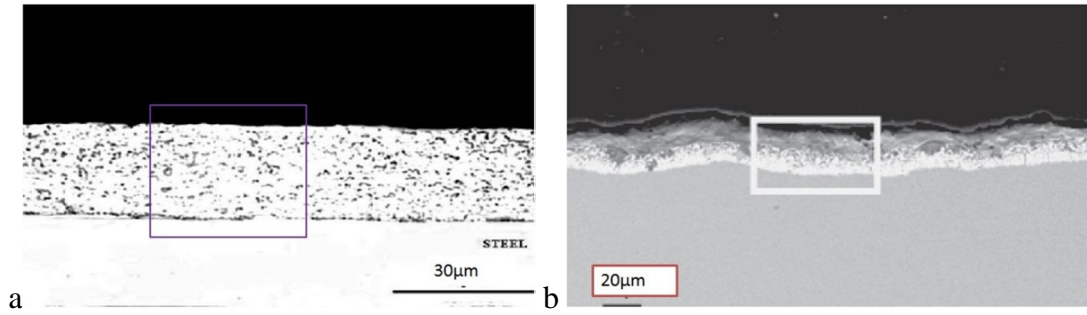


Figure 4.2 Base material microstructures a) galvanized (GI) steel b) galvannealed (GA) steel.

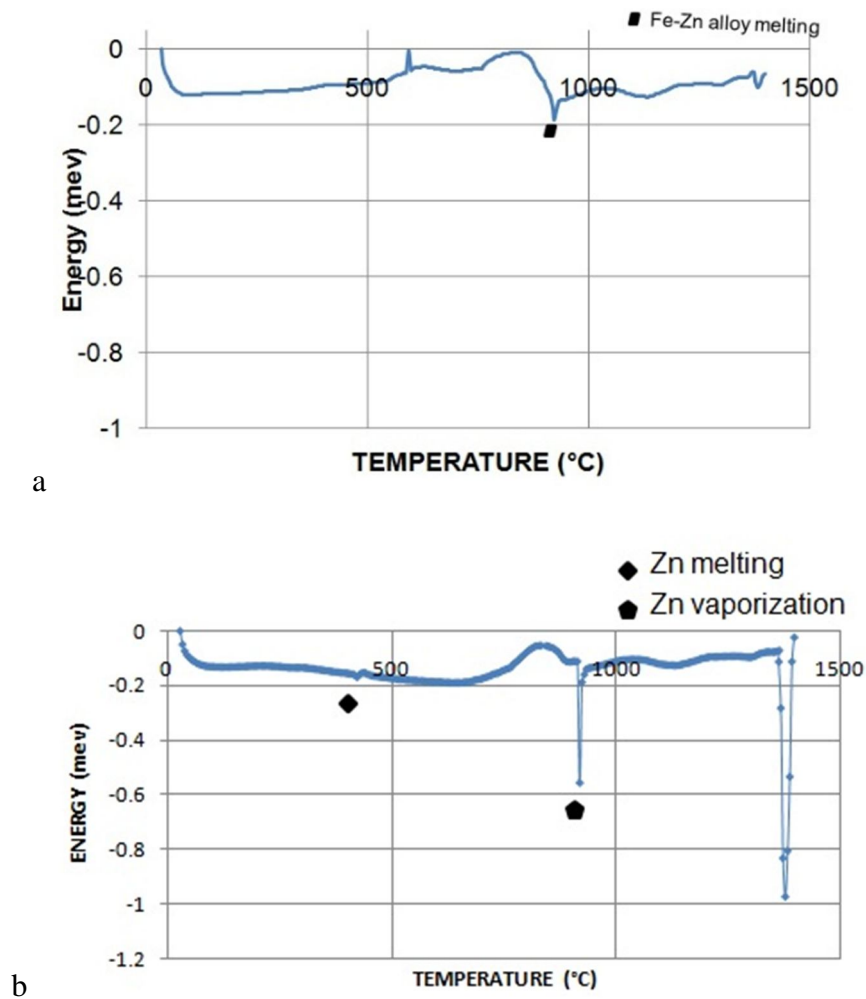


Figure 4.3 DSC curves of IF steel in two surface conditions a) galvannealed and b) galvanized.

The differential scanning calorimetric (DSC) curves of galvannealed and galvanized steel are shown in Fig 4.3. The DSC curve shown in Fig 4.3a shows a dip or an endothermic peak at a temperature of around 927 °C which indicates the melting of the Fe-Zn layer present on the surface of the galvannealed coating. The DSC curve shown in Fig 4.3b shows two major dips

or endothermic reactions one at 420 °C and the other at around 910-912 °C. 420 °C indicates the melting and 910-912 °C indicates the vaporisation of the Zn layer present on the galvanized steel.

4.3 Thermal transient measurements

Fig 4.4 shows the thermal cycles measured in P-GMAW braze-welding of aluminum and steel using 4043 filler wire. The schematic showing the position of the thermocouple is shown in Fig 3.8. Peak temperature has almost reached melting temperature. In fact, P-MIG specimen remained at higher temperature through the completion of the 150 mm braze bead.

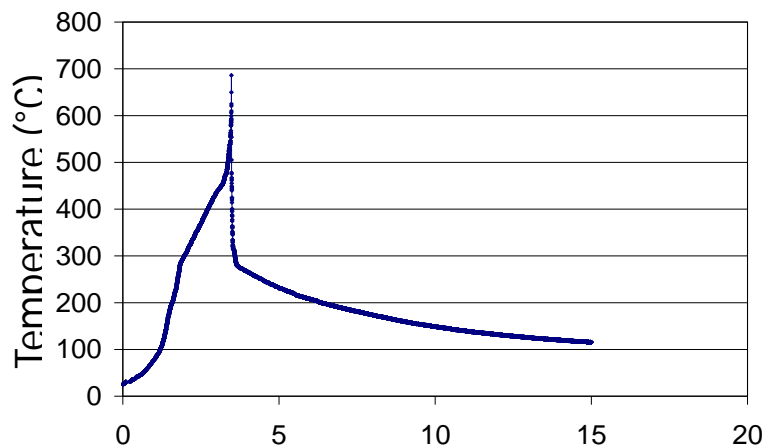


Figure 4.4 Thermal transient recorded in P-MIG brazing of aluminium and steel with 4043 filler wire.

4.4 Study of effect of various parameters

The effect of the following weld-brazing parameters has been evaluated

- angle of tilt of the lapped sheet assembly
- torch orientation
- steel surface chemistry
- gap between overlapping sheets

- filler wire composition; and
- heat input

4.4.1 Angle of tilt

4.4.1.1 Macrostructure

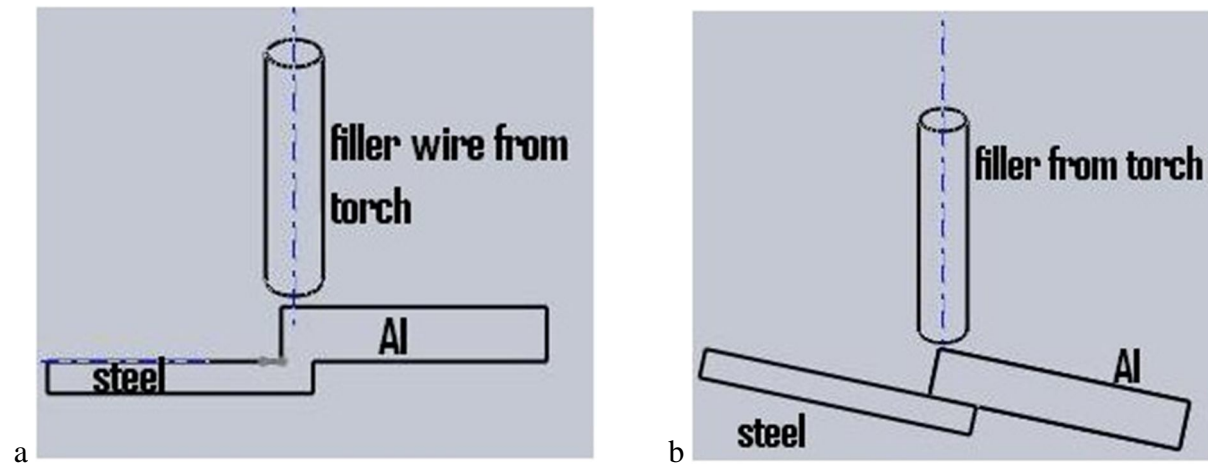


Figure 4.5 Schematic of brazing assembly a) 0° tilt b) 12° tilt.

Fig 4.5 shows schematic of brazing assembly with variation in tilting angle of the lapped sheet assembly.

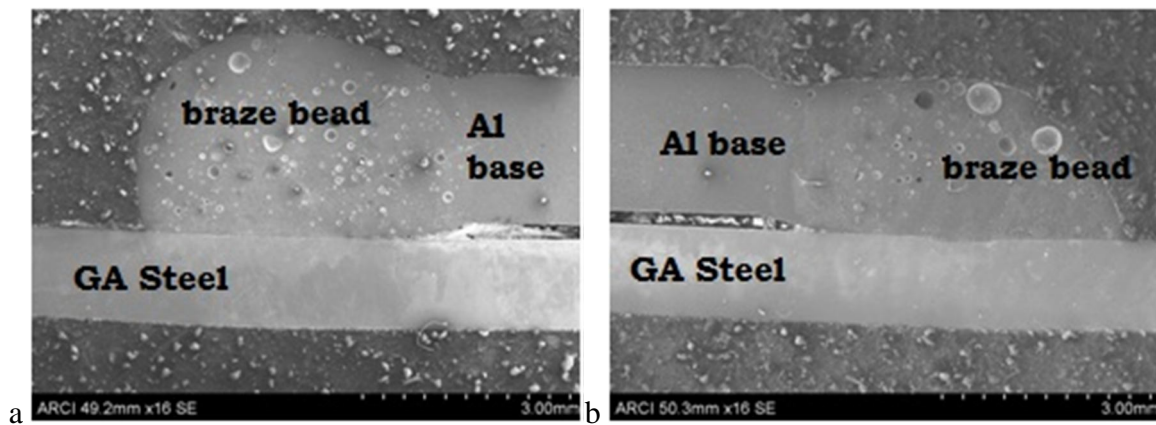


Figure 4.6 Transverse cross sectional SEM macrostructures of aluminium/GA steel joints.

Table 4.3 Bead geometry measurements of aluminium/GA IF steel joints

Measurement	0° tilt	12° tilt
Bead width (mm)	2.2-2.5	3.5-3.8
Bead height (mm)	2.2-2.4	1.6-1.65
Wetting angle (°)	108-110	59-63

Fig 4.6 shows the cross-sectional macrostructures of aluminium/GA IF steel joints welded at 0° and 12° tilt and bead geometry measurements are given in Table 4.3. It is observed that at 0° tilt, a convex bead is formed with a width of 2.5-2.8 mm, whereas bead widened to 3-3.5 mm in case of 12° tilt. Improved wetting and reduced convexity of the bead is observed with an increase in tilting angle. This may be due to higher volume of aluminium being exposed to arc causing more melting of aluminium, also resulting in improved wetting. Significant porosity is observed in both the cases.

4.4.1.2 Microstructure

The aluminium/bead interface, braze bead and bead/steel interface are the regions of microstructural interest in a dissimilar aluminium/steel joint. Fig 4.7 shows optical micrographs of various regions of microstructural interest of aluminium/GA IF steel joint at 500X magnification. During brazing operation the arc melts some part of base aluminium along with filler wire that wets the steel surface to form a joint. Therefore Al/bead interface showed solidified structure with elongated grains at the fusion line as shown in Fig 4.7a. Braze bead also showed solidified dendrites of Al-Si alloy as shown in Fig 4.7b. Fig. 4.7c shows a typical bead/steel interface microstructure. The bead/steel interface shows a thin layer at the interface as shown in Fig 4.7c. This layer is a reaction product of molten aluminium and solid steel. A variation in morphology along the interface is observed and the

schematic of different regions of microstructural observation of steel/bead interface is shown in Fig 4.8.

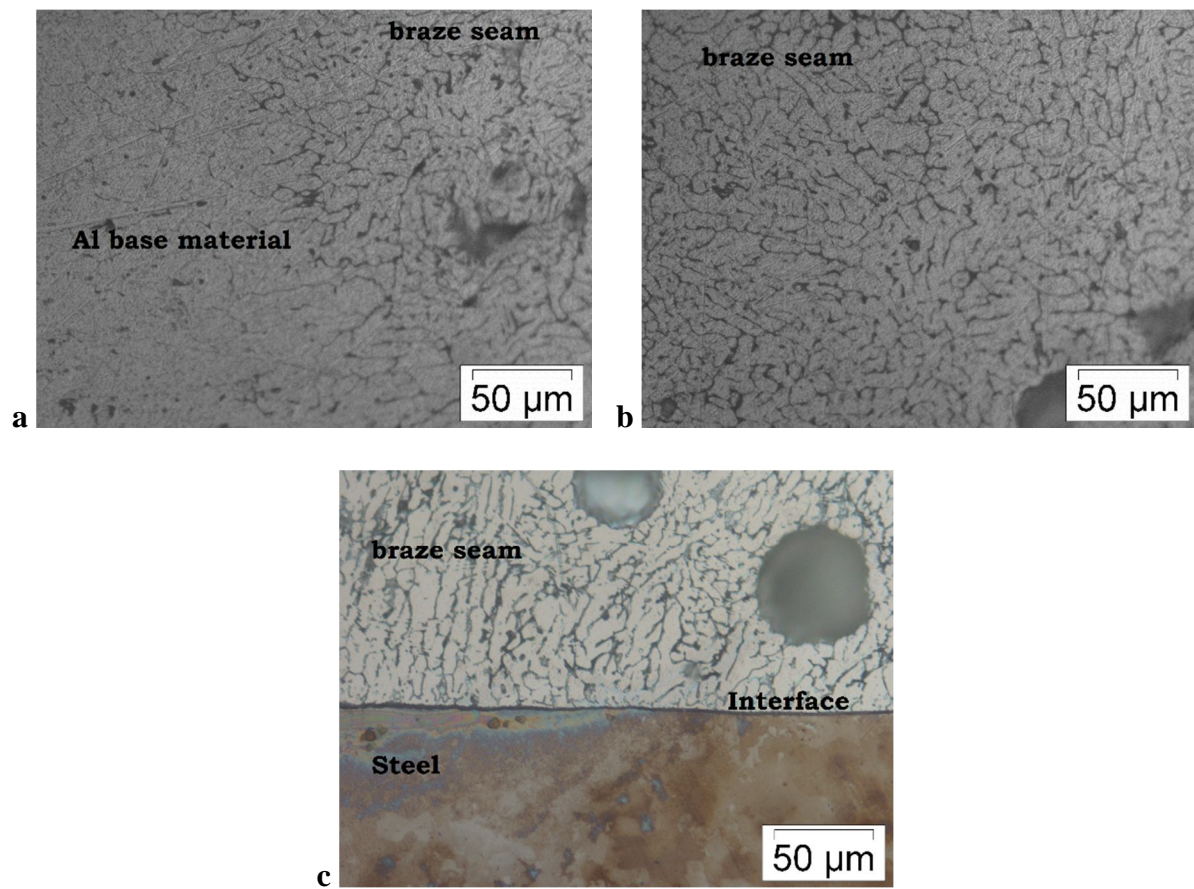


Figure 4.7 Optical images of microstructure at various locations of aluminium/GA IF steel joint at 500X magnification a) aluminium/bead interface b) braze bead c) bead/steel interface.

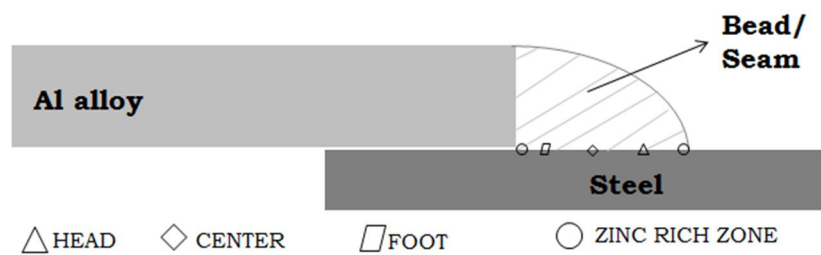


Figure 4.8 Schematic indicating various locations of bead/steel interface.

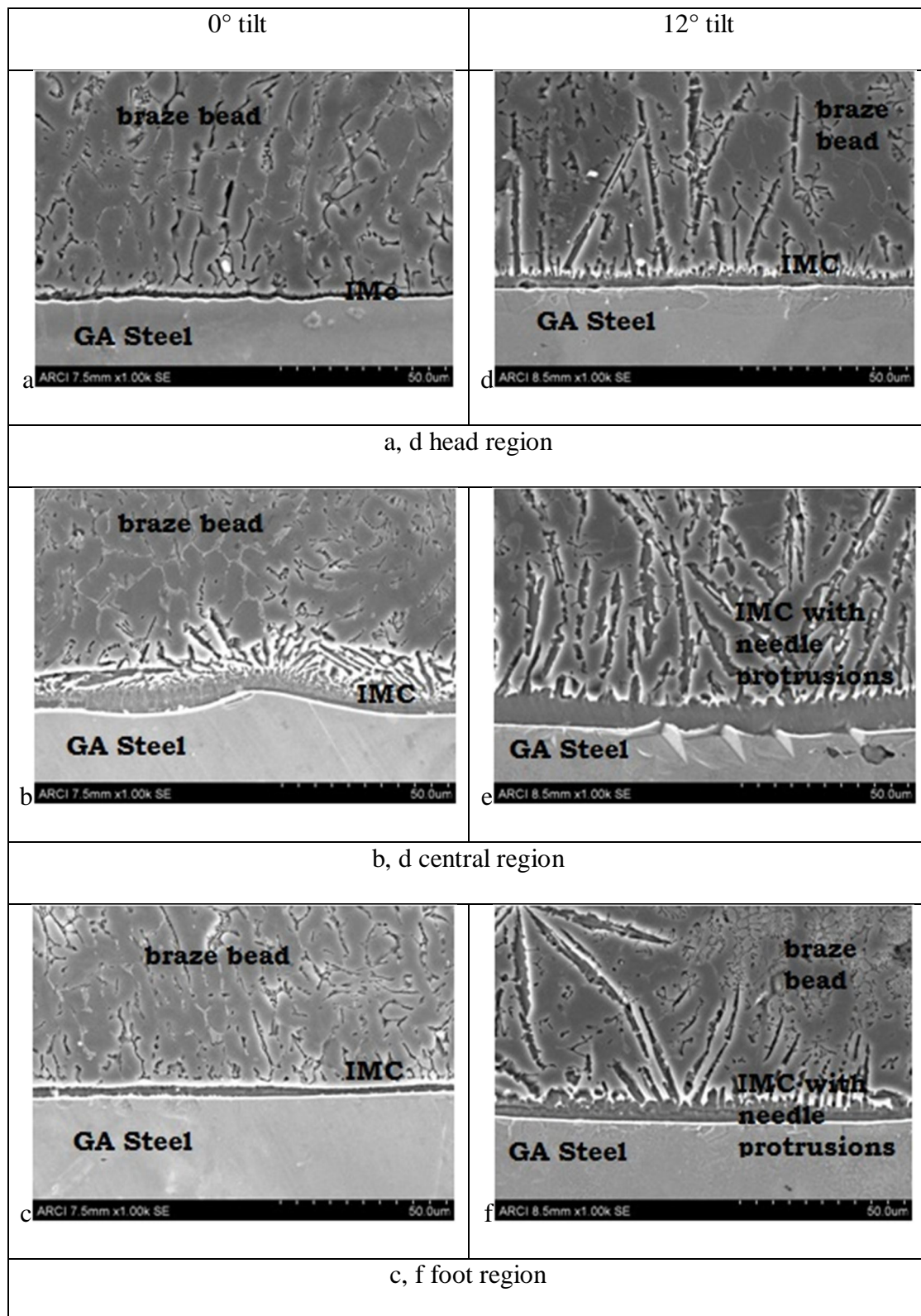


Figure 4.9 SEM microstructures of bead/steel interface at 1000x magnification.

Steel/bead interface shows three different regions in the plane of interface, such as head, center and foot as shown in Fig 4.8. SEM micrographs of the specimens are shown in Fig.4.9.

It was observed that the dilution between the base materials is high in case of 12° tilt. This is

perhaps due to higher melting of steel side in tilt condition. Interface region experiences the highest temperature gradient than any other location in the weld that resulted in planar mode of Solidification. A typical interface comprising possibly the intermetallic (IMC) layer is clearly seen. Thickness of this layer in three different regions is given in Table 4.4. The layer is higher in case of tilt specimen due to higher dilution. Head region (Fig.4.9 a, c, d, f) shows an interface with less IMC thickness in both the conditions, whereas needle like protrusions towards the bead are observed in case of tilting. At the center region (Fig.4.9 b, e) IMC growth is higher than head and foot regions due to high heat intensity at the center. Needle like protrusions extended up to 50 μm in case of 12° tilt whereas it is restricted to 15 μm in case of 0° tilt. Foot region (Fig.4.9 c, f) also shows similar trend in microstructure. The EDAX analysis of IMC layer shows that it is composed of variable composition such as Al: 52-63% (at.%), Fe: 36-48% (at. %).

Table 4.4 IMC layer thickness at various locations of bead/steel interface

S.No	Location	IMC layer thickness (μm)	
		0° tilt	12° tilt
1	Head	1-2	4-5
2	Center	10-12	15-16
3	Foot	2-3	7-9

4.4.1.3 Lap shear test

Table 4.5 shows the lap shear test results obtained for two sets of specimens. In spite of bead porosity the weld specimen failed at the interface. The strength improved by 20% in case of tilted specimen, even though IMC layer thickness is slightly high. The strength of the braze joint (lap or fillet) is a function of the wetting or bead width. Increase in wetting or bead width enhances load bearing capability and improves the strength of the joint.

Table 4.5 Lap shear test results

S.No	Sample id	Load per unit length (N mm^{-1}) (failure location)	
		0° tilt	12° tilt
1	S ₁	105±5 (interface)	125±5 (interface)
2	S ₂	103±5(interface)	127±5 (interface)
3	S ₃	104±5 (interface)	124±5 (interface)

4.4.1.4 Conclusions

- Tilting of the weld joint assembly affects the bead geometry and interface formation in terms of thickness of intermetallic layer as well as wetting of steel surface by aluminium.
- Bead geometry affects joint properties, viz., increase in wetting bead width helps in improving joint efficiency.

4.4.2 Torch orientation

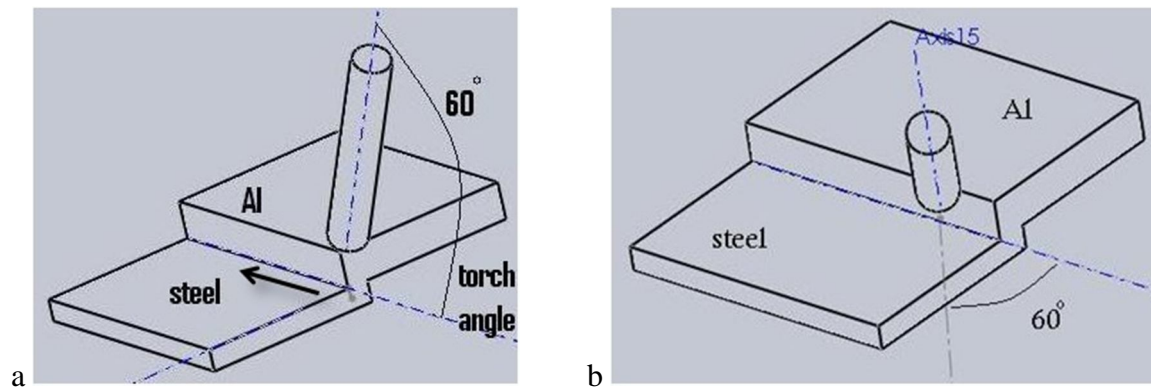


Figure 4.10 Schematic of brazing assembly with variation in torch orientation.

Fig 4.10 shows the schematic of brazing assembly with variation in torch orientation with respect to welding direction. At 0° (with respect to brazing direction) torch orientation and 3.5 m/min of wire feed rate a discontinuous bead is formed. Discontinuities are reduced when the wire feed rate is increased to 5 m/min and a good joint was formed. This indicates a

threshold in terms of amount of filler to be deposited and heat input required to cause adequate wetting to form a bead. According to wetting theory, wetting depends mainly on temperature and viscosity of the wetting media, temperature differential between the substrate and wetting media, surface energy of the substrate. Therefore, at high heat input conditions the temperature differential between the molten pool and the substrate is minimized and that resulted in improved wetting above 5 m/min. In the specimen welded by altering the torch orientation to 60° (with respect to brazing direction) continuous bead formation occurred even at a wire feed rate of 3.5 m/min. Here the change in fluid flow or molten pool flow has been attributed due to the change in torch orientation. The pushing action of the arc could probably be the reason for improved wetting. Hence, even at lower heat input and material deposition conditions an interface could be formed with continuity. This result is of significant importance while carrying out joint designs and process optimization for such dissimilar materials joining applications.

4.4.2.1 Summary

- Torch orientation is an important parameter in joining aluminium to steel using pulsed MIG brazing using an aluminium filler wire owing to fluid flow effects on wetting.
- Joints can be made at low heat input conditions by changing the torch orientation with reduced formation of intermetallic at the interface.

4.4.3 Surface chemistry of steel

The following section explains the effect of surface chemistry of steel on the bead formation ability and mechanical properties of the joints formed. IF steel with three surface conditions viz. galvanized, galvanealed and uncoated are chosen for this part of work.

4.4.3.1 Macrostructure

Effect of chemical composition on wetting and porosity

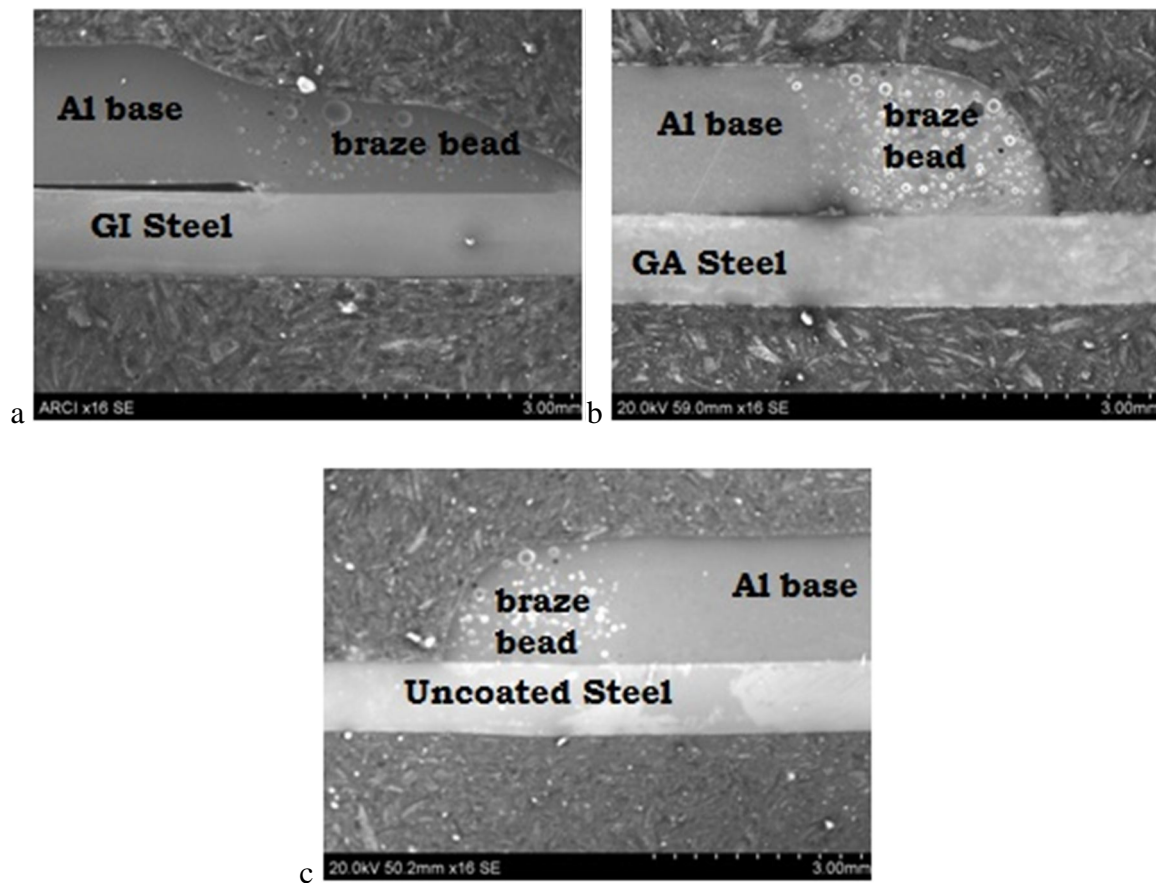


Figure 4.11 SEM macrographs of aluminium/steel joints under different surface conditions of steel a) Al/GA steel, b) Al/GI steel, c) Al/uncoated steel

Table 4.6 Bead geometry measurements

S. No	Bead profile	Surface condition of steel		
		GI	GA	U
1	Bead width (mm)	4.2-4.4	2.6-2.7	2.2-2.3
2	Bead height (mm)	1.4-1.55	1.8-2	1.85-2
3	Wetting angle (°)	32-36	82-85	83-88

Transverse cross sectional macrostructures of brazed Al-steel joints are shown in Fig 4.10 and the bead geometry measurements are given in Table 4.6. It is observed that bead widths vary with the surface condition. Galvanized steel (Fig.4.11a) showed better wetting behaviour than galvanized (Fig 4.11b) and uncoated (Fig 4.11c) steel. The surface chemical composition of the steel seems to be significantly effecting the wetting behaviour. Zn is present in elemental form on galvanized steel, whereas in the form of Fe-Zn alloy on galvanized steel and no Zn on uncoated steel. According to Young's equation [1], wetting is favoured by a liquid with less surface tension and/or wide difference in Solid surface energy and Solid/liquid interfacial energy. In actual brazing conditions, molten Al-Si alloy is expected to wet the surface comprising zinc, iron-zinc alloy and iron in case of galvanized, galvanized and uncoated steel, respectively. The welding arc vaporizes the zinc surface layer, melts the iron-zinc alloy layer in case of galvanized and galvanized steel, respectively. In case of uncoated steel the arc only heats the surface. In case of galvanized steel the rise in surface free energy owing to zinc vaporization renders the steel surface thermodynamically unstable. Hence, the molten aluminium coming in contact with this unstable surface facilitates better wetting and spreading resulting in more spreading. In reactive systems such as this, the wetting action is governed by the final chemistry at the triple line (S/L/V interface). Zinc vapour alloys with molten aluminium forming Al-Zn Solid solution at the triple line, resulting in a pulling action on the melt at triple line facilitating more spreading. Hence, rise in surface energy of steel caused by vaporization of zinc layer, low viscous Al-Zn alloy at the triple line exerting pulling action, enhanced triple line velocity due to movement of zinc vapours in the gap between the plates may be the probable reasons for improved wetting of galvanized steel [2]. Zhang, et al. [3] reported the presence of Al-ZN eutectic phases towards the toe and foot of the joint. Lack of rise in surface free energy due to surface melting in case of galvanized steel and only heating in case of uncoated steel

resulted in limited wetting and spreading action. Other difference observed is that the galvanized steel showed reduction in bead height compared to other combinations resulting in undercut like feature in bead height. Zhang et al. [3] reported the superior wetting and spreading behaviour of Zn coated steel compared to aluminized steel.

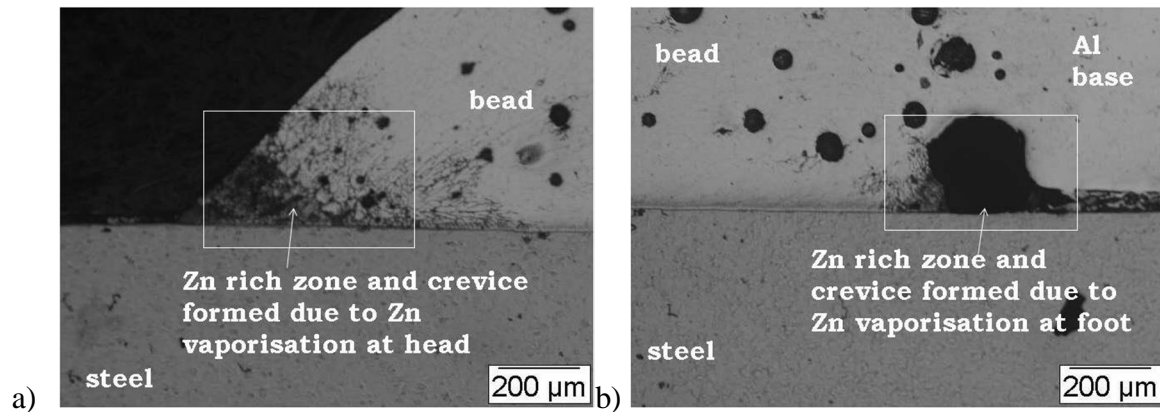


Figure 4.12 Optical micrographs of crevice and Zn rich zone at head and foot regions a) head region and b) foot region.

The arc struck between the filler wire and base material rises the surface temperature of the steel instantaneously leading to vaporization of Zn layer. The Zn vapour tries to escape from gap between the plates. If the molten metal solidifies first, escaping Zn vapours get entrapped and leave crevice at the ends of bead/steel interface. The crevice formed is shown in Fig.4.12. Fig 4.12a shows the opening up of the bead/steel interface at head region whereas the restricted conditions at the foot region have resulted in crevice of slightly larger size as shown in Fig.4.12 b. The crevice formed at the foot region has extended into bead region due to restrictions caused by base material sheets.

4.4.3.1.1 Effect of gap on wetting and porosity

In order to avoid the entrapment of Zn vapours in the bead, a gap between the overlapping sheets was envisaged. Accordingly, experiments were carried out with varying gap to identify the optimum interfacial gap.

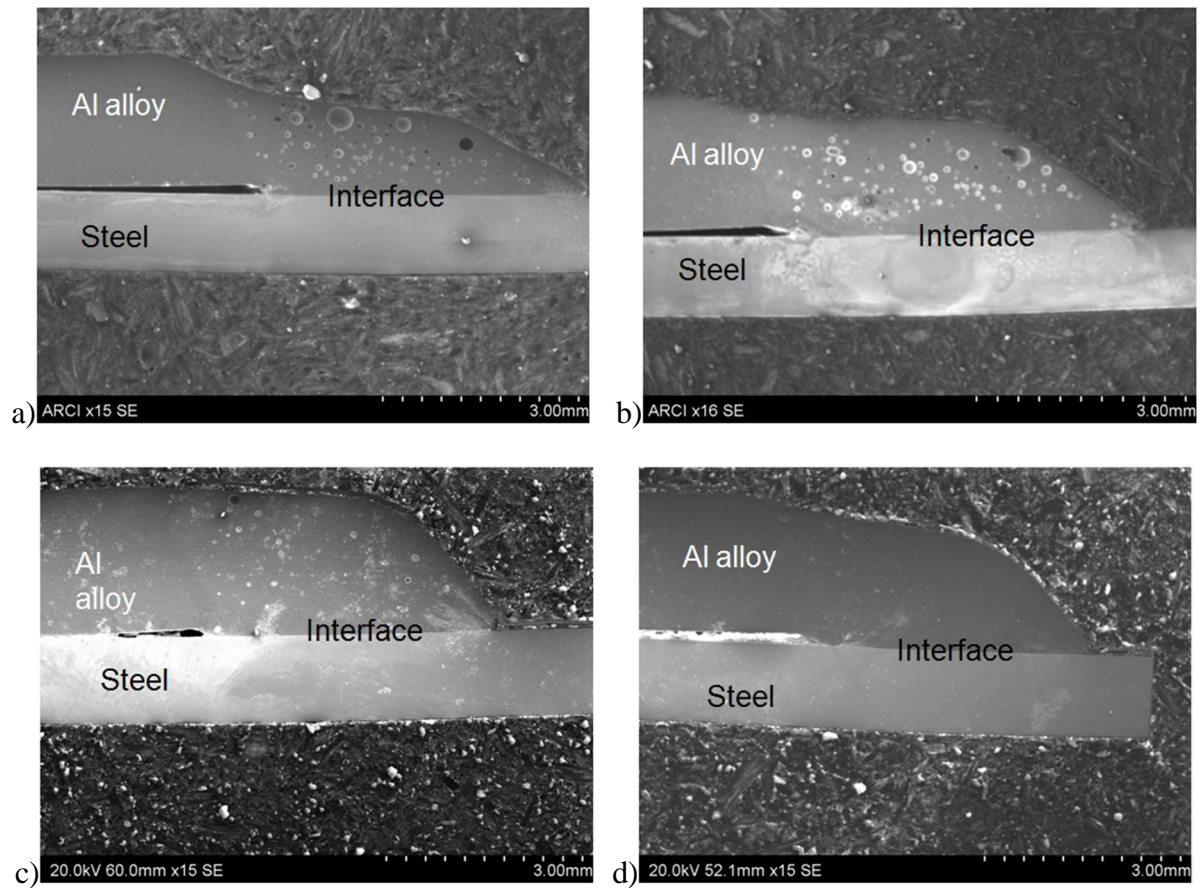


Figure 4.13 Transverse cross-section SEM macrographs of Al/GI steel joints at different interfacial gaps a) < 50 μm b) 200 μm c) 300 μm and d) 500 μm .

Table 4.7 Bead geometry measurements with variation in interfacial gap

S.No	Bead geometry measurements	Interfacial gap (μm)			
		< 50	200	300	500
1	Bead width (mm)	4.2-4.4	4-4.1	3.8-3.95	3.8-3.9
2	Bead height (mm)	1.4-1.55	1.65-1.75	1.7-1.8	1.7-1.8
3	Wetting angle ($^{\circ}$)	32-36	43-45	50-52	52-53

Transverse cross-section macrographs of Al/GI steel joints brazed with variation in interfacial gap are shown in Fig.4.13 and bead geometry measurements are given in Table 4.8. Change in interfacial gap altered the wetting behaviour. Increase in interfacial gap slowed down the spreading kinetics of the molten metal pool. The reduced region (undercut) in case of joints

made at $<50\text{ }\mu\text{m}$ gap (Fig 4.13a) is not seen in joints made with higher interfacial gaps (Fig 4.13b, c, d). The reduction in capillary action and the force exerted by the escaping Zn vapours at the triple line may be the probable reason for reduced wetting at high interfacial gaps.

Fig 4.14 shows the macrographs near to head and foot regions of bead/steel interface. It is observed that the intensity of crevice formation due to Zn vaporization is minimized. Increase in interfacial gap paid an easy way for Zn vapours to escape and resulted in minimal or nearly no crevice condition as shown in Figs 4.14a & b. Hence, there is a significant reduction in crevice and porosity formation for joints made with interfacial gap.

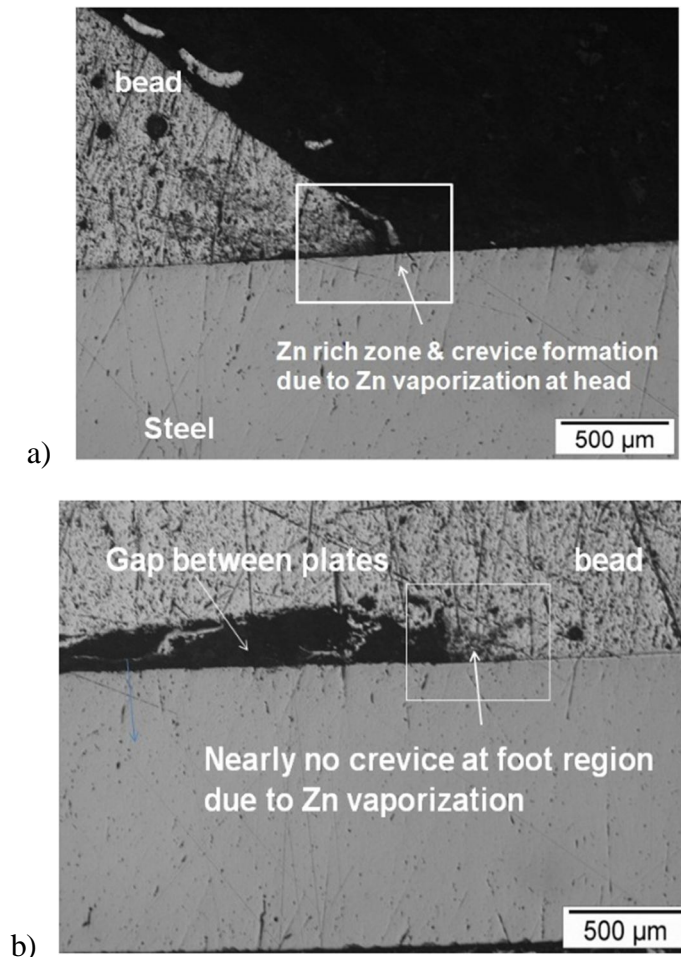


Figure 4.14 Optical micrographs of crevice formation and Zn rich zones in joints made with increased gap (300 μm).

4.4.3.2 Microstructure

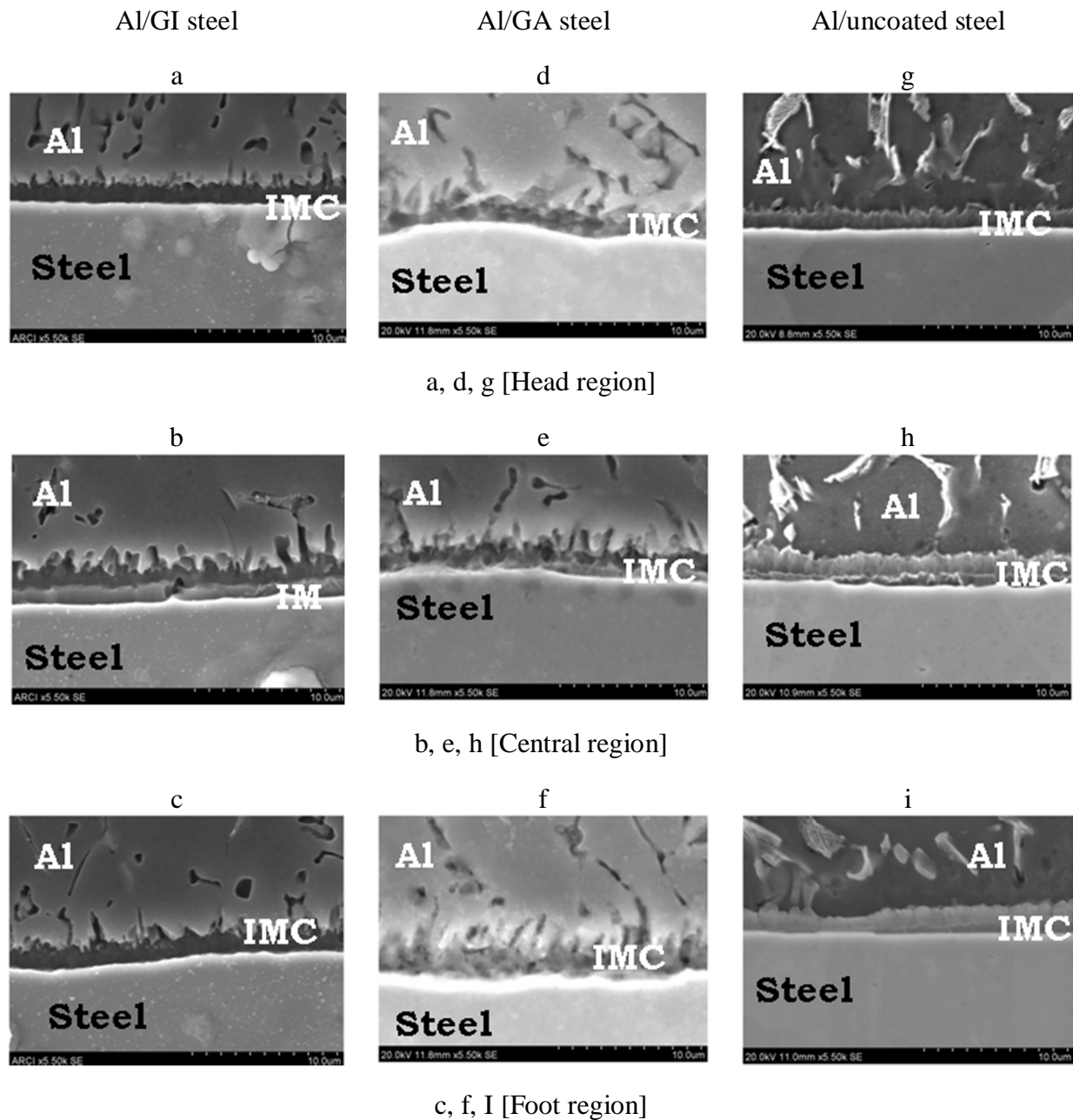


Figure 4.15 SEM micrographs at different locations of bead/steel interface at 5.5 kX magnification a) head region (Al/GI steel interface) b) central region (Al/GI steel interface) c) foot region (Al/GI steel interface) d) head region (Al/GA steel interface) e) central region (Al/GA steel interface) f) foot region (Al/GA Steel interface) g) head region (Al/uncoated steel interface) h) central region (Al/uncoated steel interface) I) foot region (Al/uncoated steel interface).

Al/bead interface, braze bead, bead/steel interface are the three different zones of interest for microstructural observation. Al/bead interface and braze bead show similar microstructure as

in Figs 4.7a & b. Bead/steel interface showed variation in microstructural features along the interface. Different regions marked along the interface - head, center, and foot along with a Zn rich zone at head and foot regions are shown in Fig 4.8.

Fig 4.15 shows the bead/steel interfacial microstructures at three different locations head, center & foot of joints made under different surface conditions of steel. It is observed that the IMC layer thickness is varying along the interface from head to the foot regions; (the IMC layer thickness variations are given in Table 4.8. In all the three cases the IMC layer thickness is higher at the center than the head and foot regions. The interface consists of a planar type solidified region with a needle like formation protruding into the aluminium bead. The needle structures are sharper at head and foot regions whereas needles with slightly rounded edges are seen at the central region. Further, the head and foot regions consist of two layers one is bright and the other is dark in colour with some needles like protrusions towards the aluminium melt. The central region comprises of one additional grey coloured region along with the two bright and dark layers as shown in Fig 4.15b, e & h. The grey coloured region is distinctly seen in all the three cases only at the central region. This may be due to high heat intensity experienced by the central region that resulted in growth of an additional layer.

Table 4.8 IMC layer thickness at different locations of bead/steel interface

S. No	Location	IMC layer thickness (μm)		
		Al/GI	Al/GA	Al/uncoated
1	Head	1.8-2.2	1.9-2.3	1.8-2.2
2	Center	2.9-3.5	3.3-4	3.2-3.8
3	Foot	1.5-2	1.7-2	1.6-2

It is also observed that the interface of joints of galvanized and uncoated steel possesses slightly thicker IMC layer than galvanized steel. In case of galvanized steel large amount of supplied energy is expended in vaporization of zinc and low amount is consumed for nucleation and growth of IMC layer. This can be confirmed by DSC curves of different steels conducted under Ar (inert) atmosphere as galvanized and galvanized shown in Fig.4.3. In both Fig 4.3a & b an endothermic peak is observed at 930 °C, which corresponds to melting of Fe-Zn alloy. In Fig 4.3a an additional intense endothermic peak is obtained at 910 °C which corresponds to vaporization of zinc. Availability of high amount of energy for diffusion and growth of IMC layer resulted in thicker IMC layer in galvanized and uncoated steel. It is observed from EDS analysis that there is a compositional gradient across the interface from steel to aluminium side. According to EDS spot analysis the bright layer towards the steel comprises of 16-18 at% Al, 80-82 at. % Fe, 0.5-2 at. % Si 0-0.5 at. % Zn, grey region comprises of 40-60 at. % Al, 35-59 at. % Fe, 1-3 at. % Si, 0-0.55 at. % Zn, dark region comprises of 63-75 at. % Al, 20-31 at. % Fe, 3-3.5 at. % Si, 0-0.5 at. % Zn. It indicates that Fe-rich IMC layer towards steel side and Al-rich IMC layer towards bead side have formed.

4.4.3.3 Lap shear test

Table 4.9 Lap shear properties with gap < 50 µm

Specimen No	Load per unit length (N mm ⁻¹)		
	Al/GI	Al/GA	Al/uncoated
S1	180±5 (undercut)	120 ±5 (interface)	110±5 (interface)
S2	176±5 (undercut)	126±5 (interface)	105±5 (interface)
S3	178±5 (undercut)	118 ±5 (interface)	106±5 (interface)

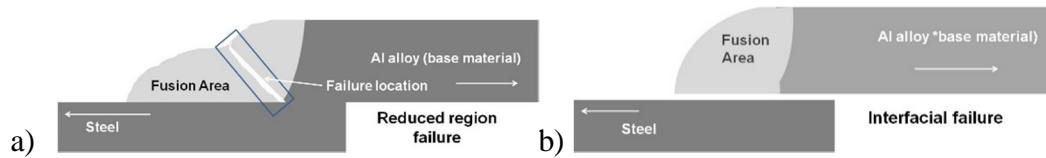


Figure 4.16 Schematic of different modes of failure a) reduced region failure and b) interfacial failure.

Results of lap shear tests of brazed specimens for above mentioned condition with an interfacial gap of $< 50 \mu\text{m}$, fracture load per unit length and location of failure are given in Table 4.9. Joints with galvanized steel behaved differently compared to joints with galvanized and uncoated steel in terms of load bearing capacity and failure location. Two modes of failure are recorded as shown in Fig 4.16 a) reduced region failure and b) interfacial failure. It is observed that under similar heat input/brazing conditions the joint with galvanized steel performed better compared to joints with galvanized and uncoated steel. The load bearing capacity of joints with galvanized steel at an average of 178 N/mm is higher compared to that of joints with galvanized and uncoated steel with an average of 120 and 107 N/mm , respectively. Joints with galvanized steel failed in the undercut (reduced) region, whereas joints with galvanized and uncoated steel recorded interfacial failure. It has been reported in the literature that joint load bearing capacity is dependent on bead width and wetting angle[4]. Lesser bead width and improper wetting lead to interfacial failure in joints made with galvanized and uncoated steel. In case of galvanized steel due to better wetting width the interface is stronger than the braze bead, the braze bead is weaker due to reduced thickness in the undercut region and due to Zn accumulation. The zones of Zinc vaporization are leaving a crevice at head and foot regions which acts as stress concentration location and propagation point leading to failure.

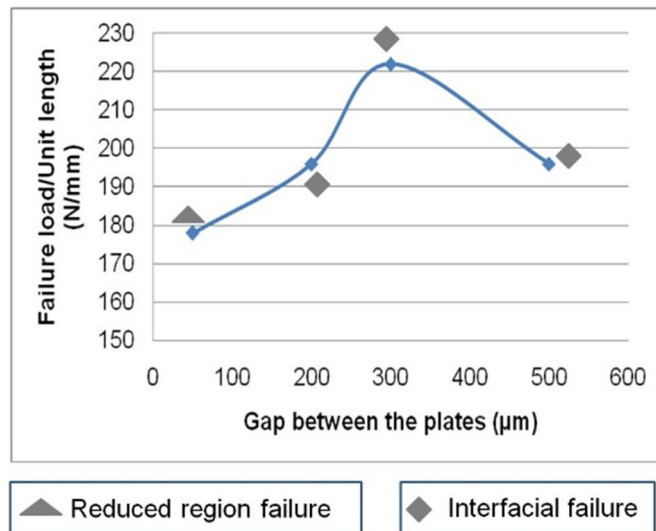


Figure 4.17 Variation in fracture load with gap between the plates.

Table.4.10 Variation in tensile properties with gap between the plates

Specimen	Fracture Load per unit length (N/mm) with variation in gap (failure location)			
	< 50 μm	200 μm	300 μm	500 μm
S₁	180±5 (undercut)	196±5 (interface)	222±5 (interface)	198 ±5 (interface)
S₂	176±5 (undercut)	197±5 (interface)	222±5 (interface)	195±5 (interface)
S₃	178±5 (undercut)	195±5 (interface)	220±5 (interface)	196±5 (interface)

As shown in Fig 4.12 the crevice formation due to Zn vaporization acted as a stress riser leading to failure. The intensity of crevice formation can be minimized by maintaining interfacial gap between the plates allowing the zinc vapours to escape. Joints were made by maintaining a gap of 200 μm, 300 μm and 500 μm. The metallographic analysis of the transverse cross-sections of the joints indicated negligible effect of gap on macrostructural and microstructural features of the joints but influenced the mechanical properties. Fig 4.17 shows the effect of gap on mechanical properties of the joint. The variation in fracture loads with gap and failure locations are indicated in Table 4.10. 9.5% & 24.7% increment in fracture load is observed with increase in gap to 200 μm and 300 μm, respectively and the

failure location is shifted from undercut region failure (Fig 4.16a) at lesser gap to interfacial failure (Fig 4.16b) at higher gap conditions. Zn vapours formed escaped through the gap, resulting in nearly a crevice free joint. Hence, the reduced crevice formation may be the cause for improved mechanical performance of the joints at higher gap conditions. Das et al [5] reported the joint strength of 250 N/mm for friction stir lap welding of AA6061-T6 (2 mm thick)/HIF-GA (1 mm thick). Zhang et al.[6] reported a joint strength of 96 MPa in a cold metal transfer brazing of wrought 6061 aluminium alloy and galvanized low carbon steel. The strength values are comparable to that of values reported in the literature with more advanced joining techniques. Zhang et al. [3] also reported that joints made with Zn coated steel show better performance than joints made with aluminised steel.

4.4.3.4 Fractography

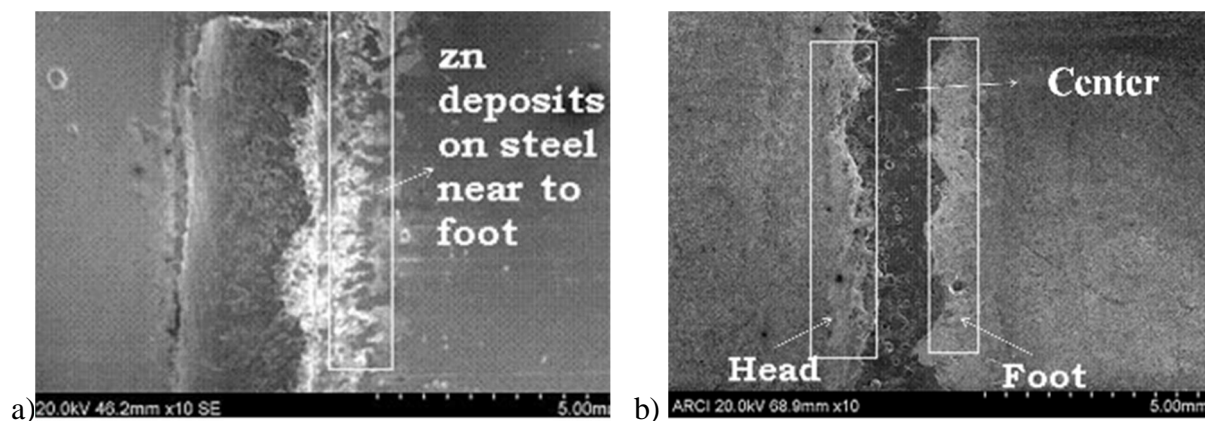


Figure 4.18 SEM macrographs of fractured surfaces a) undercut region failure (Al/GI steel) and b) interfacial failure (Al/GI, Al/GA steel, Al/uncoated steel).

Al/steel specimens tested under lap shear condition recorded two modes of failure as shown in Fig 4.16 - a) reduced region failure (Al/GI steel) and b) interfacial failure (Al/GI, Al/GA & Al/uncoated steel) (Fig.4.16b, 4.18b). The fractured surfaces are observed under SEM for knowing the nature of failure and chemical composition at the point of failure. Crevice formed due to Zn vaporization at foot region (Fig 4.12b) is the crack initiation site that propagated into the braze bead resulting in failure in reduced region as shown in Fig 4.16a.

Zn in its oxide form is detected adjacent to failure region (Fig 4.18a). Fig 4.18b shows the macrograph of interfacial failure. The surface of the interfacial failure shows a black band region with white border. The white bands at head and foot regions reveal the presence of Zinc in the form of oxide. This corroborates our inference on effect of Zn entrapment on joint strength explained in earlier section. Further investigation of the interfacial failure surface revealed the presence of high amount of Al and Si on the failed surface indicating the failure in filler metal. The magnified image taken at the central region of interfacial fracture surface of Al/GI & Al/GA steel joints (Fig 4.19a), Al/uncoated steel (Fig 4.20a) reveals somewhat ductile failure. Elemental mapping carried out in these regions showed the presence of Al (Figs 4.19, 4.20b) and Si (Figs 4.18d, 4.19d) in high amounts with little Fe (Figs 4.19b, 4.20 b). The spot analysis conducted in these regions also revealed the presence of nearly 90-98 % of Al (Tables 4.11 & 4.12) in the failed region. Hence, failure in Solidified filler metal is observed in case of interfacial failures.

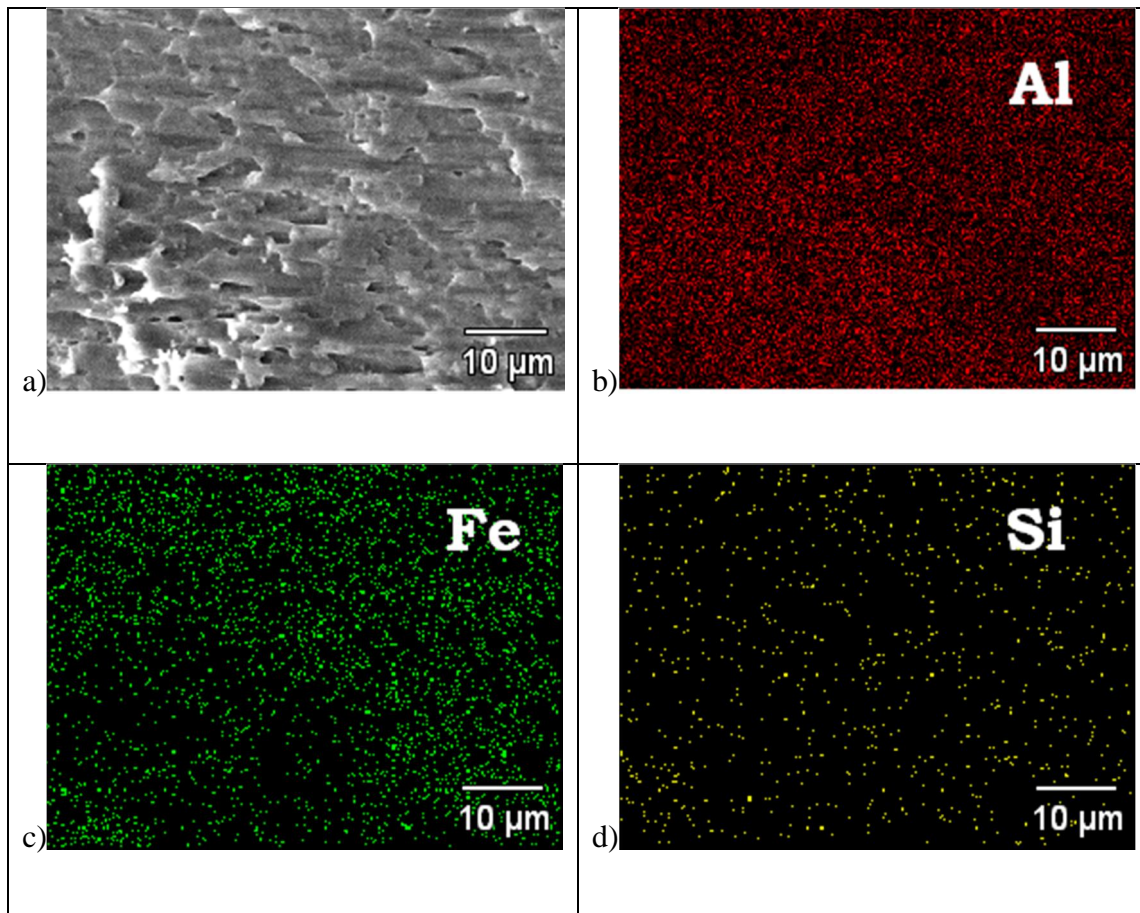


Figure 4.19 Elemental mapping at central region of interfacial failure (Al/GI & Al/GA steel) a) image indicating location of elemental mapping b) Al distribution c) Fe distribution and d) Si distribution.

Table 4.11 EDS spot analysis at central region (Al/GI & Al/GA steel)

Pt No	Atom %			
	Al	Fe	Si	Zn
1	96.15	1.73	1.69	0.43
2	96.54	2.08	0.99	0.39
3	91.44	7.75	0.71	0.10

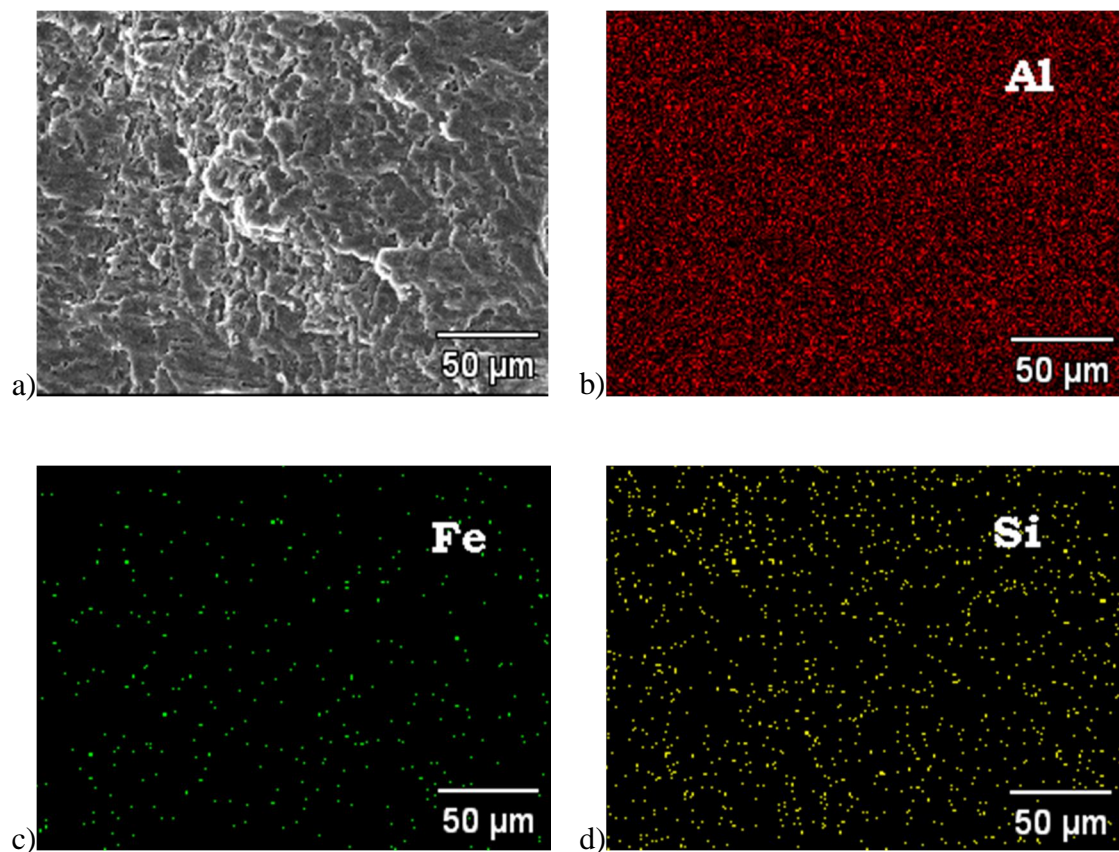


Figure 4.20 Elemental mapping at central region of interfacial failure (Al/uncoated steel) a) image indicating location of elemental mapping b) Al distribution c) Fe distribution and d) Si distribution.

Table 4.12 EDS spot analysis at central region of interfacial failure (Al/uncoated steel)

The figure is a composite image. On the left is a scanning electron micrograph (SEM) showing a textured surface with three regions of interest labeled 1, 2, and 3. Region 1 is on the left, region 2 is in the center, and region 3 is at the bottom. On the right is an EDS analysis table. The table has columns for 'Pt', 'Atom %', and five elements: 'Al', 'Fe', 'Si', and 'Zn'. The rows are numbered 1, 2, and 3, corresponding to the regions in the SEM image. The table data is as follows:

Pt	Atom %				
No	Al	Fe	Si	Zn	
1	97.56	1.17	0.92	0.34	
2	91.54	3.87	3.75	0.85	
3	98.13	0.47	0.99	0.40	

Figure 1. SEM image of the surface of the Pt/Al₂O₃/Fe₃O₄/SiO₂/ZnO nanocomposite. The inset shows the EDS analysis of the surface of the nanocomposite.

Based on the above results it may be summarized that in P-GMA weld-brazing, surface chemistry/condition of base material and interfacial gap have significant effect on wetting

behaviour, thickness and morphology of the interfacial IMC layer and porosity formation, which in turn affected the mechanical strength of the joint. The fractographic analysis also showed different chemistry in different layers that formed at the interface which needs further investigation to understand their influence on interface strength. Further, the results provide an insight into the types of failure and the weaker zones, which can be effectively used in altering the joining process and optimizing the mechanical performance of the joints. The load bearing capacity of P-GMA weld brazed fillets of 230 N/mm of bead length is quite an useful value for designers to consider incorporating in appropriate body applications.

4.4.3.5 Summary

- Pulsed-GMAW process can be used as a joining technique for dissimilar aluminium-steel combination
- Wetting and spreading behaviour is altered by the surface chemistry of steel. Presence of zinc coating on steel enhances the wetting and spreading behaviour of steel than in the form of iron zinc alloy in case of galvanized steel.
- The thickness and morphology of the intermetallic compounds formed are dependent on energy intensity and distribution.
- Joints made with galvanized steel showed stronger interface due to better wetting and recorded highest fracture load among the three steels.
- Increase in interfacial gap aided in minimizing the undercut (reduced region) in the bead and also in minimizing the entrapment of Zn vapours in the bead.
- Overall, the load bearing capacity at 230 N/mm is highest in the Al-galvanized steel lap fillet joints made with an Al-steel interfacial gap of 300 μm .

4.4.4 Effect of filler wire composition

4.4.4.1 Macrostructure

Fig 4.21 shows the transverse cross section SEM macrograph of the Al/steel brazed joint made with Al-12%Si filler wire. In the present context the molten pool generated by melting of filler wire and melting of the aluminium base material wets the steel surface to form a leak proof braze joint. Bead geometry measurements, wetting width and contact angle are reported in Tables 4.6 & 4.13.

Under similar braze-welding conditions the joints made with Al-12%Si (Fig 4.21) filler recorded higher wetting and spreading than Al-5%Si (Fig 4.11a) filler wire as seen from increased wetting width and decreased wetting angle. Enhanced fluidity of the molten metal pool due to higher Si content in case of Al-12%Si filler may have probably resulted in more spreading and wetting compared to Al-5%Si filler wire.

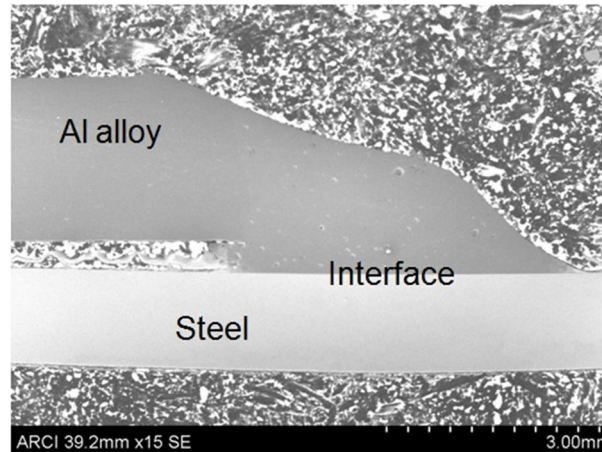


Figure 4.21 Transverse cross-section SEM macrographs of Al/steel brazed joints made with Al-12%Si filler.

Table 4.13 Bead geometry measurements

Sino	Bead geometry measurements	Range
		Al-12%Si
1	Bead width (mm)	4.5-4.6
2	Bead height (mm)	1.6-1.7
3	Wetting angle ($^{\circ}$)	19-20

4.4.4.2 Microstructure

In an aluminium-steel lap-fillet joint the regions of interest for microstructural analysis are braze bead, bead/Al alloy interface and bead/steel interface as they affect the strength of the joint. The braze bead structure and bead/Al interface are similar to micrographs shown in Fig 4.7 a & b.

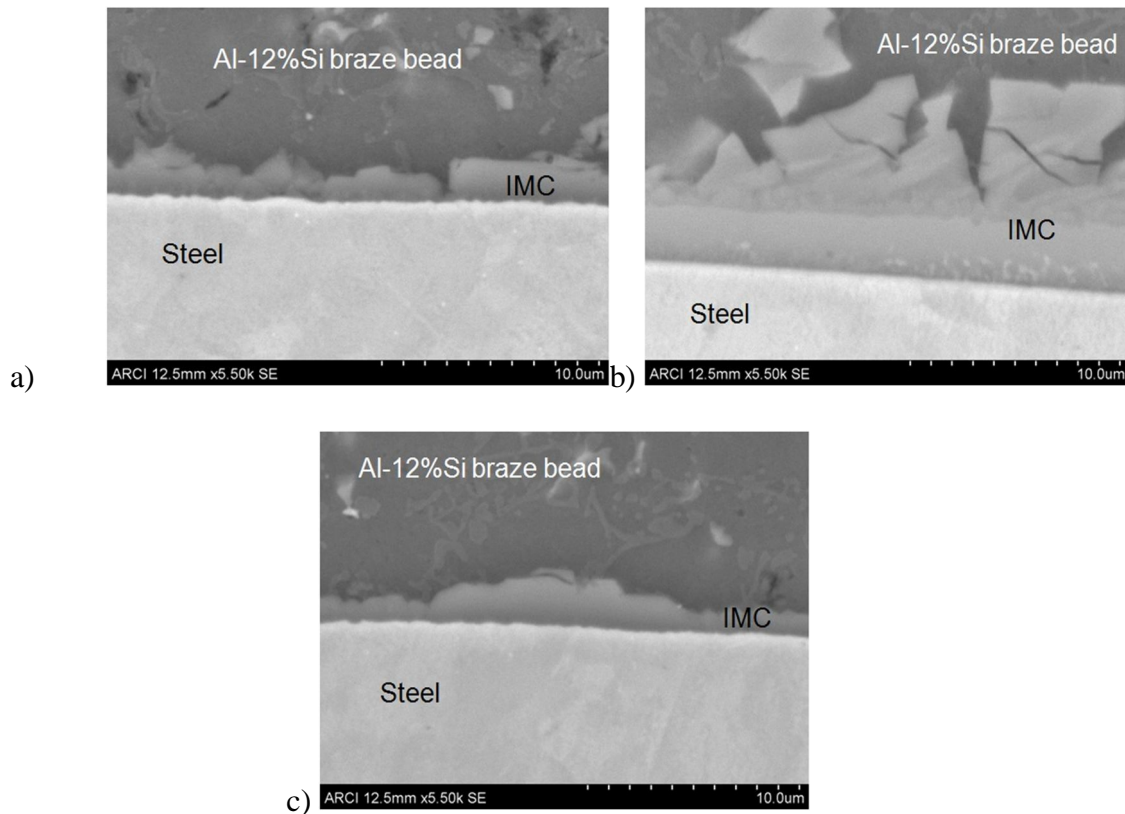


Figure 4.22 SEM micrographs at different locations of bead/steel interface at 5.5 kX magnification a) head region, b) center region and c) foot region.

Different regions of microstructural interest in bead/steel interface are head, center, foot and zinc rich region as shown in Fig 4.8. During brazing operation the elemental zinc present on the surface of steel evaporates and tries to escape from gap between the plates and condenses near the head and foot regions. At the same time higher solubility limit of zinc in aluminium compared to that of iron enables Al-Zn solution formation. It exerts a pulling action at solid-liquid-vapour triple line which enhances the triple line velocity resulting in improved spreading and wetting of molten pool on steel surface.

The reaction between solid Fe and Al-Si melt resulted in intermetallic compound (IMC) layer formation at bead/steel interface. The bead/IMC layer interface shows serrated nature whereas IMC layer/steel interface is almost flat in all the cases (Figs 4.16 & 4.22). The joints made with Al-12%Si (Fig 4.22d, e, f) filler wire recorded thicker IMC layer than joints made from Al-5%Si filler (Fig 4.15a, b, c). Al-12%Si is the eutectic composition and its melting temperature is around 577 °C whereas the melting temperature of Al-5%Si composition is around 600 °C. Hence, Al-12%Si melt Solidifies below 577 °C and Al-5%Si melt Solidifies below 600 °C. It indicates that Al-12%Si melt is in molten state for slightly longer time than Al-5%Si melt promoting diffusion and growth of IMC layer. The IMC layer varied in morphology and thickness along the interface. The central region experiencing high heat intensity recorded thicker IMC layer (Fig 4.15b & 4.22b). The head region (Fig 4.14a) with Al-5%Si filler wire shows two layers; one is white in colour and the other is dark grey in colour. The central region (Fig 4.15b) shows three layers, one is white region, second is grey region and the third is dark grey region with needles. The foot region (Fig 4.15c) shows similar layers like head region. It is observed that the dark grey region extends into aluminium melt with needle like protrusions with sharp edges in head (Fig 4.15a) and foot regions (Fig 4.15b), slightly rounded edges at the central region (Fig 4.15c). The head region (Fig 4.22a) of the joint made with Al-12% Si filler wire has 2 layers one in pale white colour towards steel side and the other in light grey colour towards the aluminium bead side. The central region (Fig 4.22b) comprises of 3 layers one in pale white colour towards steel side, second is a light cream colour band at the center and the third is light grey colour layer towards the aluminium melt. The foot region (Fig 4.22c) resembles head region. In this case the light grey colour region is slightly discontinuous and wavy towards the aluminium side rather needle like protrusions in case of joints made with Al-5%Si filler wire. The light grey region at the center shows polyhedral shaped particles arranged in a row to form a layer.

4.4.4.3 Electron Probe Micro Analysis

Fig 4.23 shows the elemental composition graphs obtained from electron probe micro analysis. It is observed that the joint interface comprises of only the combination of aluminium, iron and silicon. It is also envisaged that joints made from 4047 filler wire is richer in Si content compared to joints made from 4043 filler wire. The higher Si content in the filler wire might have resulted in enhanced Si content at the joint interface.

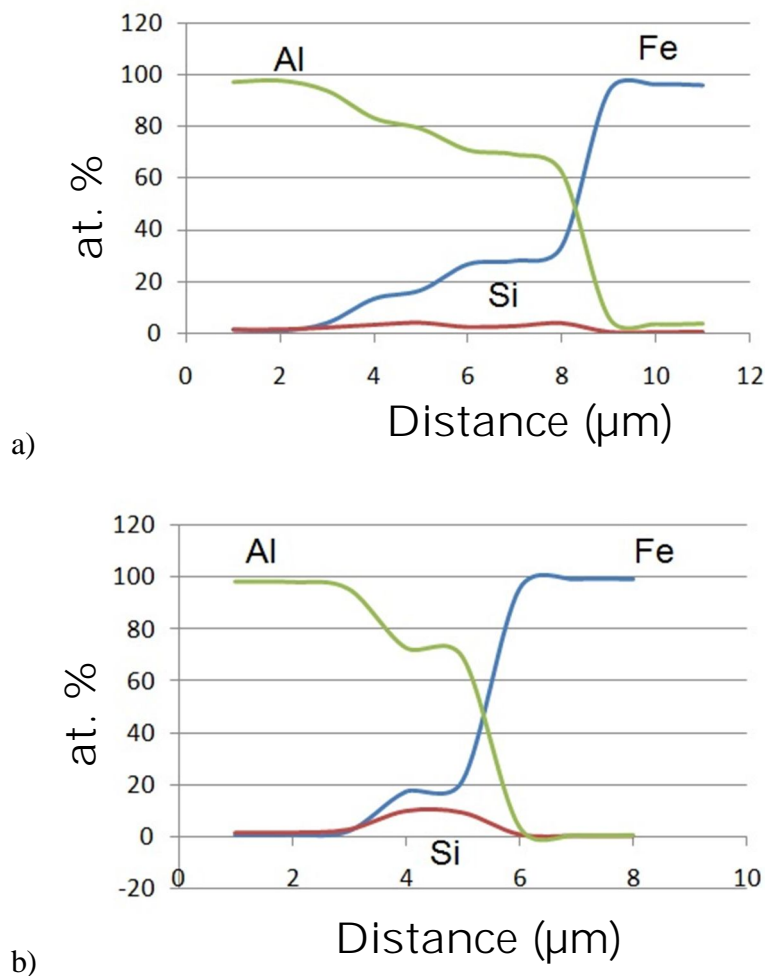


Figure 4.23 EPMA plots across the joint interface for joints made with two different filler wires a) 4043 and b) 4047.

4.4.4.4 Lap shear test

The fracture load and failure location obtained in lap shear tests of the specimens brazed with above mentioned conditions are reported in Tables 4.10 & 4.14. It is observed that the load bearing capacity of the joints brazed with Al-12%Si filler is high than the joints made with al-

5%Si filler wire. Nearly 10% increment in fracture load is recorded for the joints made with Al-12%Si filler wire. Two types of failure modes, a) interfacial failure and b) bead failure have been recorded. The joints brazed with Al-5%Si recorded interfacial failure at a fracture load of 222 N/mm and the joints made with Al-12%Si filler recorded bead failure at a fracture load of 245 N/mm. The improved wetting and spreading caused due to increased fluidity of the molten pool due to high Si content in the filler wire might probably be the reason for enhanced joint strength.

Table 4.14 Lap shear test results

S.No	Specimen id	Joint strength (failure load/unit length, N/mm)
1	S ₁	240±5 (bead)
2	S ₂	245±5 (bead)
3	S ₃	242±5 (bead)

4.4.5 Effect of heat input

4.4.5.1 Macrostructure

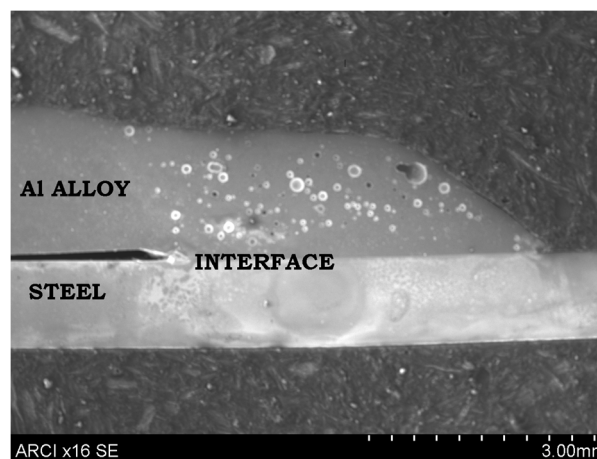


Figure 4.24 Transverse cross-section SEM macrographs of Al/steel brazed joints made with Al-5%Si filler at a wire feed rate of 4 m/min and speed of 1.2 m/min.

Fig 4.24 shows transverse cross sectional macrostructure of lap fillet joint made with Al-5%Si filler at a wire feed rate of 4 m/min and speed of 1.2 m/min. Bead geometry

measurements are given in Table 4.15. The bead height has increased with increase in wire feed rate to 4 m/min (Fig 4.24) compared to the joint made at a wire feed rate of 3.5 m/min (Fig 4.11a). However the neck region is still observed at the fusion boundary.

Table 4.15 Bead geometry measurements

S.No	Bead geometry parameters	Wire feed rate (4 m/min)
1	Bead width (mm)	4.3-4.4
2	Bead height (mm)	1.8-1.9
3	Wetting angle (°)	40-43

4.4.5.2 Microstructure

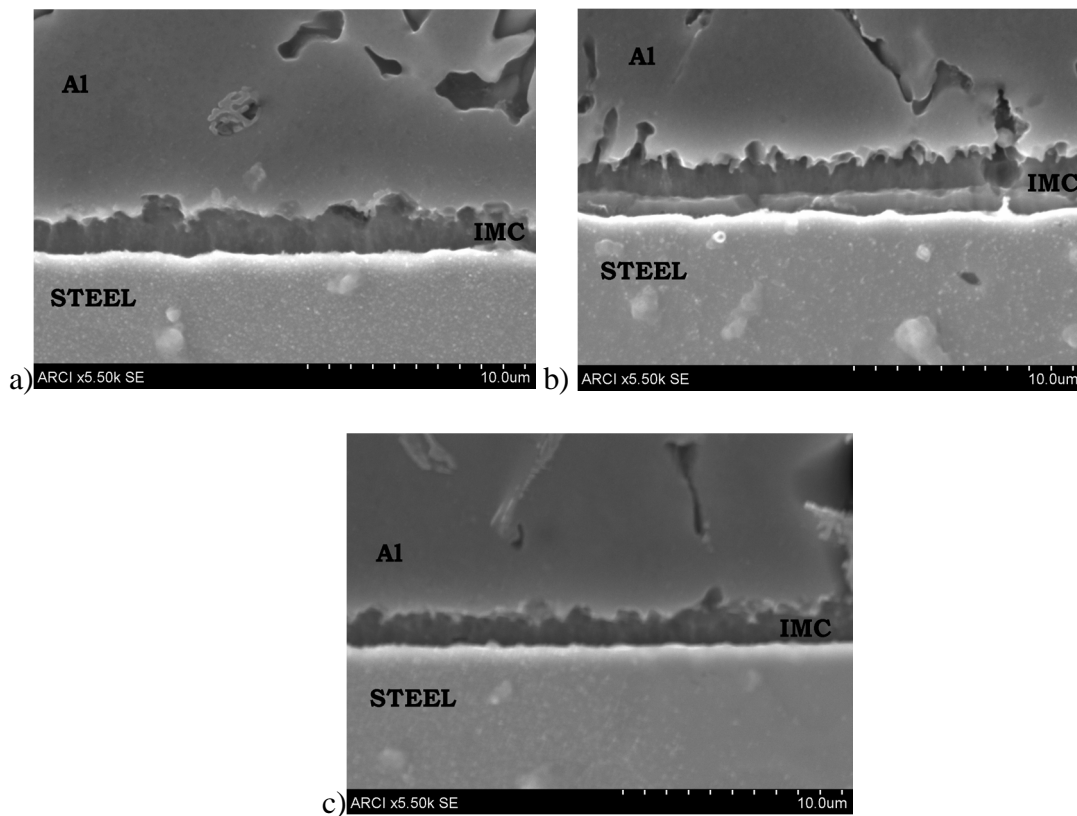


Figure 4.25 SEM micrographs of Al/steel joints at different regions of the steel/bead interface made with Al-5%Si filler wire at a wire feed rate of 4 m/min - a) head b) center and c) foot.

Table 4.16 IMC layer thickness at various locations of bead/steel interface at a wire feed rate of 4 m/min

S.No	Location	IMC thickness (μm)
1	Head	1.9-2.3
2	Center	3.2-3.8
3	Foot	1.8-2.2

The joint comprises of different regions. Bead - the fillet formed by Solidifying filler metal and the Al-steel interface. Different regions of the steel/bead interface are indicated in the schematic given Fig 4.8.

Al/bead interfaces for the wire feed rate 4 m/min are shown in Fig 4.25. Intermetallic compound (IMC) layer formed at the interface is clearly seen in all the cases. The thickness of the IMC layer is varying from head to foot region. Thickness values in different regions are given in Table 4.16. Center (Fig 4.25b) showed higher IMC layer thickness compared to that of head (Fig 4.25a) and foot (Fig 4.25c) regions. Higher energy intensity in the central region of arc may be resulting in more dilution from steel side.

IMC morphology also varied from head to the foot region. The central region had three distinct layers and needle like structures protruding into the bead, whereas the head and foot regions showed only two distinct layers and needle like structures. These needles in head and foot regions are smaller than needles in the central region. High resolution image of typical interface is shown in Fig 4.7g. The bright region along the steel-bead interface is seen in all the interfaces. Above this is seen a light grey colored layer and above that is a dark grey colored layer above which the needles of same color are protruding into the bead. The center region showed all the layers and needles. But, the head and foot regions showed only two layers followed by needles. Hence, the interface at the center is different from the interface at the head and foot regions. In an arc, the central portion is at higher intensity than the

periphery. This could be the reason for the above variation in interface morphology. It is observed that increased heat input showed negligible effect in terms of IMC layer growth but altered the morphology of the IMC layer towards aluminum side compared to low heat input. Sharpness of the needles reduced with increase in heat concentration. That is, under low heat input conditions, central region showed rounded needle compared to head and foot that showed sharp needle structure (Fig 4.11 a, b, c). Decreased cooling rates or increased heat input might be the reason for morphology alteration (Fig 4.25 a, b, c).

4.4.5.3 Lap shear test

Table 4.17 Lap shear test results at 4 m/min wire feed rate

S.No	Specimen No	Load per unit length (N/mm)	
		Pulsed-MIG	Failure location
4	S ₁	210±5	Interface
5	S ₂	212±5	Interface
6	S ₃	207±5	Undercut/reduced bead height zone

The joints made with Al-5%Si filler wire and at a wire feed rate of 4m/min and at a gap of around 300 μ m recorded the joint strength in the range of 207-212 N/mm. It recorded two types of failure that is interfacial and reduced region failure as shown in Fig 4.16. The joint strength is less than the joints made at wire feed rate of 3.5 m/min. The increased IMC layer thickness and possibly the phases involved at the bead/steel interface resulted in lesser joint strength in case of joints made with wire feed rate of 4 m/min. The intensity of groove formation is reduced with increase in wire feed rate but is not avoided completely. The groove acting as a weak zone might have led to failure in some cases.

4.5 Phase analysis

Various methods of phase identification especially micro area, selective area diffraction techniques like EBSD, TEM and micro area x-ray diffraction were employed. But the

requirement of fine polishing and selective area thinning in EBSD and TEM restricted the applicability of these techniques to phase identification. Hence, micro area x-ray diffraction is found successful in phase identification and the results are reported in the following section. There is very limited literature on interfacial phase analysis using the above mentioned techniques. Especially, the interfacial phase study of P-GMAW braze-welded aluminium/steel joints is not reported in the literature.

The crystal structure of steel is BCC, 6061 and 4043 aluminium alloys are FCC. Two conditions arise under the present context:

- Molten 4043 and 6061 on partially melted 6061 aluminium alloy (similar crystal structure)
- Molten 4043 on BCC steel surface (dissimilar crystal structure)

On steel side the base metal grains of BCC iron act as nucleation site and on aluminium side the partially melted grains of base metal FCC aluminium act as nucleation site. It is well known that the ratio G/R (temperature gradient/growth rate) determines the Solidification mode in a weld. The G/R ratio is high at the fusion line and less at the center line. Hence the Solidification mode changes from planar to cellular, cellular to columnar dendrites, and columnar dendrites to equiaxed dendrites. In the present case the base metal grains of BCC iron acting as nucleation site and due to high G/R at fusion line favours planar growth. The IMC layer grows in planar solidification mode, followed by initiation of cellular mode. Over this the Al-Si melt grows in a columnar dendritic fashion, perpendicular to the bead/steel interface as shown in Fig 4.22c. At center line the equiaxed dendrites grow in all directions and the columnar dendrite growth is restricted by the growing equiaxed dendrites.

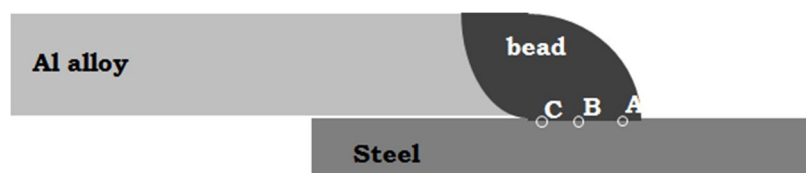
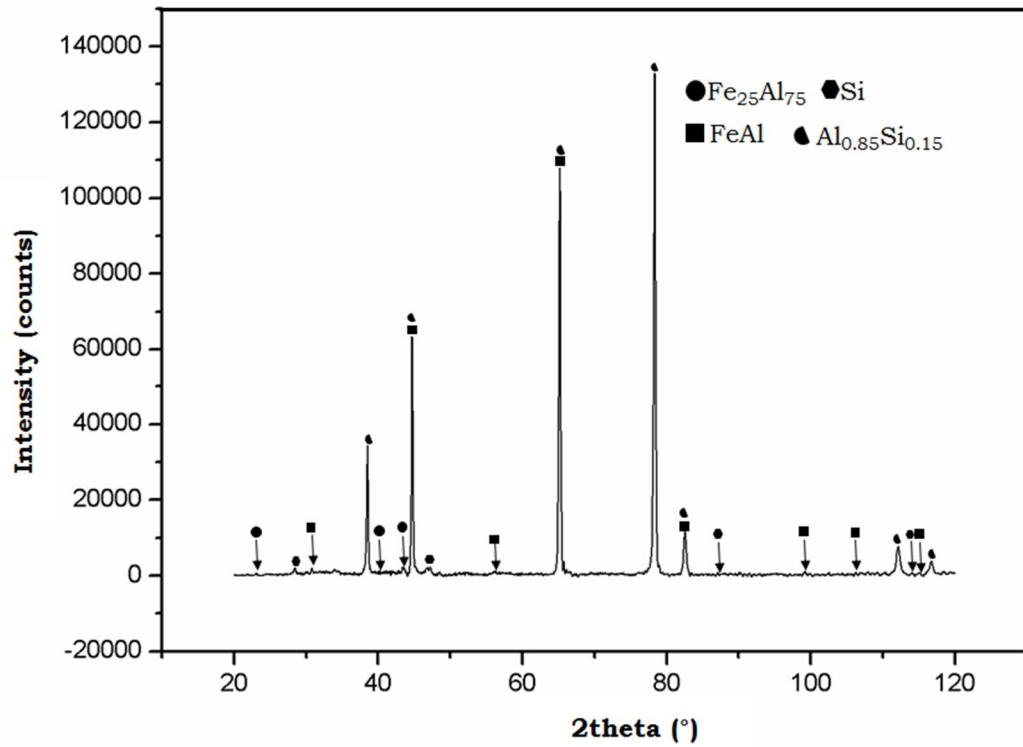
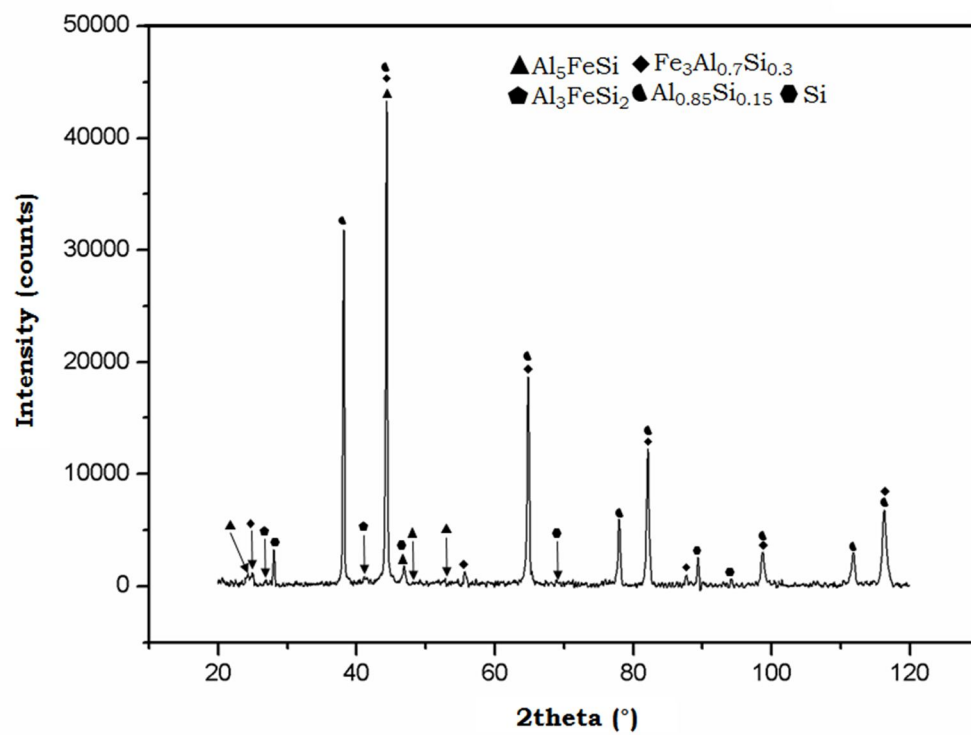


Figure 4.26 Schematic indicating locations of x-ray diffraction A) head B) center C) foot.

Fig 4.26 shows various locations of micro area x-ray diffraction study. From the above mentioned results it is found that the IMC layer morphology is found to vary along the bead/steel interface. Hence, the micro area x-ray diffraction study is carried out at three different locations as indicated in Fig 4.26.

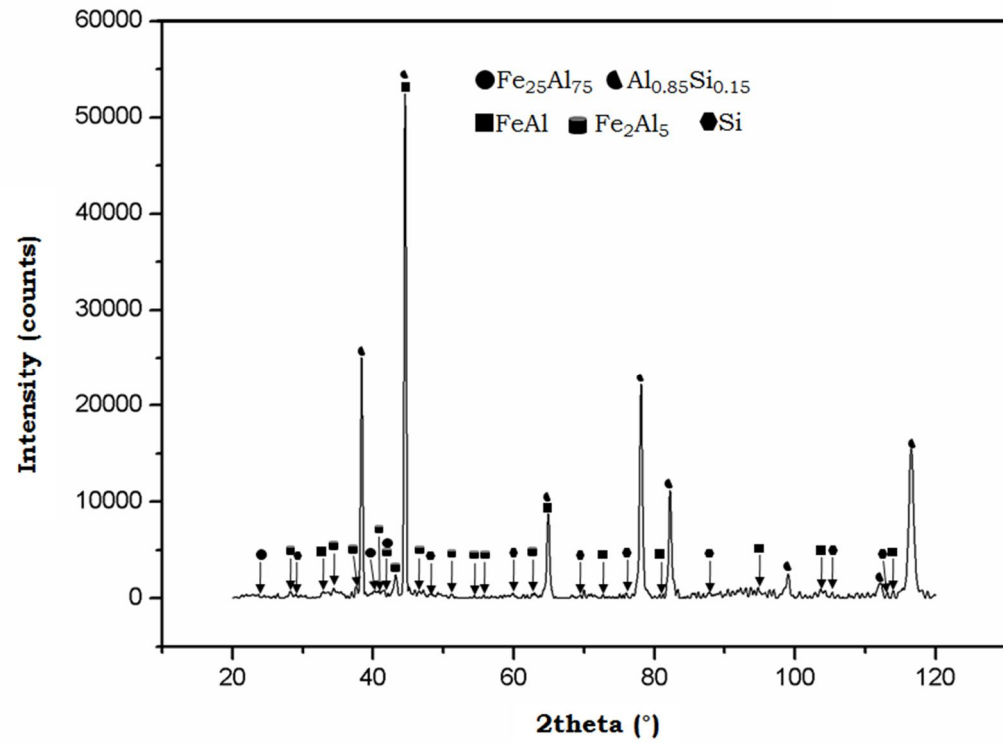


a)

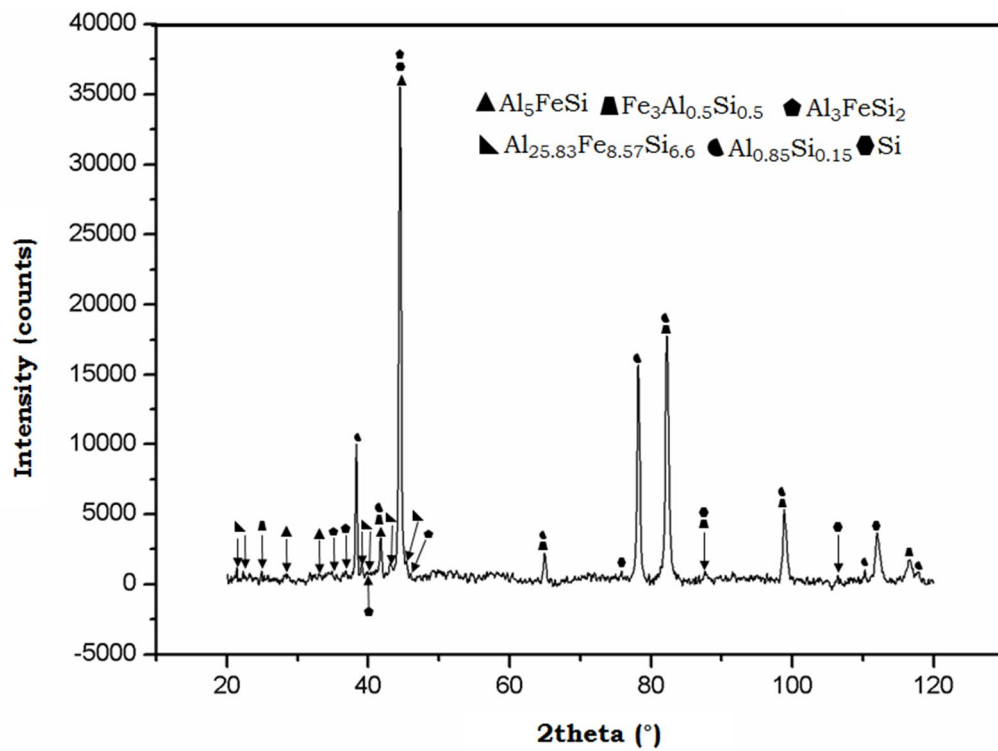


b)

Figure 4.27 Micro area XRD patterns of head region of bead/steel interface made with two filler wires a) Al-5%Si filler b) Al-12%Si filler.

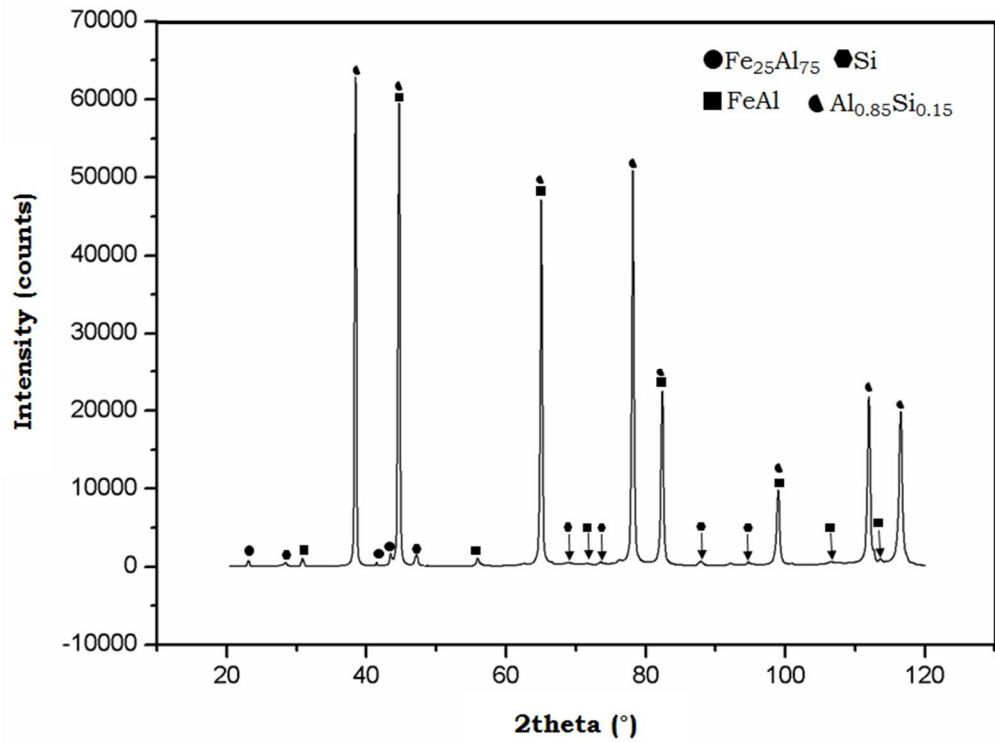


a)

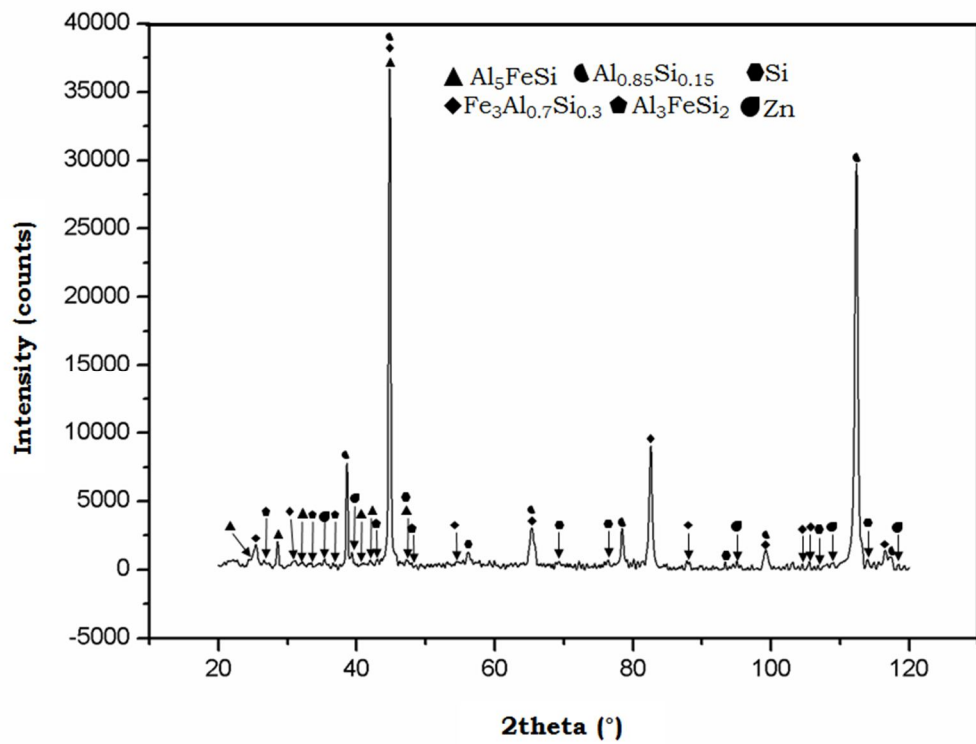


b)

Figure 4.28 Micro area XRD patterns of central region of bead/steel interface made with two filler wires a) Al-5%Si filler b) Al-12%Si filler.



a)



b)

Figure 4.29 Micro areas XRD patterns of foot region of bead/steel interface made with two filler wires a) Al-5%Si filler b) Al-12%Si filler.

Agudo et al.[7] studied the interfacial IMC phases formed in the butt joints of AW5182-H11 aluminium alloy and Zn coated DX54D steel made using Al99.5, AlMn₁, AlSi₅, AlSi₃Mn₁ filler materials using EBSD and TEM. It has been shown that the joints made with Al99.5 and AlMn₁ filler wire possess 4 µm thick IMC layer and is comprised of Fe₂Al₅ and Fe₄Al₁₃ towards the steel and filler side respectively. It is also reported that the joints made with AlSi₅ and AlSi₃Mn₁ restricts the growth of IMC layer to 2.5 µm and is comprised of AlFeSi ternary compound along with Fe₂Al₅ and Fe₄Al₁₃. Peyre et al.[8] also reported the presence of Fe₂Al₅ and FeAl₃ using EDS analysis. Zhang et al.[3] studied the fractured surface using XRD and reported the presence of Fe₄Al₁₃ and Fe₃Al_{0.7}Si_{0.3} at the interface. Murakami et al.[9] showed the presence of Fe₂Al₈Si on the fractured surface of steel using XRD analysis. Park et al.[10] using EDS analysis of the interface showed the presence of FeAl₃ and Fe₂Al₅. Figure 4.27 to 4.29 shows the x-ray diffraction patterns of the bead/steel interface made with Al-5%Si filler wire and the chemical composition of the IMC phases are given in Table 4.18. It reveals the presence of FeAl (cubic), Fe₂Al₅ (orthorhombic), Fe₂₅Al₇₅ (monoclinic) Al_{0.85}Si_{0.15} (cubic), Si (Cubic at central (Fig 4.28a) region and FeAl (cubic), Fe₂₅Al₇₅ (monoclinic), Al_{0.85}Si_{0.15} (cubic), Si (Cubic) at head (Fig 4.27a) and foot (Fig 4.29a) region. It is mentioned that the head and foot regions recorded two layered interface whereas central region showed three layered interface. From EPMA it is observed that across the interface, the concentration of Fe is found to be high towards steel side and decreases going towards the bead side. Therefore, the cubic FeAl phase is most likely to be present towards the steel side of the interface (white region in Fig 4.15 a, b, c) and Fe₂₅Al₇₅ being rich in Al among the phases present is most likely to be present towards the bead side of the interface (dark grey region with needle like protrusions in Fig 4.15 a, b, c). Along with these phases the central region has an additional light grey region adjacent to the white region (Fig 4.15b). This layer is in between white and dark grey region and is supposed to possess slightly more Fe content than white layer and

slightly less Al content than dark grey region. As observed from x-ray diffraction patterns it may be represented to be Fe_2Al_5 phase. Hence, the white layer towards steel is FeAl , followed by light grey region of Fe_2Al_5 followed by $\text{Fe}_{25}\text{Al}_{75}$ towards the bead side of the interface at central region and FeAl towards steel side and $\text{Fe}_{25}\text{Al}_{75}$ towards bead side of the interface at head and foot regions. The adjacent layer to steel being cubic renders the steel/IMC interface flat and the adjacent layer to bead is monoclinic renders the IMC/bead interface weak. The diffraction spot of size $10\text{ }\mu\text{m}$ focuses bead also along with the interface. Hence Al-Si based binary phase is coming from the bead. Si being inherently present in the filler wire and one of the major reaction products of the ternary Al-Fe-Si system, is predominantly seen in x-ray diffraction patterns.

Table 4.18 Details of intermetallic phases formed

S.No	Phase	Composition (at. %)			Crystal structure	Enthalpy of formation (kJ/mol)
		Al	Fe	Si		
	FeAl	50	50	-	cubic	-32.1564
	$\text{Fe}_{25}\text{Al}_{75}$	75	25	-	monoclinic	-19.1799
	Fe_2Al_5			-	orthorhombic	-21.8547
	$\text{Fe}_3\text{Al}_{0.5}\text{Si}_{0.5}$	12.50	75	12.50	cubic	-18.2414
	$\text{Fe}_3\text{Al}_{0.7}\text{Si}_{0.3}$	17.50	75	7.50	cubic	-19.9806
	Al_5FeSi	71.43	14.29	14.29	monoclinic	-14.835
	$\text{Al}_{25.83}\text{Fe}_{8.57}\text{Si}_{6.6}$	63	20.90	16.10	rhombohedral	-22.3587
	Al_3FeSi_2	50	16.67	33.33	tetragonal	-10.0945

Figs 4.27 to 4.29 shows the x-ray diffraction patterns obtained from the bead/steel interface of the joints made with Al-12%Si filler wire. It reveals the presence of $\text{Fe}_3\text{Al}_{0.7}\text{Si}_{0.3}$ (cubic),

Al_5FeSi (monoclinic), $\text{Al}_{0.85}\text{Si}_{0.15}$ (cubic), Si (cubic), trace amounts of Al_3FeSi_2 (tetragonal) at head and foot regions, $\text{Fe}_3\text{Al}_{0.5}\text{Si}_{0.5}$ (cubic), $\text{Al}_{25.83}\text{Fe}_{8.57}\text{Si}_{6.6}$ (rhombohedral), Al_5FeSi (monoclinic), $\text{Al}_{0.85}\text{Si}_{0.15}$ (cubic), Si (cubic) along with trace amount of Al_3FeSi_2 (tetragonal) at central region of the bead/steel interface. $\text{Fe}_3\text{Al}_{0.7}\text{Si}_{0.3}$ and $\text{Fe}_3\text{Al}_{0.5}\text{Si}_{0.5}$ are the form of Fe_3Al with different Al/Si ratios with Si substituting for Al. The central region experiencing more heat than head and foot regions might have resulted in slightly more substitution of Al with Si resulting in $\text{Fe}_3\text{Al}_{0.5}\text{Si}_{0.5}$ whereas at head and foot regions it is limited. This cubic phase is likely to be present towards the steel side of the interface (pale white region towards the steel side Fig 4.22 a, b, c). The phases Al_5FeSi and $\text{Al}_{25.83}\text{Fe}_{8.57}\text{Si}_{6.6}$ (Al_3FeSi approx.) are two phases with different Al/Fe ratio. Al_5FeSi being the richest in Al among the observed phases may be present towards the bead side of the interface (grey region towards bead side, Fig 4.22 a, b, c). At central region the white band between pale white and light grey region comprised of less Al content than light grey region and more Fe content than white layer. Hence this band may be of $\text{Al}_{25.83}\text{Fe}_{8.57}\text{Si}_{6.6}$. Cubic $\text{Fe}_3\text{Al}_{0.7}\text{Si}_{0.3}$ is present towards the steel side followed by Al_5FeSi towards the bead side at head and foot regions and cubic $\text{Fe}_3\text{Al}_{0.5}\text{Si}_{0.5}$ towards the steel side followed by rhombohedral $\text{Al}_{25.83}\text{Fe}_{8.57}\text{Si}_{6.6}$ followed by monoclinic Al_5FeSi towards the bead side. The tetragonal Al_3FeSi_2 is a reaction product that forms along with Al_5FeSi and hence is evident in trace amounts across the interface. X-ray spot covering some part of bead revealed the presence of Al-Si based binary phase in all the cases. Zn appears to have settled towards head and foot regions and hence is identified in x-ray diffraction pattern of head region. Agudo et al.[7] reported that the presence of Si in the filler wire restricts the growth of Fe_2Al_5 . Fe_2Al_5 grows along the c-axis by diffused Al atoms occupying the vacant sites along the c-axis. In presence of Si, the Si atoms diffuse into the vacant sites and restrict the Al atom diffusion into these sites, therefore restricting its growth. In the present study the joints made with Al-5%Si filler showed the presence of Fe_2Al_5

whereas in the joints made with Al-12%Si filler this particular Fe_2Al_5 phase is absent. Therefore, increase in Si content in the filler wire restricted the growth of deleterious Fe_2Al_5 phase.

Recent reports show that the complex Al-Fe-Si system comprises of nearly ten ternary intermetallic compounds and nineteen invariants reactions at various temperatures [11]. The following equations can explain the formation of the above identified interfacial IMC phases.

U_2 at 1120°C



U_4 at 1020°C



The phase Fe_2Al_3 is the high temperature phase which can be seen in Fe-Al binary phase diagram. This high temperature phase reacts with the liquid to form ordered FeAl and Fe_2Al_5 phase. Fe_2Al_5 then reacts with the liquid to form $\text{Fe}_4\text{Al}_{13}$ phase. The phase $\text{Fe}_{25}\text{Al}_{75}$ is similar to $\text{Fe}_4\text{Al}_{13}$ phase. There are reports that at 550°C Fe_2Al_5 can dissolve up to 2at%Si, $\text{Fe}_4\text{Al}_{13}$ can dissolve up to 4 wt.%Si and FeAl can dissolve up to 1-6 at.%. [11]. Few reports show that ordered FeAl can dissolve up to 16-17 at.% [11]. Hence, the solubility of sufficient amount of Si in the respective phases obtained may have resulted in the formation of Fe-Al based binary phases with Si solubility. Hence ordered FeAl, Fe_2Al_5 and $\text{Fe}_{25}\text{Al}_{75}$ are the reaction products of the above 1 & 2 eutectic reactions. The presence of phase T_1 is not detected. The T_1 phase may probably be present in trace amount and hence not detected in micro area x-ray diffraction pattern.

The joint interface of the samples made from 4047 filler wire recorded the presence of $\text{Fe}_3\text{Al}_{0.7}\text{Si}_{0.3}$, Al_5FeSi (T_6), Si, $\text{Al}_{0.85}\text{Si}_{0.15}$ towards head and foot regions and $\text{Fe}_3\text{Al}_{0.5}\text{Si}_{0.5}$, Al_5FeSi , $\text{Al}_{25}\text{Fe}_{8.57}\text{Si}_{6.6}$ (T_3/T_2 approx), Si, $\text{Al}_{0.85}\text{Si}_{0.15}$ at the central region. The trace amount of Al_3FeSi_2 (T_4) is also observed in all the regions. The isothermal section of Al-Fe-Si phase

diagram at 550 °C is shown in Fig 4.30 [12]. The Fe corner and Si corner does not show any significant intermetallic phases. The maximum ternary intermetallic phases are located or concentrated at the aluminium corner of the phase diagram. Fig 4.30 [12] reveals various phase fields in equilibrium. There are totally 10 ternary intermetallic phases and 19 invariant reactions taking place in this Al-Fe-Si system which makes it complex.

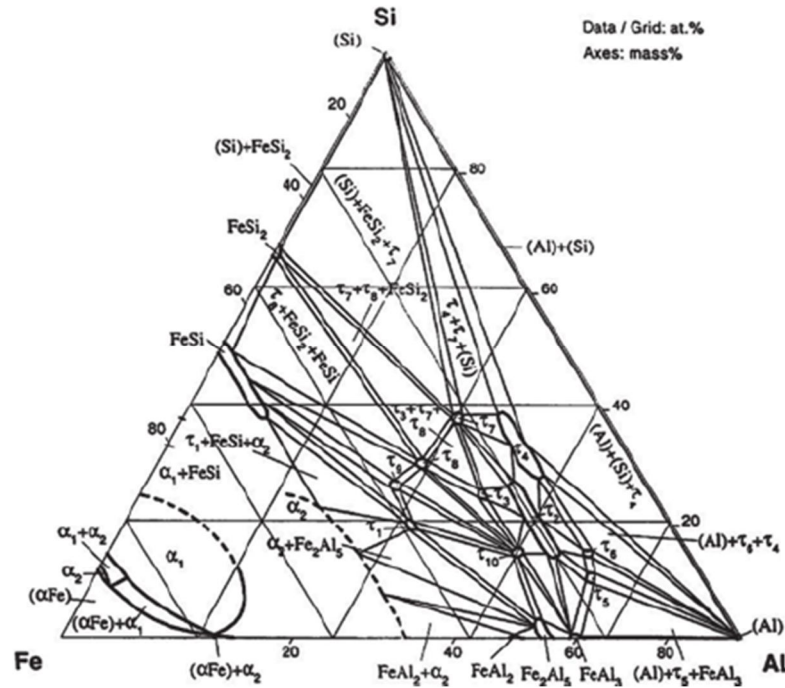


Figure 4.30 Isothermal section of Al-Fe-Si system at 550°C[12]

The following invariant reactions explain the formation of several ternary phases identified in the above micro area x-ray diffraction patterns.

Fe_3Al based compounds with little Si solubility like $\text{Fe}_3\text{Al}_{0.7}\text{Si}_{0.3}$ and $\text{Fe}_3\text{Al}_{0.5}\text{Si}_{0.5}$ were formed from the reaction mentioned in equation 3 with replacement of some Al with Si. This replacement is a diffusion aided process and the central region showed little more diffusion than head and foot region which is confirmed by their level of heat intensity. The central region of the sample experiences high heat intensity than head and foot regions due to bell shape of the arc. Hence the central region recorded slightly more diffusion of Si atoms resulting in ternary phase with slightly more amount of Si than head and foot regions.

U₁ at 1150 °C



Equation 3 also resulted in formation of Fe-Si based intermetallic compound. During analysis of the respective micro area x-ray diffraction patterns the presence of trace amounts of Fe-Si based binary compounds is noted. But the occurrence in trace amount made it highly difficult to be identified and indicated in x-ray diffraction patterns. Hence the binary Fe-Si based phases are not indicated in the above micro area x-ray diffraction patterns.

The following sequence of reactions may explain the formation of τ_2 τ_6 phase

P₂ at 940 °C



P₃ at 935 °C



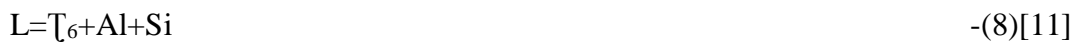
U₈ at 835 °C



U₁₂ at 600 °C



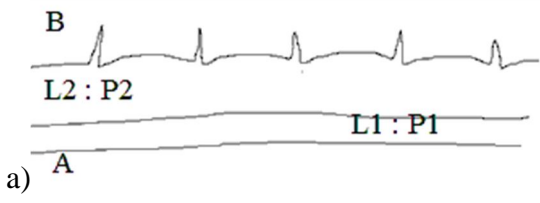
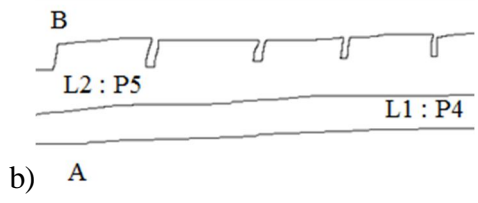
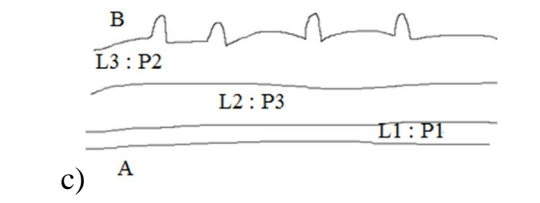
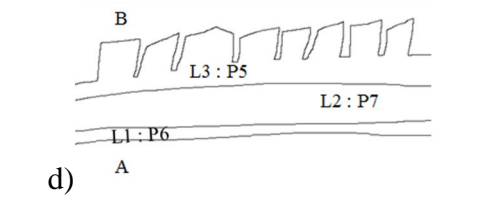
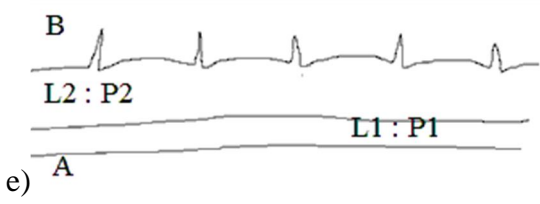
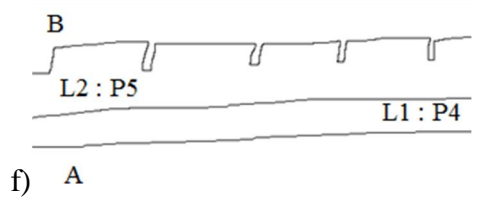
E₁ at 573°C



The ternary phase τ_2 is formed as a reaction product of equation 4. The phases τ_1 and $\text{Fe}_4\text{Al}_{13}$ are the reaction products of equation 9 & 10. According to equation 5 the formed ternary phases τ_1 , τ_2 reacts with liquid to form τ_7 . τ_7 again reacts with liquid phase to form τ_2 and τ_4 . Now τ_4 reacts with liquid to form τ_6 and Si. The phase τ_6 can also be formed from reaction mentioned in equation 8. The major observation from the above reactions is that along with the ternary intermetallic phases elemental Si is also formed as a major reaction product. This is also supported from micro area x-ray diffraction patterns indicating

strong Si peaks. τ_4 and τ_7 are also the reaction products of the above mentioned reactions. The presence of τ_7 is not detected from the micro area x-ray diffraction pattern. But the presence of τ_4 in trace amounts is detected in micro area x-ray diffraction patterns. This can be supported from the isothermal section of Al-Fe-Si ternary system at 550 °C as shown in Fig 4.30 which reveals the presence of three phase fields having wide range of formation like $\tau_2+\tau_4+\tau_6$, $\tau_6+\text{Al}+\text{Si}$, $\tau_4+\tau_6+\text{Si}$ at the aluminium corner confirming the possibility of coexistence of the above mentioned phases.

The schematic of interface morphologies at each location with corresponding phases are represented in Fig 4.31. In all the cases the steel/IMC interface is flat. The presence of cubic structure adjacent to steel (cubic) might probably have resulted in a flat steel/IMC interface. Nearly four major types of morphologies are observed at bead/IMC interface, viz., wavy and needles with sharp end (Fig 4.29a, e), wavy and needles with rounded end (Fig 4.31c), rectangular block with flat interface (Fig 4.31c, f) and irregular blocks with flat interface (Fig 4.31d). The wavy and needles with sharp end morphology is evident in head and foot regions of the joints made with Al-5%Si filler wire. These needles will grow in all directions with increase in diffusion aided by heat input. As the needles grow with increased heat input, the central region experiencing slightly more heat than head and foot region recorded wavy and needle with rounded end morphology. This needle structure is comprised of Al rich monoclinic $\text{Fe}_{25}\text{Al}_{75}$ phase adjacent to cubic bead. There may be incoherency between the monoclinic and cubic structure. The third and fourth types of interfacial morphologies are evident in joints made with Al-12%Si filler wire. It is observed that even the bead/IMC interface is irregular in shape and it has intimate contact with bead without delamination or gaps.

Location	Interface morphology/phases	
	Al-5%Si	Al-12%Si
Head		
Center		
Foot		

A: Steel (cubic), B: braze bead (Al-Si) (cubic), P1 : FeAl (cubic), P2 : $\text{Fe}_{25}\text{Al}_{76}$ (monoclinic), P3 : Fe_2Al_5 (orthorhombic), P4 : $\text{Fe}_3\text{Al}_{0.7}\text{Si}_{0.3}$ (cubic), P5 : Al_5FeSi (monoclinic), P6: $\text{Fe}_3\text{Al}_{0.5}\text{Si}_{0.5}$ (cubic) $\text{Al}_{25.83}\text{Fe}_{8.57}\text{Si}_{6.6}$ (rhombohedral)

Figure 4.31 Schematic of interfacial morphology of P-GMAW brazed specimen with two different filler wires a) Al-5%Si (head) b) Al-12%Si (head) c) Al-5%Si (center) d) Al-12%Si (center) e) Al-5%Si (foot) f) Al-12%Si (foot).

The rectangular blocks with flat surface are evident at head and foot regions of joints made with Al-12%Si filler wire. The irregular block with flat edges is evident at central region of the joints made with Al-12%Si filler wire. The growth of IMC at central region is more predominant than head and foot regions. Therefore the irregular blocks grow as a result of high heat input at the central region.

4.5.1 Summary

- The increase in filler wire Si content enhanced the wetting and spreading behaviour.
- In spite of thicker IMC layer the joints made with Al-12%Si recorded better performance in lap shear test.
- The interface of joints made with Al-5%Si is comprised of Fe-Al based binary IMC phases whereas the interface of joints made with Al-12%Si filler wire shows Al-Fe-Si based ternary intermetallic phases.
- The interface type and morphology are affected by heat input and chemical composition of the filler wire.
- The joint strength is effected by the type and morphology of the bead/steel interface. Rectangular block type interface with flat surfaces facilitates improved joint strength.

4.6 Conclusions

- At 0° torch orientation to welding direction, a dissimilar Al/GA steel joint can be formed only at higher wire feed rates in the range of 5 m/min, and a convex bead formation is observed. Under similar conditions tilting the whole brazing assembly to 12° helps in increasing wetting width, a concave bead formation is observed. Tilting aided in 15% improvement in joint strength. Hence, Al/GA steel joints demands high heat input conditions at 0° torch orientation and tilting showed positive effect on wetting and in turn increased the joint strength.
- Changing the torch orientation to 60° to the brazing direction helps in obtaining a leak proof Al/GA steel joint at low heat input conditions. Hence orienting the torch with respect to welding direction is favorable for Al/GA steel and Al/uncoated steel combinations.

- Dissimilar aluminum/steel joints with acceptable strength could be formed in a wide range of parameters. The bead formation is found to be affected by parameters like wire feed rate, processing speed, angle of tilt, torch orientation, and surface chemistry of steel and filler wire composition.
- Under similar brazing conditions, galvanized steel recorded better properties than galvanealed and uncoated steel. Hence Al/GI steel joints are found to be stronger among the above mentioned three combinations.
- In Al/GI steel joints the presence of elemental Zn lead to formation of crevice towards head and foot regions which results in fracture. Increase in gap between the plates of base materials aided in escape of Zn and reduction in intensity of crevice formation and hence enhanced the joint strength. Hence maintaining gap between the plates shows a positive effect on joint properties.
- The joints made with Al-12%Si filler wire showed better properties compared to joints made with Al-5%Si filler wire. Increase in Si content of the filler wire is supposed to improve wetting and spreading, in turn improving the joint strength. Hence joints made with 4047 filler wire have performed better compared to 4043 filler wire.
- By controlling the brazing parameters, the interfacial IMC layer thickness could be restricted to less than 10 μm
- The interfacial IMC layer morphology and thickness are influenced by parameters like wire feed rate, angle of tilt, torch orientation, surface chemistry of steel and filler wire composition.
- Under similar brazing conditions joints made with Al-12%Si filler wire recorded bead failure whereas joint made with Al-5%Si filler wire recorded interfacial failure. The failure modes are found to be effected by the interfacial morphologies especially the

bead/IMC interfacial morphology. Hence tailoring the interfacial morphologies by altering the parameters like filler wire composition, heat input the joint strength and failure mode could be altered.

- The joints made with Al-5%Si filler wire shows the presence of binary Fe-Al intermetallic whereas the joints made with Al-12%Si filler wire showed the presence of Al-Fe-Si ternary intermetallic phases. Hence by varying the Si content of the filler wire the interfacial phases can be altered.

References

- [1] M.G.N. Nicolas Eustathopoulos, Batrice Drevet, Wettability at High Temperatures, Pergamon, UK, 1999.
- [2] H.T. Zhang, J.C. Feng, P. He, Materials Science and Technology, 24 (2008) 1346-1349.
- [3] H. Zhang, J. Liu, Materials Science and Engineering a-Structural Materials Properties Microstructure and Processing, 528 (2011) 6179-6185.
- [4] G. Sierra, P. Peyre, F.D. Beaume, D. Stuart, G. Fras, Materials Characterization, 59 (2008) 1705-1715.
- [5] A. Das, M. Shome, C.R. Das, S.-F. Goecke, A. De, Science and Technology of Welding and Joining, 20 (2015) 402-408.
- [6] J. An, X.X. Shen, Y. Lu, Y.B. Liu, R.G. Li, C.M. Chen, M.J. Zhang, Surface & Coatings Technology, 200 (2006) 5590-5597.
- [7] L. Agudo, N. Jank, J. Wagner, S. Weber, C. Schmaranzer, E. Arenholz, J. Bruckner, H. Hackl, A. Pyzalla, Steel Research International, 79 (2008) 530-535.
- [8] P. Peyre, L. Berthe, X. Scherpereel, R. Fabbro, Journal of Materials Science, 33 (1998) 1421-1429.
- [9] T. Murakami, K. Nakata, H.J. Tong, M. Ushio, Isij International, 43 (2003) 1596-1602.
- [10] H.J. Park, S. Rhee, M.J. Kang, D.C. Kim, Materials Transactions, 50 (2009) 2314-2317.
- [11] G. Ghosh, Ternary Alloys, A Comprehensive Compendium of Evalu- 52. B. Sundman, B. Jansson, and J.-O. Andersson: CALPHAD, 1985, vol. ated Constitutional Data and Phase Diagrams, VCH Publishers, New York, 1992.
- [12] V. Raghavan, Journal of Phase Equilibria and Diffusion, 33 (2012) 322-326.

CHAPTER 5

COLD METAL TRANSFER WELD-BRAZING OF

ALUMINIUM ALLOY TO STEEL

5.1 Introduction

Cold metal transfer welding is a reduced energy arc welding process with precise control of heat input even lower than the P-GMAW process, discussed in the previous chapter. This is due to its “zero” current metal transfer taking place during the process. It also has a variant, Pulse-CMT wherein a pulse cycle is superimposed on CMT cycle. This feature is used to increase the arc intensity and heat input for greater feasibility of operation depending on the need. As reported in Chapter-3, several processes related and material related parameters have effect on joint formation and properties. Accordingly, CMT joining investigations have been conducted keeping most of the parameters fixed viz, galvanized surface of the steel base material, 200-300 μm interfacial gap and torch orientation in melt pool pushing mode. Effects of the following major parameters are investigated in detail with respect to the CMT process, with emphasis on the aluminium-steel interface morphology and consequent mechanical performance of the joint.

- effect of filler wire composition
- effect of pulsing (P-CMT)
- effect of heat input.

The effect of each parameter is reported in the subsequent sections in detail.

5.2 Effect of pulsing and filler wire composition

5.2.1 Thermal transient measurements

Fig 5.1 shows typical CMT cycle and the resultant thermal history of the cold metal transfer (CMT) and pulsed cold metal transfer (P-CMT) process under similar processing conditions. It can be seen that for similar parameters CMT process (Fig 5.1a) records a peak temperature of 640 °C whereas P-CMT process (Fig 5.1b) records 685 °C and the variation in cooling rate is also noted. It is noticed that base materials are forced to retain heat for slightly more time in P-CMT than CMT process. The super imposed current or pulsing in P-CMT process enhanced the energy input resulting in high peak temperature and heat retention

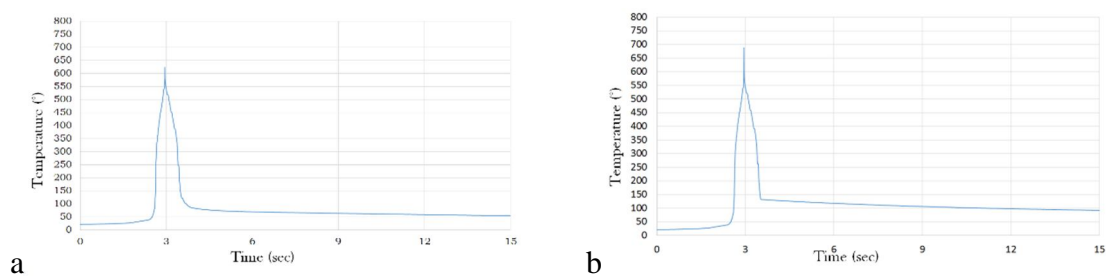


Figure 5.1 Thermal history measurement a) CMT process b) P-CMT process.

5.2.2 Macrostructure

Preliminary experiments revealed that bead formation could not take place in CMT brazing of aluminium alloy and steel at a wire feed rate of 3.5 m/min, whereas pulsing enabled the bead formation even at 3.5 m/min of wire feed rate. So, for the purpose of comparison the common 4 m/min wire feed rate parameter is chosen. All the results reported here are of 4 m/min of wire feed rate.

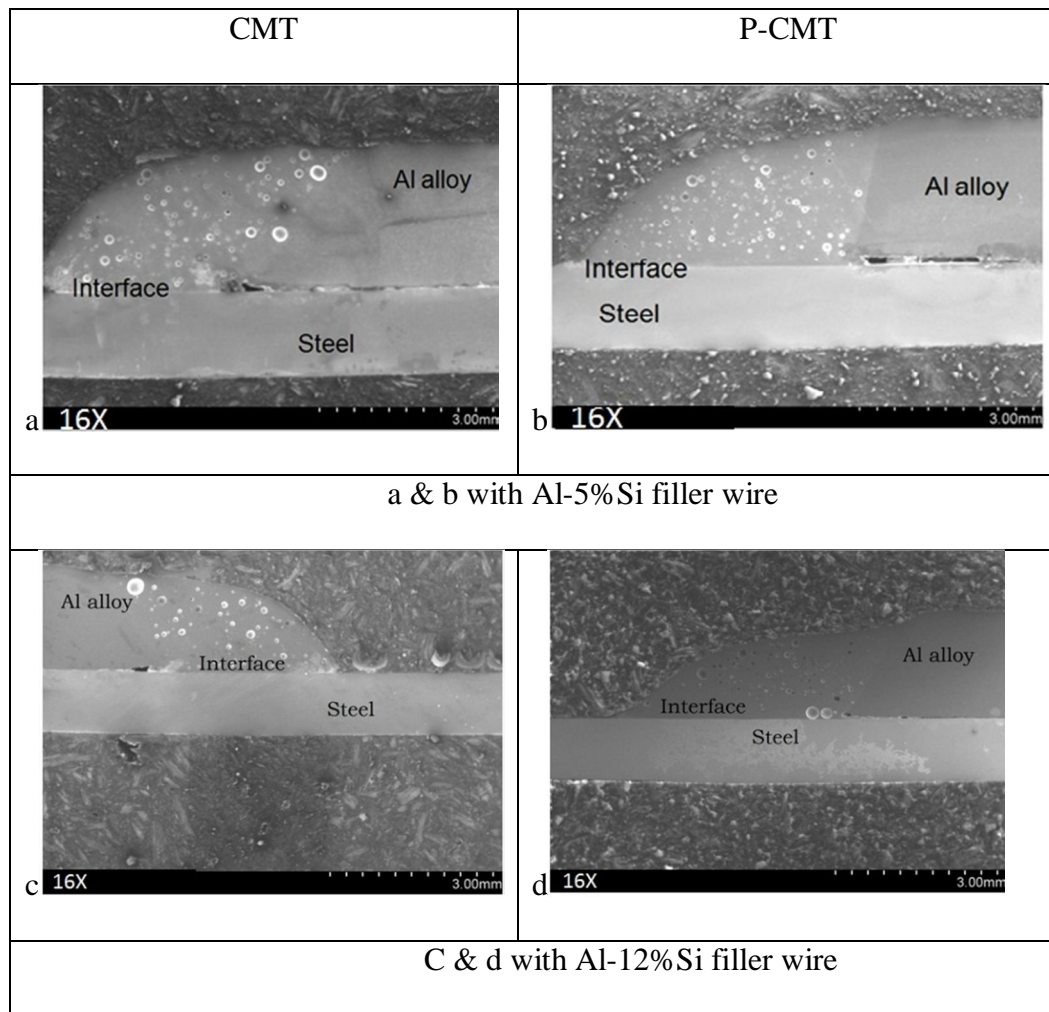


Figure 5.2 Transverse cross-section SEM micrographs of aluminium/steel joints a) CMT (Al-5%Si filler); b) P-CMT (Al-5%Si filler); c) CMT (Al-12%Si filler); and d) P-CMT (Al-12%Si filler).

Table 5.1 Bead geometry measurements

S.No	Bead geometry measurements	Range			
		Al-5%Si		Al-12%Si	
		CMT	P-CMT	CMT	P-CMT
1	Bead width (mm)	3.2-3.3	3.5-3.6	3.8-3.9	4.0-4.1
2	Bead height (mm)	1.8-1.9	1.7-1.8	1.6-1.7	1.6-1.7
3	Wetting angle (°)	60-65	55-60	43-47	40-45

Scanning electron macrographs of transverse cross-sections of aluminium/steel joints made under different conditions at 16x magnification are shown in Fig 5.2. Braze bead formation is found to be varying with the process as well as filler wire composition. The respective bead geometry measurements such as bead width, bead height and wetting angle are reported in Table 5.1. Compared to CMT (Fig 5.2a, c) an increase in bead width, reduction in wetting angles are noted in P-CMT braze-welded specimens (Fig 5.2b, d). Slightly lower temperature differential between steel and molten pool and possible enhanced fluidity of melt pool due to higher peak temperature associated with P-CMT process resulted in improved wetting and spreading of melt on steel. The joints made using Al-12%Si (Fig 5.2b, d) filler recorded low contact angles and high bead widths than joints made using Al-5%Si filler (Fig 5.2a, c). The increase in Si content in the filler wire assisted the wetting and spreading action. The addition of Si to aluminium alloys diminishes the viscosity of the melt. Therefore, Al-12%Si filler possessing high fluidity than Al-5%Si filler wire aided in improved wetting and spreading. Kang, et al.,[1] studied the joining of A5052 aluminium to aluminized and galvanized steel using various filler wires. It is reported that under similar heat input conditions the galvanized steel showed better wetting and spreading compared to aluminized steel. It is also reported that in case of joints made with galvanized steel the joints made with 4047 filler wire showed better wetting and spreading behaviour which is similar to the present observation.

5.2.3 Microstructure

Fig 5.3 shows different regions of microstructural interest in aluminium-steel dissimilar joint. Aluminium/bead interface (Fig 5.3a), braze bead (Fig 5.3b) and bead/steel interface (Fig 5.3c) are the three regions of microstructural interest. The aluminium/bead interface and braze bead shows a pure dendritic microstructure in all the cases. The bead/steel interface possesses the reaction product of aluminium melt and solid steel. The reaction product

formed at the bead/steel interface has a significant effect on mechanical properties of the joint. Therefore the study of the reaction product in terms of morphology, type of phase could yield a lot of interface information. Fig 5.4 shows a schematic with different regions; hence microstructural observation has been carried out on the bead/steel interface. Fig 5.5 shows the SEM micrographs of different locations of bead/steel interface at 2kX magnification. The bead/steel interface comprises of steel/IMC layer interface and IMC layer/bead interface. The steel/IMC layer interface is almost flat and IMC layer/bead interface showed variation in morphology. This is because the base material grain acting as nucleation sites grows the IMC without altering the orientation. The reaction product/bead interface is wavy in nature. This is because the IMC layer grows from steel side into the aluminium melt. Zhang, et al.[2] reported the interfacial characteristics of the wrought 6061 aluminium alloy and Zn coated IF steel made with 4043 filler wire. It is reported that the steel/IMC layer interface is serrated and the toothlike structures are growing into the steel. Delamination at IMC layer/bead interface is noticed (Fig 5.5 a, b, c, d, e, f). This delamination is evident in the specimens made with Al-5%Si filler. This delamination is observed only in a particular type of solidification sequence and will be explained in later section.

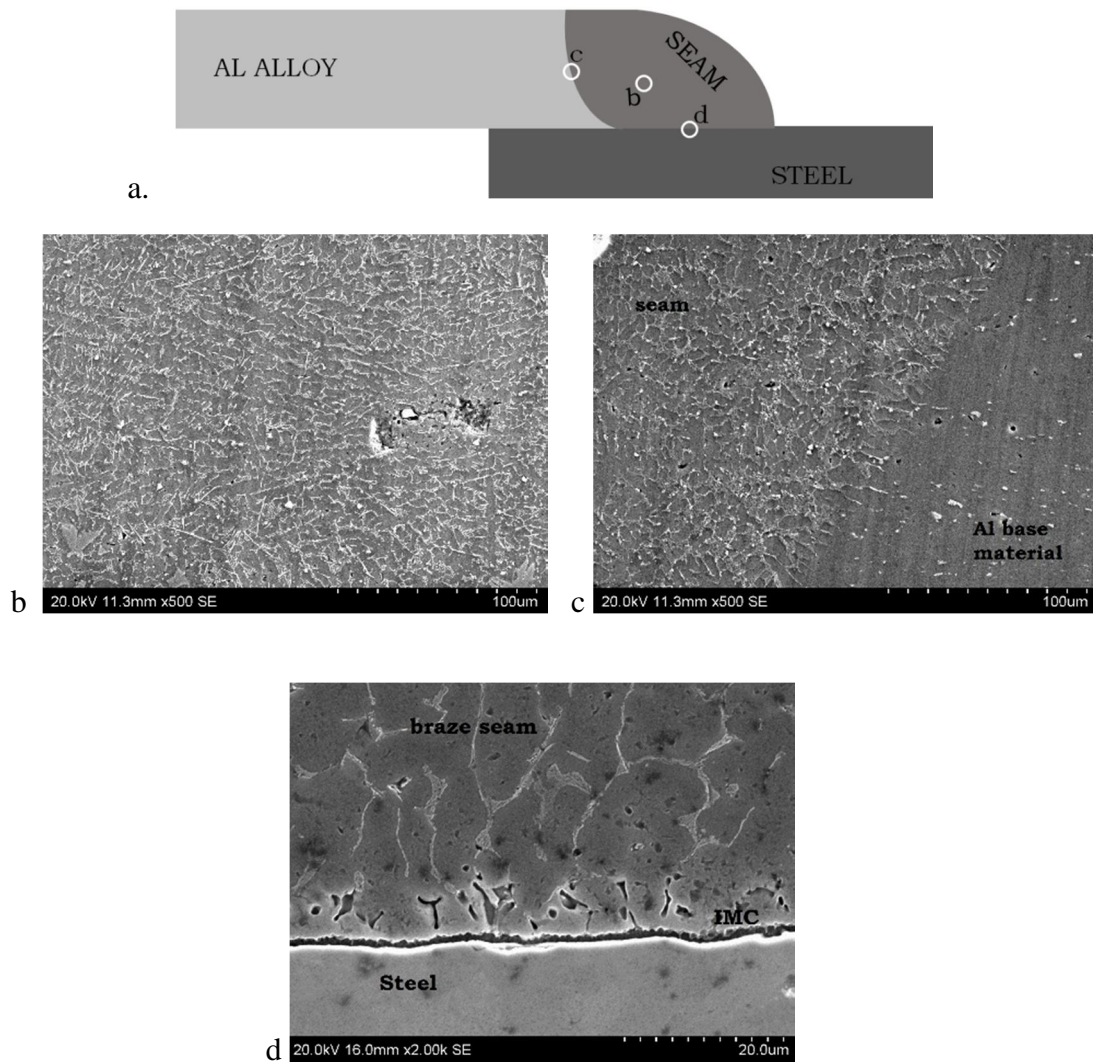


Figure 5.3 SEM micrographs of the aluminium-steel joint – a) schematic indicating different regions of microstructural observation b) braze bead c) aluminium/bead interface and d) bead/steel interface.

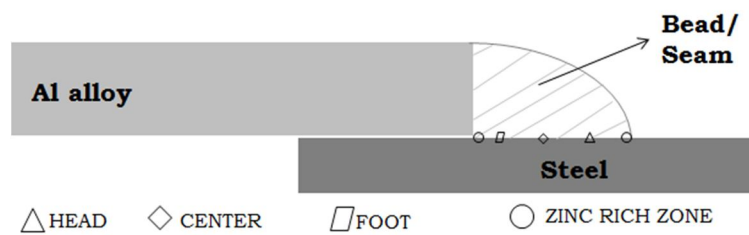


Figure 5.4 Schematic of different regions of bead/steel interface.

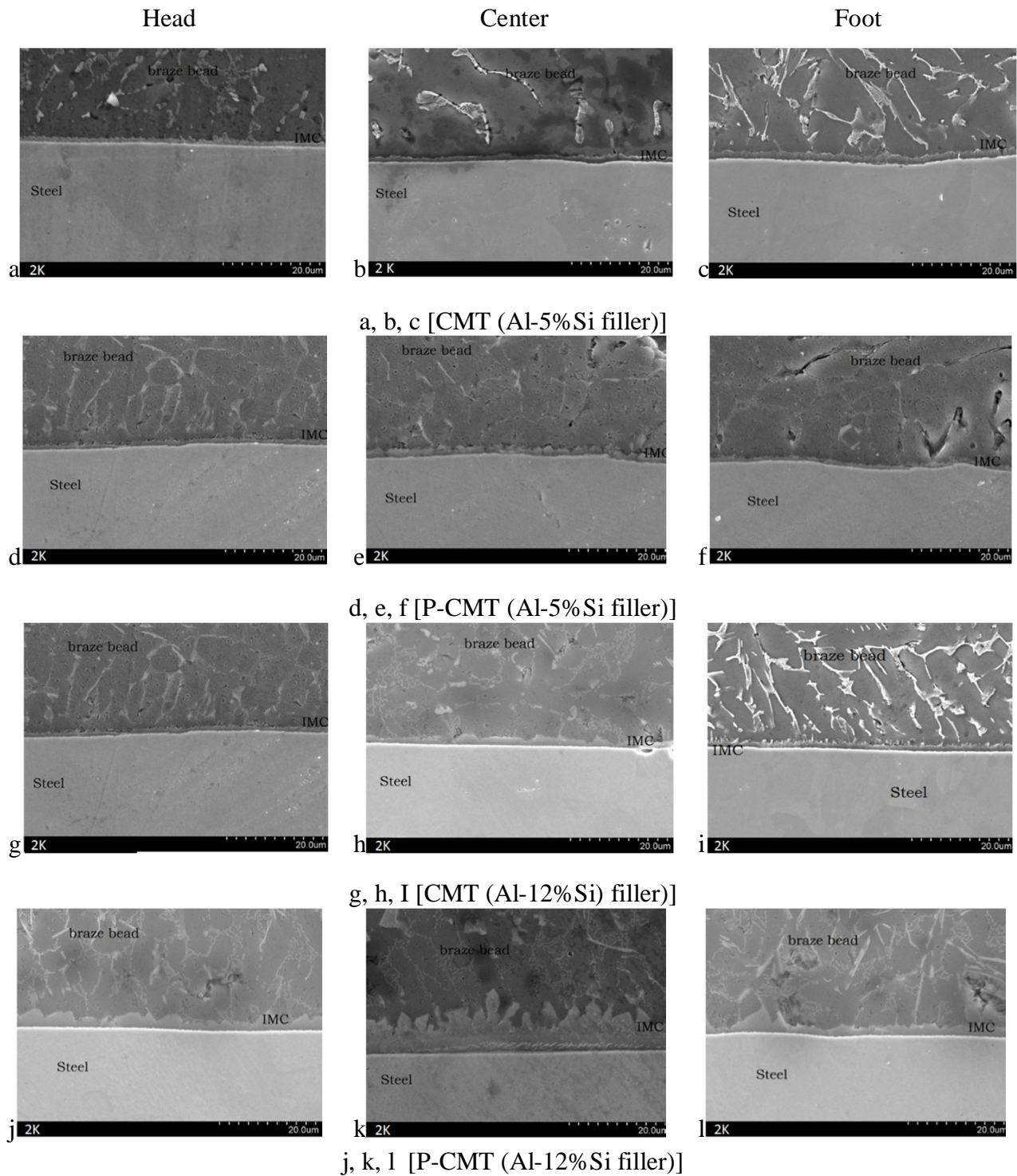


Fig 5.5 SEM micrographs of various locations of bead/steel interface at 2kX magnification – a) head (CMT Al-5%Si filler), b) center (CMT Al-5%Si filler), c) foot (CMT Al-5%Si filler); d) head (P-CMT Al-5%Si filler); e) center (P-CMT Al-5%Si filler), f) foot (P-CMT Al-5%Si filler), g) head (CMT Al-12%Si filler). H) center (CMT Al-12%Si filler), i) foot (CMT Al-12%Si filler), j) head (P-CMT Al-12%Si filler), k) center (P-CMT Al-12%Si filler) and l) foot (P-CMT Al-12%Si filler).

It is observed that the central region (Fig 5.5 b, e, h, k) recorded thicker IMC layer than head (Fig 5.5 a, d, g, j) and foot (Fig 5.5 c, f, i, l) regions. The high heat intensity of the central region of the welding arc could be the reason for increased thickness of the IMC layer in this region. The interface of the joints made from P-CMT (Fig 5.5 d, e, f, j, k, l) process possesses thicker IMC layer compared to joints made from CMT process (Fig 5.5 a, b, c, g, h, i). The high heat input and intensity involved in P-CMT process aids the diffusion process resulting in thickening of the IMC layer. Almost all the regions (Fig 5.5 a, b, c, d, e, f, g, h, i, j, l) show two layered reaction product except the central region of P-CMT brazed joint interface (Fig 5.5k) made using Al-12%Si filler wire. A bright white coloured layer towards steel and light grey region towards bead, are the two layers (Fig 5.5 a, b, c, d, e, f, g, h, i, j, l). It is also noted that under similar brazing parameters the joints made using Al-12%Si filler wire (Fig 5.5 g, h, i, j, k, l) possess thicker IMC layer than the joints made using Al-5%Si filler wire (Fig 5.5 a, b, c, d, e, f). The Al-12%Si is a eutectic composition having melting temperature of 577 °C and Al-5%Si melts at around 600 °C. The eutectic composition is in liquidus state till 577 °C whereas Al-5%Si solidifies below 600°C. Hence Al-12%Si is in molten state for slightly longer time than Al-5%Si which aids the diffusion process causing formation of thicker IMC layer. It is also noted that the central region (Fig 5.5k) of P-CMT brazed joint using Al-12%Si filler solidified into a three layer region. It comprised of bright white layer towards steel side, followed by dark grey region and light grey region with needle like protrusions towards the bead. Zhang, et al.[3] reported the interfacial characteristics of A1060 aluminium alloy and Zn coated low carbon steel. It is reported that with increase in heat input the IMC layer will increase in thickness and even in number of compounds present which is similar to the present situation. It is also reported that with increase in heat input the IMC layer grow into the weld metal. This is comparable to the present case where the joint interface phase of P-CMT brazed specimen showed an increase in IMC layer thickness and needles protruding

into the filler metal. Morphology of the solidified structure is also found to vary with filler wire, especially the morphology of the IMC layer towards the bead side. In the joints made using Al-5%Si filler wire the IMC layer/bead interface is wavy in nature with curved or rounded surface towards the bead (Fig 5.5 a, b, c, d, e, f). But for the joints made using Al-12%Si filler wire, the IMC layer/bead interface is uneven with blocky particles with flat surface towards the bead. High and activated diffusion rates in Al-12%Si filler are expected to be the reason for this variation in morphology. This has to be further investigated. The effect of morphology of the IMC layer on mechanical properties of the joint is discussed in detail in the subsequent section.

Table 5.2 IMC layer thickness under various conditions

S.No	Location	IMC layer thickness (μm)			
		Al-5%Si		Al-12%Si	
		CMT	P-CMT	CMT	P-CMT
1	Head	1-1.2	1.7-1.9	1-1.2	2.2-2.4
2	Center	1.4-1.7	2.7-3.2	3.3-3.6	8-9
3	Foot	≤ 1	1.2-1.4	1.4-1.6	1.8-2

5.2.4 Lap shear test

Table 5.3 Lap shear test results

S.No	Sample id	Fracture load (N/mm) & failure location			
		Al-5%Si		Al-12%Si	
		CMT	P-CMT	CMT	P-CMT
1	S ₁	236 \pm 5 (interface)	209 \pm 5 (interface)	260 \pm 5 (bead)	242 \pm 5 (bead)
2	S ₂	232 \pm 5 (interface)	210 \pm 5 (interface)	260 \pm 5 (bead)	240 \pm 5 (bead)
3	S ₃	233 \pm 5 (interface)	206 \pm 5 (interface)	257 \pm 5 (bead)	238 \pm 5 (bead)

The fracture loads and failure location for the joints tested under lap shear condition are given in Table 5.3. It is observed that the joints made with CMT process showed better load bearing capacity than P-CMT brazed specimens. High energy inputs compared to CMT involved in P-CMT process resulted in thicker IMC layer and resulted in low fracture loads in spite of higher bead width in P-CMT process. It is observed that the joints made using Al-5%Si filler wire have recorded low fracture loads than joints made using Al-12%Si filler wire. It is also observed that joints made using Al-5%Si filler recorded interfacial failure whereas joints made using Al-12%Si filler wire recorded bead failure in all the cases indicating a stronger interface. Better wetting and spreading of Al-12%Si filler on steel as well as favourable IMC layer probably resulted in high fracture loads. The joint strength of nearly 262 N/mm with failure in the bead can be achieved using CMT weld brazing process. Zhang et al. [2] reported the shear strength around 96 MPa for A6061 wrought aluminium alloy and Zn coated IF steel. Yang et al.[4] reported the shear strength around 270 N/mm for the similar material combination. Therefore the strengths achieved in the present work are comparable with the reported values in the literature.

5.3 Effect of heat input

5.3.1 Macrostructure

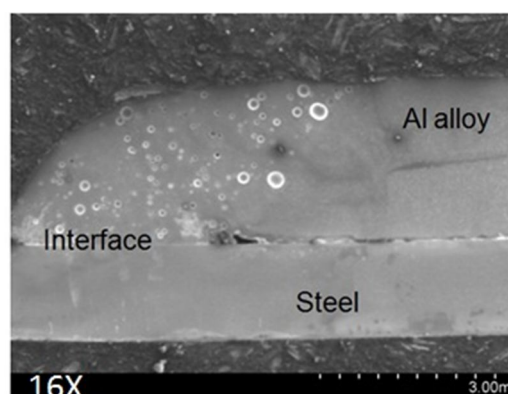


Figure 5.6 Transverse cross-section SEM micrographs of CMT brazed aluminium/steel joints made with Al-5%Si filler wire.

Table 5.4 Bead geometry measurements of CMT brazed joints made with Al-5%Si filler wire

S.No	Bead geometry measurements	Range	
		Al-5%Si - WFR	
		(m/min)	
		4	4.5
1	Bead width (mm)	3.2-3.3	3.4-3.8
2	Bead height (mm)	1.8-1.9	1.7-1.8
3	Wetting angle (°)	60-65	55-58

Fig 5.6 shows the SEM transverse cross-section macrographs of the Al/steel joints made with Al-5%Si filler at different wire feed rates at 16x magnification and bead geometry measurements are given in Table 5.4. It is clearly seen that there is an increase in bead width and height with increase in wire feed rate. The wetting angle also increased from 60-65° to 64-67°. The increase in wire feed rate increases the deposition rate and therefore increased the bead width, height and wetting angle.

5.3.2 Microstructure

Aluminium/bead interface, braze bead, bead/steel interface are the different regions of microstructural interest. The microstructures at these locations are similar to microstructures shown in Fig 5.3. Various locations of bead/steel interface are identified in Fig 5.4. Fig 5.7 shows microstructures at three different locations of the bead/steel interface made with Al-5%Si filler wire at 5.5kX magnification. The measured thicknesses of IMC layer at various locations for both wire feed rates are given in Table 5.5. It is observed in both heat input

conditions that the central region recorded thicker IMC layer than head and foot regions. The high heat intensity experienced by the central region of the arc resulted in high IMC growth

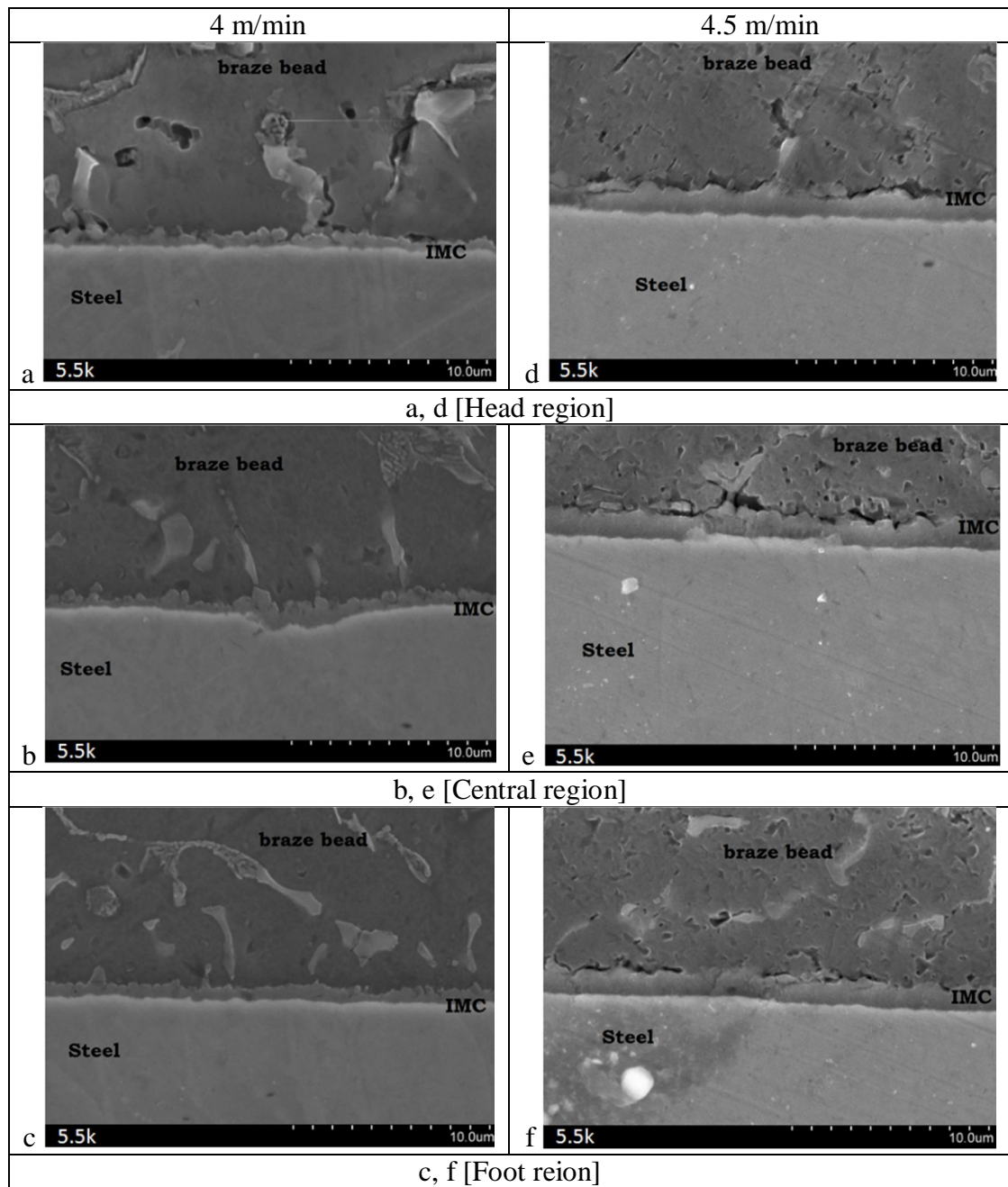


Fig 5.7 SEM micrographs of various locations of bead/steel interface of CMT brazed joints made with 4043 filler wire with variation in heat input at 5.5kX magnification - a) head (WFR : 4m/min), b) center (WFR : 4m/min), c) foot (WFR : 4m/min), d) head (WFR : 4.5m/min), e) center (WFR : 4.5m/min) and f) foot (WFR : 4.5m/min).

at the central region which was observed in P-GMAW joints also. The joint made with higher wire feed rate recorded thicker IMC layer than the joints made at low wire feed rate. With

increase in wire feed rate, the heat input and deposition rate increases, which in turn increases the growth of IMC layer. Two layered IMC layer is observed in all the cases as shown in Fig 5.7. A pale white layer towards the steel side and a grey region towards the bead are observed. Delamination at IMC/bead interface is observed. This delamination tendency is intense in joints made at higher wire feed rate. This delamination may be because of incoherency between the crystal structures of the IMC layer and bead adjacent to it. This delamination may affect the mechanical performance of the joint and its failure location.

Table 5.5 IMC layer thickness under various heat input conditions

S.No	Location	IMC layer thickness (μm)	
		Al-5%Si WFR (m/min)	
		4	4.5
1	Head	1-1.2	1.4-1.6
2	Center	1.4-1.7	1.85-2.05
3	Foot	≤ 1	1.3-1.5

5.3.3 Lap shear test

Table 5.6 Lap shear test results under various heat input conditions

S.No	Sample id	Fracture load (N/mm) & failure location	
		Al-5%Si/WFR (m/min)	
		4	4.5
1	S ₁	236 \pm 5 (interface)	240 \pm 5 (interface)
2	S ₂	232 \pm 5 (interface)	242 \pm 5 (interface)
3	S ₃	233 \pm 5 (interface)	245 \pm 5 (interface)

The results of lap shear test are given in Table 5.6. The joint strengths in the range of 232-236 N/mm were observed in case of joints made at a wire feed rate of 4m/min and 240-245 N/min were observed in case of joints made at a wire feed rate of 4.5 m/min. Slight increase in joints strength with increase in wire feed rate is observed. This may be attributed to an increase in bead width at wire feed rate of 4.5 m/min. Interfacial failure is recorded in all the cases. The delamination at IMC/bead interface acted as a crack initiation site and lead to interfacial failure in all the cases.

5.4 Phase analysis

The mechanical performance of an aluminium/steel dissimilar joint is influenced by the type and morphology of the IMC layer formed at the bead/steel interface. The maximum thickness of the IMC layer formed is around 9 μm . SEM microstructures also revealed the occurrence of two and three layered regions. An extremely thin and multiple layers present in the IMC layer posed problem in phase analysis, micro area x-ray diffraction technique was attempted in order to overcome this problem.

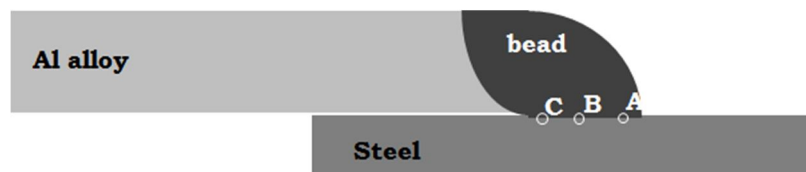
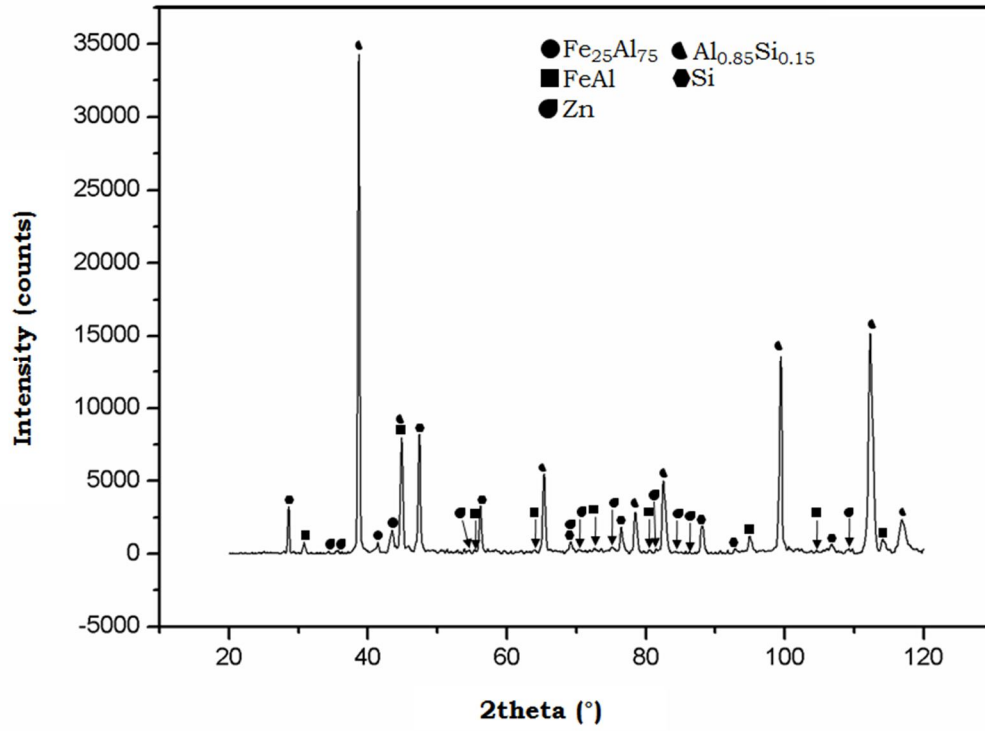


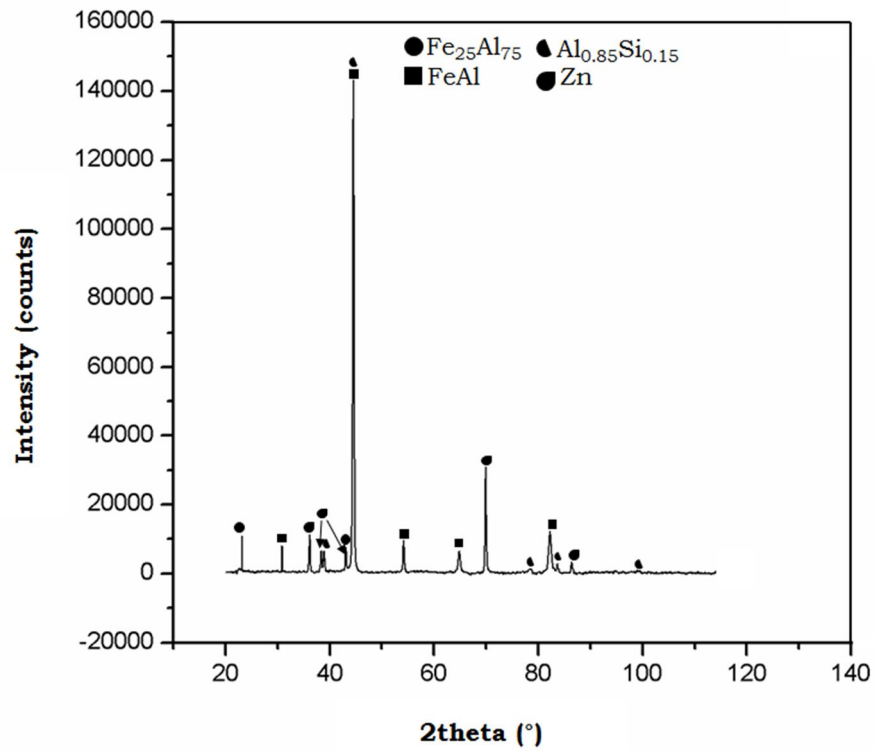
Figure 5.8 Schematic indicating various locations of x-ray diffraction A) head B) center C) foot.

Agudo et al.[5] studied the interfacial IMC phases formed in the butt joints of AW5182-H!!! aluminium alloy and Zn coated DX54D steel made using Al99.5, AlMn₁, AlSi₅, AlSi₃Mn₁ filler materials using EBSD and TEM. It has been shown that the joints made with Al99.5 and AlMn₁ filler wire possess 4 μm thick IMC layer and is comprised of Fe₂Al₅ and Fe₄Al₁₃ towards the steel and filler side respectively. It is also reported that the joints made with AlSi₅

and AlSi_3Mn_1 restricts the growth of IMC layer to $2.5\ \mu\text{m}$ and is comprised of AlFeSi ternary compound along with Fe_2Al_5 and $\text{Fe}_4\text{Al}_{13}$. Peyre et al.[6] also reported the presence of Fe_2Al_5 and FeAl_3 using EDS analysis. Fig 5.8 shows the schematic of bead/steel interface indicating different locations of x-ray diffraction spots. Figs 5.9 to 5.11 shows the x-ray diffraction patterns of bead/steel interface made with Al-5%Si filler wire. The calculated enthalpies of formation of the phases formed are given in Table 5.7. The x-ray diffraction pattern of CMT brazed bead/steel interface made with Al-5%Si filler wire reveals the presence of FeAl (cubic), $\text{Fe}_{25}\text{Al}_{75}$ (monoclinic), $\text{Al}_{0.85}\text{Si}_{0.15}$ (cubic), Zn (HCP), Si (cubic) at head (Fig 5.9a) region, FeAl (cubic), $\text{Fe}_{25}\text{Al}_{75}$ (monoclinic), $\text{Al}_{0.85}\text{Si}_{0.15}$ (cubic), Si (cubic) at center (Fig 5.10a) and foot (Fig 5.11a) regions. The P-CMT brazed bead/steel interface showed the presence of FeAl (cubic), $\text{Fe}_{25}\text{Al}_{75}$ (monoclinic), $\text{Al}_{0.85}\text{Si}_{0.15}$ (cubic), Zn (HCP) at head region (Fig 5.9b), FeAl (cubic), $\text{Fe}_{25}\text{Al}_{75}$ (monoclinic), $\text{Al}_{0.85}\text{Si}_{0.15}$ (cubic), Si (cubic) at center (Fig 5.10b) and foot regions (Fig 5.11b). FeAl and $\text{Fe}_{25}\text{Al}_{75}$ are the two observed binary Fe-Al based IMC compounds at bead/steel interface made with Al-5%Si filler wire.

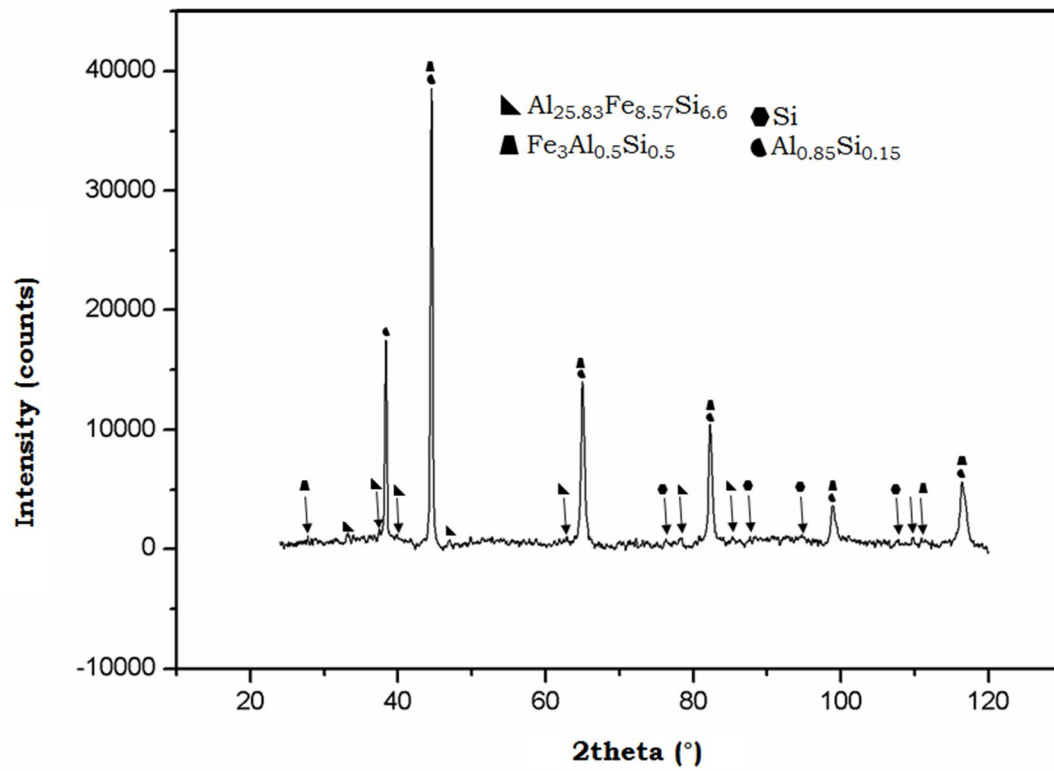


a

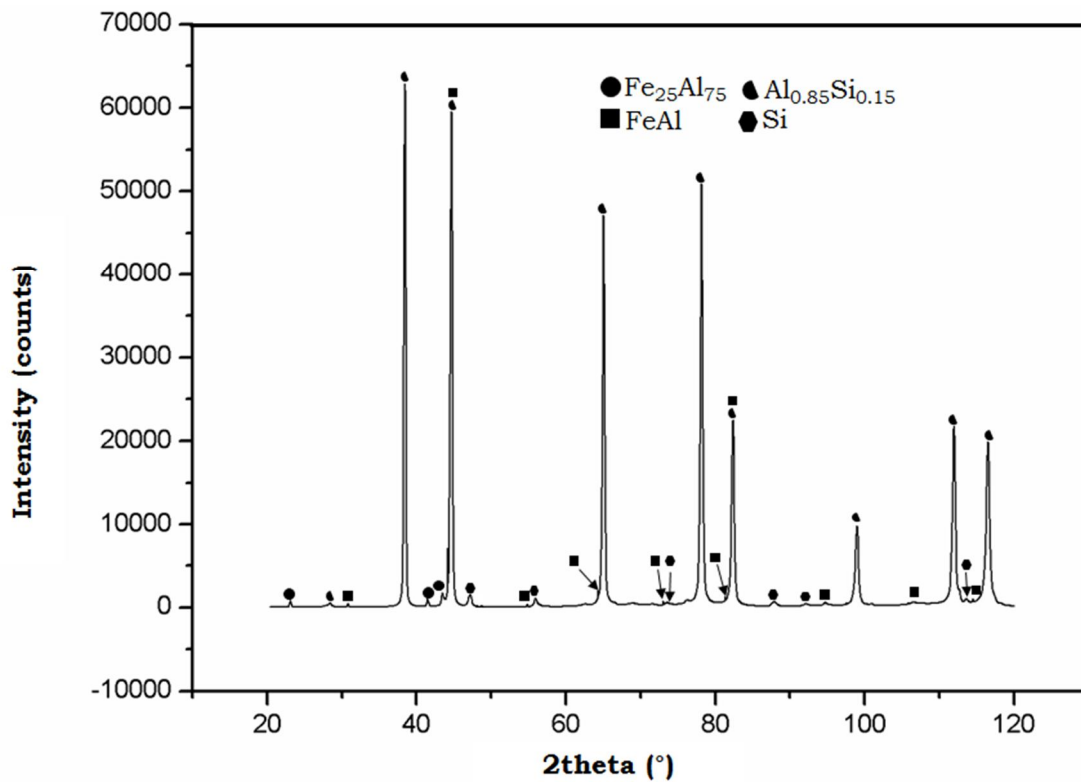


b

Figure 5.9 Micro area XRD patterns of head region of bead/steel interface made with Al-5%Si filler wire a) CMT b) P-CMT.

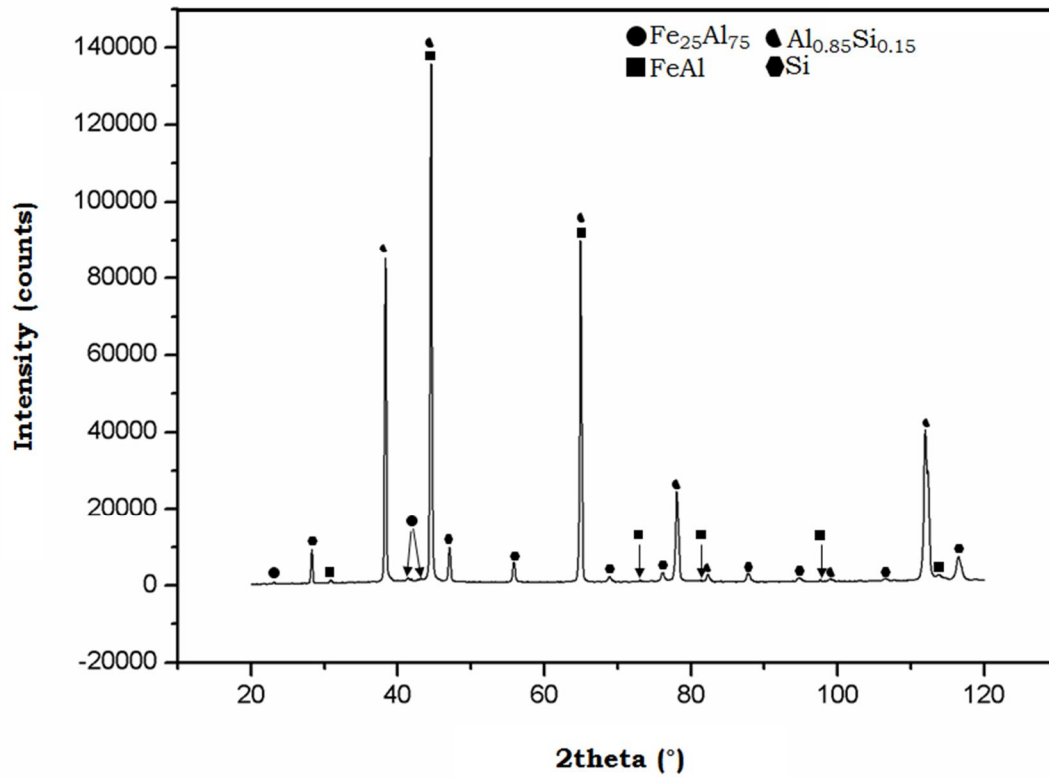


a

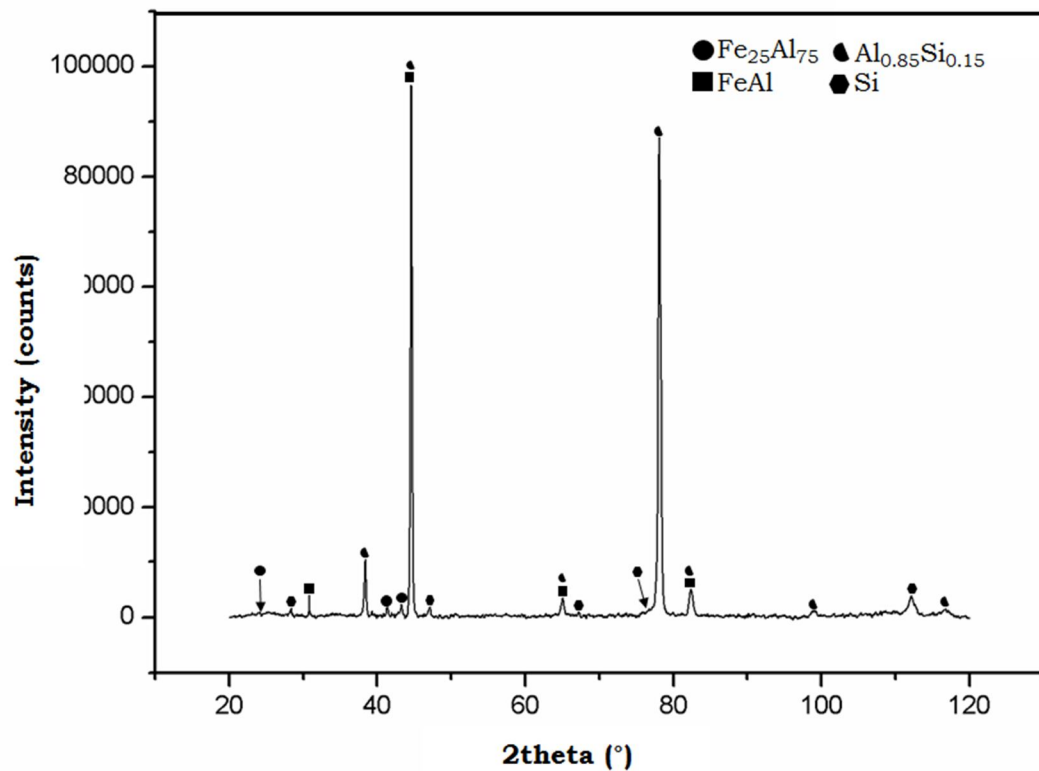


b

Figure 5.10 Micro area XRD patterns of central region of bead/steel interface made with Al-5%Si filler wire a) CMT b) P-CMT.

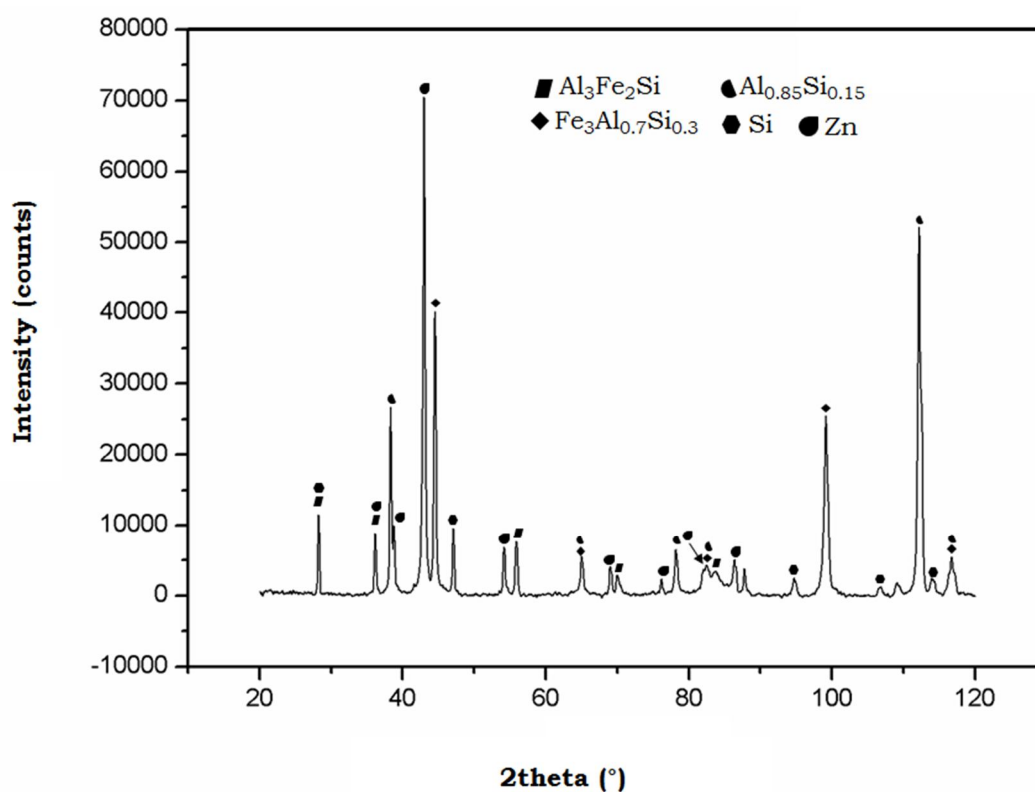


a

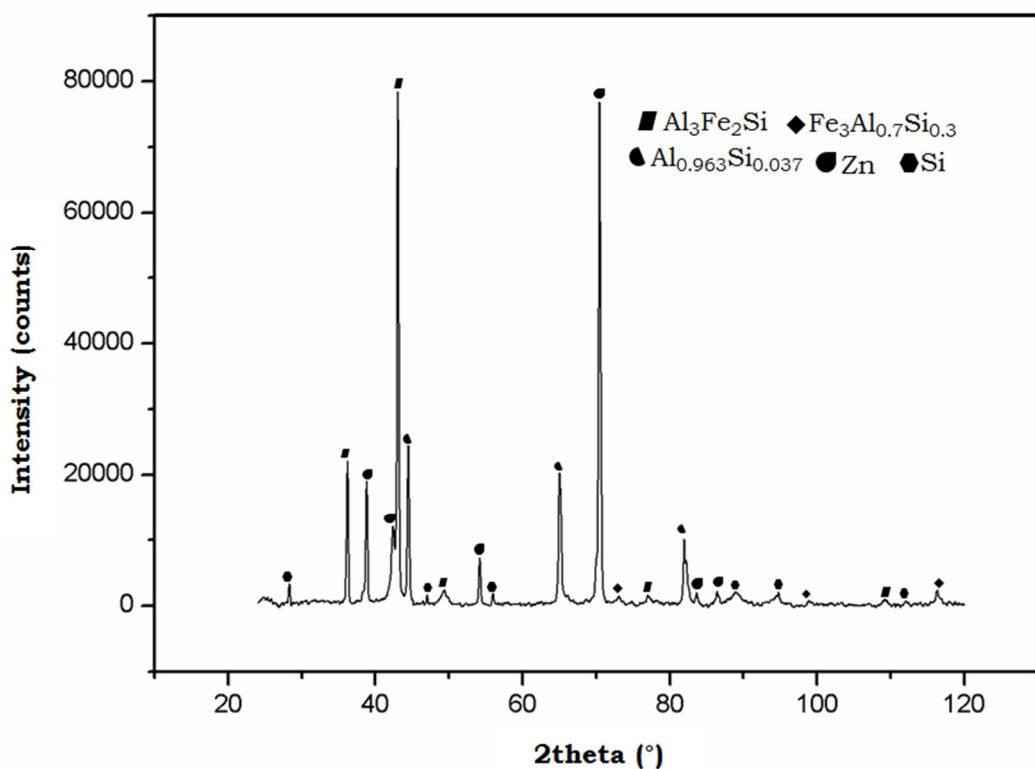


b

Figure 5.11 Micro area XRD patterns of foot region of bead/steel interface made with Al-5%Si filler wire a) CMT b) P-CMT.



a



b

Figure 5.12 Micro area XRD patterns of head region of bead/steel interface made with Al-12%Si filler wire a) CMT b) P-CMT.

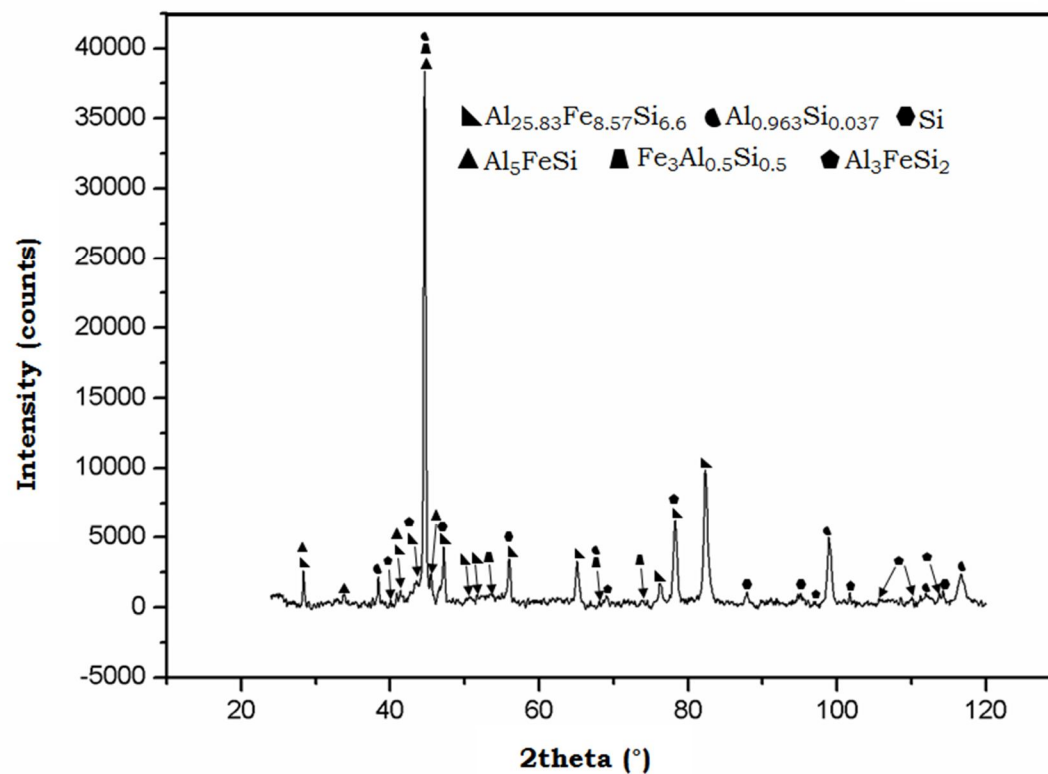
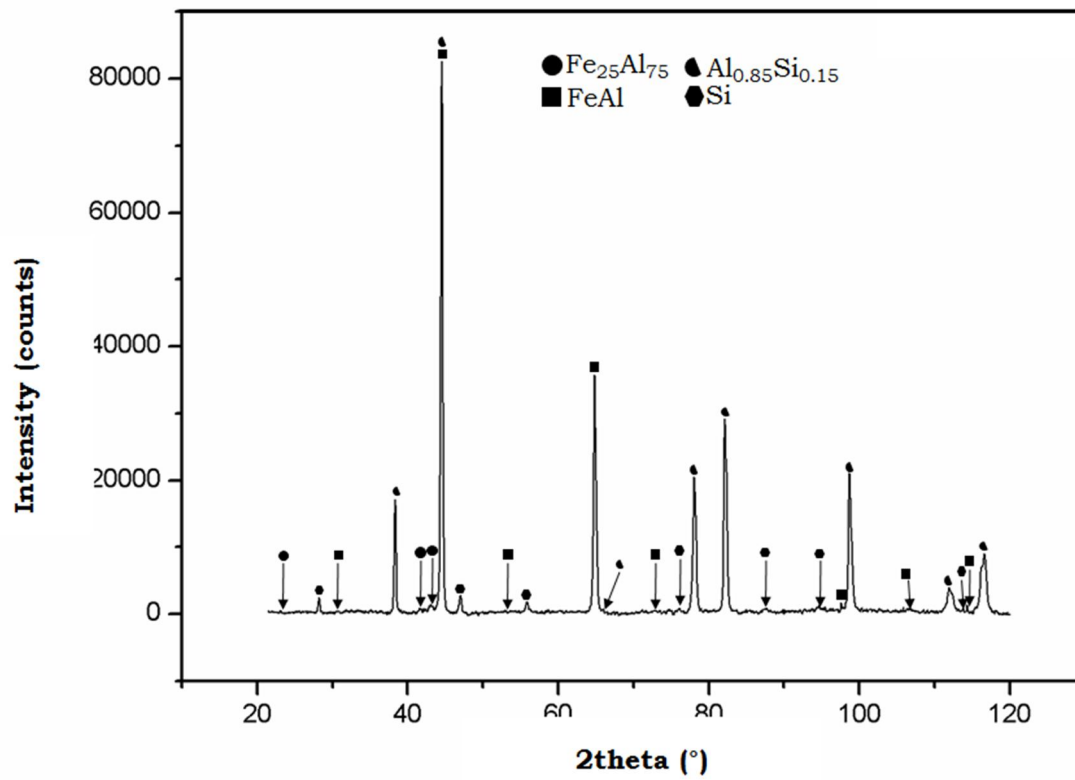


Figure 5.13 Micro area XRD patterns of central region of bead/steel interface made with Al-12%Si filler wire a) CMT b) P-CMT.

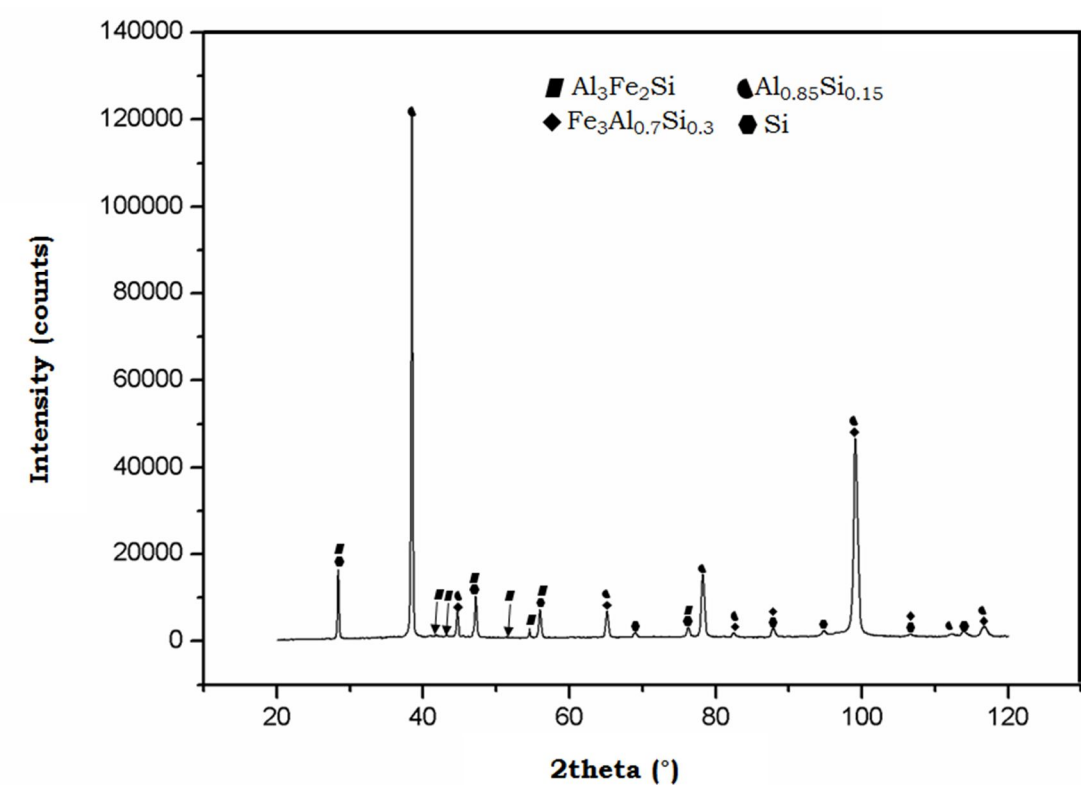
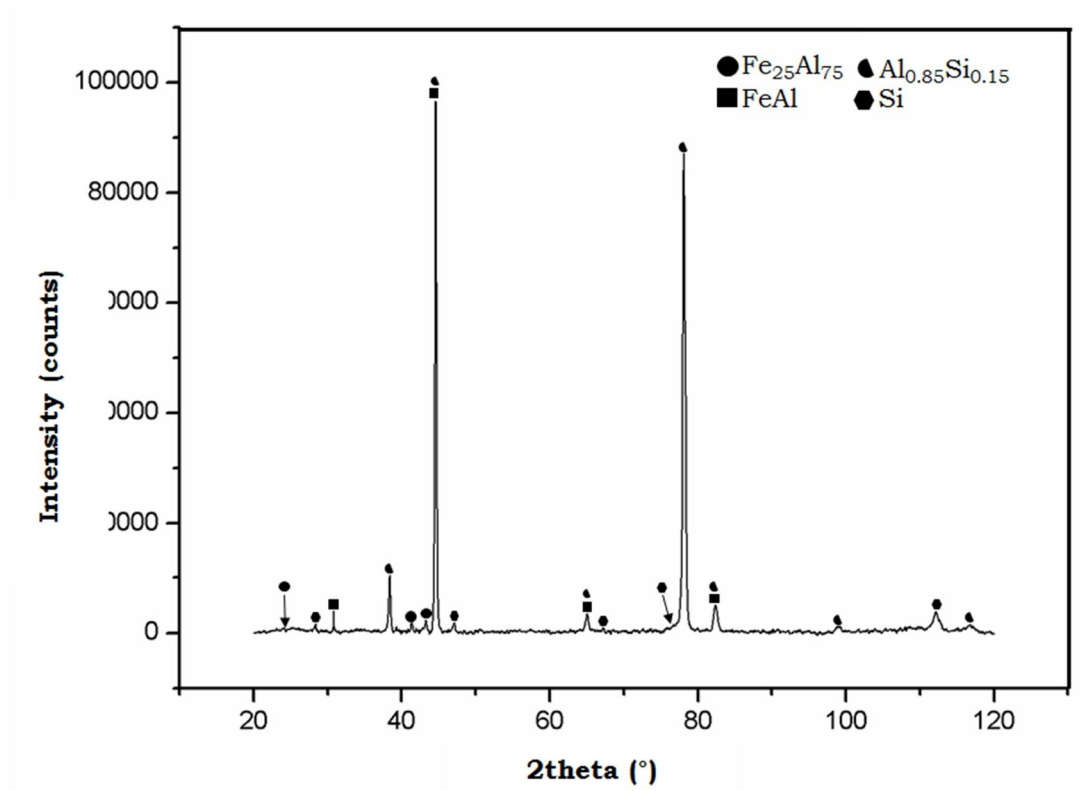


Figure 5.14 Micro area XRD patterns of foot region of bead/steel interface made with Al-12%Si filler wire a) CMT b) P-CMT.

Table 5.7 Phase data (composition, crystal structure & enthalpy of formation)

S.No	Phase	Composition (at. %)			Crystal structure	Enthalpy of formation (kJ/mol)
		Al	Fe	Si		
1	FeAl	50	50	-	Cubic	-32.15
2	Fe ₂₅ Al ₇₅	75	25	-	Monoclinic	-19.2
3	Al ₃ Fe ₂ Si	50	333.33	16.67	Cubic	-32.9
4	Al _{25.83} Fe _{8.57} Si _{6.6}	63	20.90	16.10	Rhombohedral	-22.3
5	Fe ₃ Al _{0.5} Si _{0.5}	12.50	75	12.50	Cubic	-18.2
6	Fe ₃ Al _{0.7} Si _{0.3}	17.50	75	7.50	Cubic	-19.9
7	Al ₅ FeSi	71.43	14.29	14.29	Monoclinic	-14.8
8	Al ₃ FeSi ₂	50	16.67	33.33	Tetragonal	-10.1

The respective microstructures showed the presence of two layered IMC region at bead/steel interface (Fig 5.5a-f). Therefore, two IMC compounds form two layers of the bead/steel interface. In general, the layer towards the steel side will be rich in Fe and the layer towards the aluminium will be rich in Al. Hence, the layer towards the steel side may comprise of FeAl; because enthalpy of mixing of aluminium in iron for FeAl phase (i.e. -32 kJ/mole) was less than that of other IMC phases, as shown in Table 5.7. The layer towards aluminium side may be Fe₂₅Al₇₅. Along with these Fe-Al based IMC compounds, Al_{0.85}Si_{0.15}, Si are also observed in all the regions. This is because the 10 µm spot used in x-ray diffraction covers some part of braze bead also. Si is inherently present in the filler wire and it is a reaction product in most of the binary and ternary invariant reactions of Al-Fe-Si system. During the joining process Zn might tend to escape from gap between the plates, settles towards head

and foot region. Therefore the x-ray diffraction patterns of head region revealed the presence of Zn. The type of IMC layer formed is not affected by pulsing.

Table 5.8 XRD analysis of the IMC layer

Sr. No	Location		Al-5%Si		Al-12%Si	
			CMT	P-CMT	CMT	P-CMT
1	Head	Major peaks	$\text{Al}_{0.85}\text{Si}_{0.15}$, Si, Zn	$\text{Al}_{0.85}\text{Si}_{0.15}$, Si, Zn	$\text{Al}_{0.85}\text{Si}_{0.15}$, Si, Zn, $\text{Al}_3\text{Fe}_2\text{Si}$, $\text{Fe}_3\text{Al}_{0.7}\text{Si}_{0.3}$	$\text{Al}_{0.85}\text{Si}_{0.15}$, Zn, $\text{Fe}_3\text{Al}_{0.7}\text{Si}_{0.3}$, $\text{Al}_3\text{Fe}_2\text{Si}$
		Minor peaks	FeAl, $\text{Fe}_{25}\text{Al}_{75}$	FeAl, $\text{Fe}_{25}\text{Al}_{75}$	-	Si,
2	Center	Major peaks	$\text{Al}_{0.85}\text{Si}_{0.15}$, Si	$\text{Al}_{0.85}\text{Si}_{0.15}$, Si	$\text{Al}_{0.85}\text{Si}_{0.15}$, Si	$\text{Al}_{0.85}\text{Si}_{0.15}$, Al_5FeSi , $\text{Al}_{25.83}\text{Fe}_{8.57}\text{Si}_{6.6}$,
		Minor peaks	FeAl, $\text{Fe}_{25}\text{Al}_{75}$	FeAl, $\text{Fe}_{25}\text{Al}_{75}$	$\text{Fe}_3\text{Al}_{0.5}\text{Si}_{0.5}$, $\text{Al}_{25.83}\text{Fe}_{8.57}\text{Si}_{6.6}$	$\text{Al}_{25.83}\text{Fe}_{8.57}\text{Si}_{6.6}$, Al_3FeSi_2 , $\text{Fe}_3\text{Al}_{0.5}\text{Si}_{0.5}$
3	Foot	Major peaks	$\text{Al}_{0.85}\text{Si}_{0.15}$, Si	$\text{Al}_{0.85}\text{Si}_{0.15}$, Si	$\text{Al}_{0.85}\text{Si}_{0.15}$	$\text{Al}_{0.85}\text{Si}_{0.15}$, Zn, $\text{Al}_3\text{Fe}_2\text{Si}$
		Minor peaks	FeAl, $\text{Fe}_{25}\text{Al}_{75}$	FeAl, $\text{Fe}_{25}\text{Al}_{75}$	Si, $\text{Al}_3\text{Fe}_2\text{Si}$, $\text{Fe}_3\text{Al}_{0.7}\text{Si}_{0.3}$	$\text{Fe}_3\text{Al}_{0.7}\text{Si}_{0.3}$

Figs 5.12 to 5.14 show the x-ray diffraction patterns of bead/steel interface made with Al-12%Si filler wire. It revealed the presence of $\text{Fe}_3\text{Al}_{0.7}\text{Si}_{0.3}$ (cubic) $\text{Al}_3\text{Fe}_2\text{Si}$ (cubic), $\text{Al}_{0.85}\text{Si}_{0.15}$ (cubic), Si (cubic), Zn (HCP) at head region (Fig 5.12a), $\text{Fe}_3\text{Al}_{0.5}\text{Si}_{0.5}$ (cubic), $\text{Fe}_{8.57}\text{Al}_{25.83}\text{Si}_{6.6}$ (rhombohedral), $\text{Al}_{0.85}\text{Si}_{0.15}$ (cubic), Si (cubic) at central region (Fig 5.13a) and $\text{Fe}_3\text{Al}_{0.7}\text{Si}_{0.3}$ (cubic), $\text{Al}_3\text{Fe}_2\text{Si}$ (cubic), $\text{Al}_{0.85}\text{Si}_{0.15}$ (cubic), Si (cubic) at foot region (Fig 5.14a). Head and foot regions showed two cubic IMC compounds whereas central region showed one cubic and one rhombohedral phase. The respective microstructures of the CMT brazed bead/steel

interface made with Al-12%Si filler wire showed two layered IMC region throughout the cross-section (Fig 5.5g-i). Therefore the presence of two layered IMC is confirmed from x-ray diffraction pattern. The two phases $\text{Fe}_3\text{Al}_{0.7}\text{Si}_{0.3}$ (head & foot) and $\text{Fe}_3\text{Al}_{0.5}\text{Si}_{0.5}$ (center) are the forms of Fe_3Al with varied Al/Si ratio. This ratio is based on the diffusion rate of Al & Si which is governed by temperature and enthalpy of mixing of aluminium in iron. The central region experiencing higher heat intensity than head and foot regions may have resulted in slightly more diffusion resulting in Fe_3Al form of IMC compound with varied Al/Si ratio. $\text{Al}_3\text{Fe}_2\text{Si}$ and $\text{Al}_{25.83}\text{Fe}_{8.57}\text{Si}_{6.6}$ (approx Al_3FeSi) are the two phases with varied Al to Fe ratio observed in head, foot region and central region, respectively. The variation in diffusion rates due to varied temperature and cooling rate at center and foot regions may probably have resulted in formation of phases with varied Al/Fe ratio. $\text{Fe}_3\text{Al}_{0.7}\text{Si}_{0.3}$ and $\text{Fe}_3\text{Al}_{0.5}\text{Si}_{0.5}$ are the Fe rich cubic phases which are expected to be present towards the steel side of the interface. $\text{Al}_3\text{Fe}_2\text{Si}$ and $\text{Al}_{25.83}\text{Fe}_{8.57}\text{Si}_{6.6}$ are the Al rich phases and are expected to be present towards the bead side of the interface. As mentioned above Si is the reaction product of many invariant ternary reactions occurring in Al-Fe-Si system. $\text{Al}_{0.85}\text{Si}_{0.15}$ and Zn are coming from bead and entrapped Zn at head region, respectively.

The x-ray diffraction patterns of P-CMT brazed bead/steel interface made with Al-12%Si revealed the presence of $\text{Fe}_3\text{Al}_{0.7}\text{Si}_{0.3}$ (cubic) $\text{Al}_3\text{Fe}_2\text{Si}$ (cubic), $\text{Al}_{0.85}\text{Si}_{0.15}$ (cubic), Si (cubic), Zn (hcp) at head region (Fig 5.12b), $\text{Al}_{25.83}\text{Fe}_{8.57}\text{Si}_{6.6}$ (rhombohedral), Al_5FeSi (monoclinic), $\text{Fe}_3\text{Al}_{0.5}\text{Si}_{0.5}$ (cubic), Si (cubic) and traces of Al_3FeSi_2 (tetragonal) at central region and $\text{Fe}_3\text{Al}_{0.7}\text{Si}_{0.3}$ (cubic) $\text{Al}_3\text{Fe}_2\text{Si}$ (cubic), $\text{Al}_{0.85}\text{Si}_{0.15}$ (cubic), Zn (hcp) at foot region. As mentioned above the Fe rich cubic phases $\text{Fe}_3\text{Al}_{0.7}\text{Si}_{0.3}$ and $\text{Fe}_3\text{Al}_{0.5}\text{Si}_{0.5}$ have formed towards steel side with varied Al/Si ratio. As the central region experiences slightly high heat intensity, more Al appears to have been replaced by Si than that in head and foot regions. Similarly, $\text{Al}_3\text{Fe}_2\text{Si}$ is the other IMC phase present in head and foot regions. Therefore the

microstructure of the head and foot regions of P-CMT brazed samples made with Al-12%Si shows two layered IMC region at head and foot regions which agrees with the x-ray diffraction analysis. But the central region shows three layered IMC region at the interface as shown in Fig 5.5k. This reflects in x-ray diffraction pattern where three IMC compounds namely $\text{Fe}_3\text{Al}_{0.5}\text{Si}_{0.5}$, Al_5FeSi , $\text{Al}_{25.83}\text{Fe}_{8.57}\text{Si}_{6.6}$ in appreciable amounts and traces of Al_3FeSi_2 are observed. As Al_3FeSi_2 is a reaction product that forms along with the compound Al_5FeSi in a ternary system, it also has been observed in trace amounts. Therefore the Fe rich compound like $\text{Fe}_3\text{Al}_{0.7}\text{Si}_{0.3}$ is expected to be present towards the steel side of the interface and $\text{Al}_3\text{Fe}_2\text{Si}$ is expected to be present towards the bead side of the interface in head and foot regions. The Fe rich compound $\text{Fe}_3\text{Al}_{0.5}\text{Si}_{0.5}$ is expected to be present towards the steel side, $\text{Al}_{25.83}\text{Fe}_{8.57}\text{Si}_{6.6}$ may be present above the Fe rich layer followed by Al rich Al_5FeSi towards the bead side of the interface at central region. As mentioned above, $\text{Al}_{0.85}\text{Si}_{0.15}$ comes from bead, Si is a reaction product of many ternary invariant reactions of the Al-Fe-Si system and Zn is coming from settled Zn towards head and foot region.

The composition of the phases observed are given in Table 5.8. From XRD analysis it is observed that the phases are becoming rich in Al at the central region compared to head and foot regions in all the cases. High heat intensity of the central region may be aiding in more diffusion of Al resulting Al rich phases. Therefore, increase in heat input encourages the formation of Al rich IMC compounds. P-CMT compared to CMT having high heat input facilitated more Al rich IMC compounds.

The binary Fe-Al system comprises of 5 intermetallic compounds. The ternary Al-Fe-Si system comprises of ten ternary intermetallic compounds and nineteen invariant reactions. The invariant reactions involved in binary and ternary systems can be used for explaining the

phase formation in this case. The formation of FeAl and Fe₂₅Al₇₅ phases can be explained as follows:

U₂ at 1120 °C



U₄ at 1020 °C



The phase Fe₂Al₃ is the high temperature phase which can be seen in Fe-Al binary phase diagram. This high temperature phase reacts with the liquid to form ordered FeAl and Fe₂Al₅ phase. Fe₂Al₅ then reacts with the liquid to form Fe₄Al₁₃ phase. The phase Fe₂₅Al₇₅ is similar to Fe₄Al₁₃ phase. There are reports that at 550 °C Fe₂Al₅ can dissolve upto 2at%Si, Fe₄Al₁₃ can dissolve up to 4wt%Si and FeAl can dissolve up to 1-6at%. Some reports show that ordered FeAl can dissolve up to 16-17at%. Therefore, the solubility of sufficient amount of Si in the respective phases may result in formation of Fe-Al based binary phases with Si solubility. Therefore, ordered FeAl and Fe₂₅Al₇₅ are the reaction products of equations 1 & 2. The presence of phase T₁ is not detected. The presence of T₁ in trace amount may be the probably reason for the difficulty in identifying this in micro area x-ray diffraction patterns

The formation of Al_{25.83}Fe_{8.57}Si_{6.6}, Al₅FeSi, Al₃FeSi₂, Fe₃Al_{0.5}Si_{0.5}, Fe₃Al_{0.7}Si_{0.3}, Si can be explained as follows. Fe₃Al based compounds were formed from the following reaction mentioned in equation 3

U₁ at 1150°C



The Fe₃Al formed from the above reaction showed some solubility of Si in it by replacement of Al atoms. The solubility of Si demands diffusion. Diffusion is a thermally activated process. The central region of the sample experiences high heat intensity than head and foot regions due to bell shape of the arc. Therefore the central region recorded slightly more diffusion of Si atoms resulting in ternary phase with slightly more amount of Si than head and foot regions. Equation 3 also resulted in formation of Fe-Si based intermetallic compound. This may be the probable reason for the observation of trace amounts of Fe-Si based intermetallic phases in all the regions.

The following sequence of reactions may explain the formation of T₂ T₆ phase

P₂ at 940 °C



P₃ at 935 °C



U₈ at 835 °C



U₁₂ at 600 °C



E₁ at 573 °C



The ternary phase T₂ may form from the reaction mentioned in equation 4. The phases T₁ and Fe₄Al₁₃ are the reaction products of equation 1 & 2. According to equation 5 the

formed ternary phases τ_1 , τ_2 reacts with liquid to form τ_7 . τ_7 again reacts with liquid phase to form τ_2 and τ_4 . Now τ_4 reacts with liquid to form τ_6 and Si. The phase τ_6 can also be formed from reaction mentioned in equation 8. The major observation from the above reactions is that along with the ternary intermetallic phases elemental Si is also formed as a major reaction product. This is also supported from x-ray diffraction patterns indicating strong Si peaks. τ_4 and τ_7 are also the reaction products of the above mentioned reactions. The presence of τ_7 is not detected from the x-ray diffraction pattern. But the presence of τ_4 in trace amounts is detected in x-ray diffraction study. This can be supported from Fig.14 which reveals the presence of three phase equilibrium or three phase fields having wide range of formation like $\tau_2+\tau_4+\tau_6$, $\tau_6+\text{Al}+\text{Si}$, $\tau_4+\tau_6+\text{Si}$ at aluminium corner of the phase diagram which confirms the possibility of coexistence of above identified IMC phases.

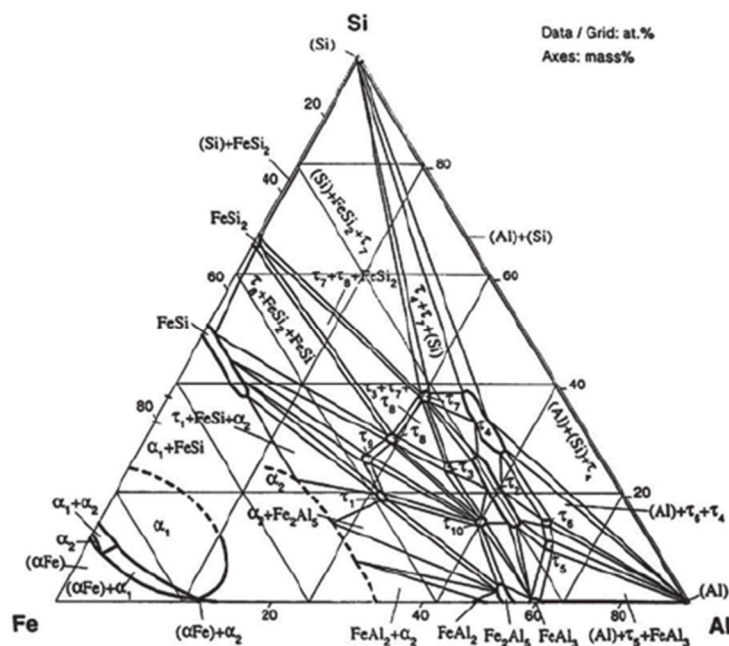


Figure 5.15 Al-Fe-Si isothermal section at 600°C [8].

5.5 Effect of interfacial morphology on failure

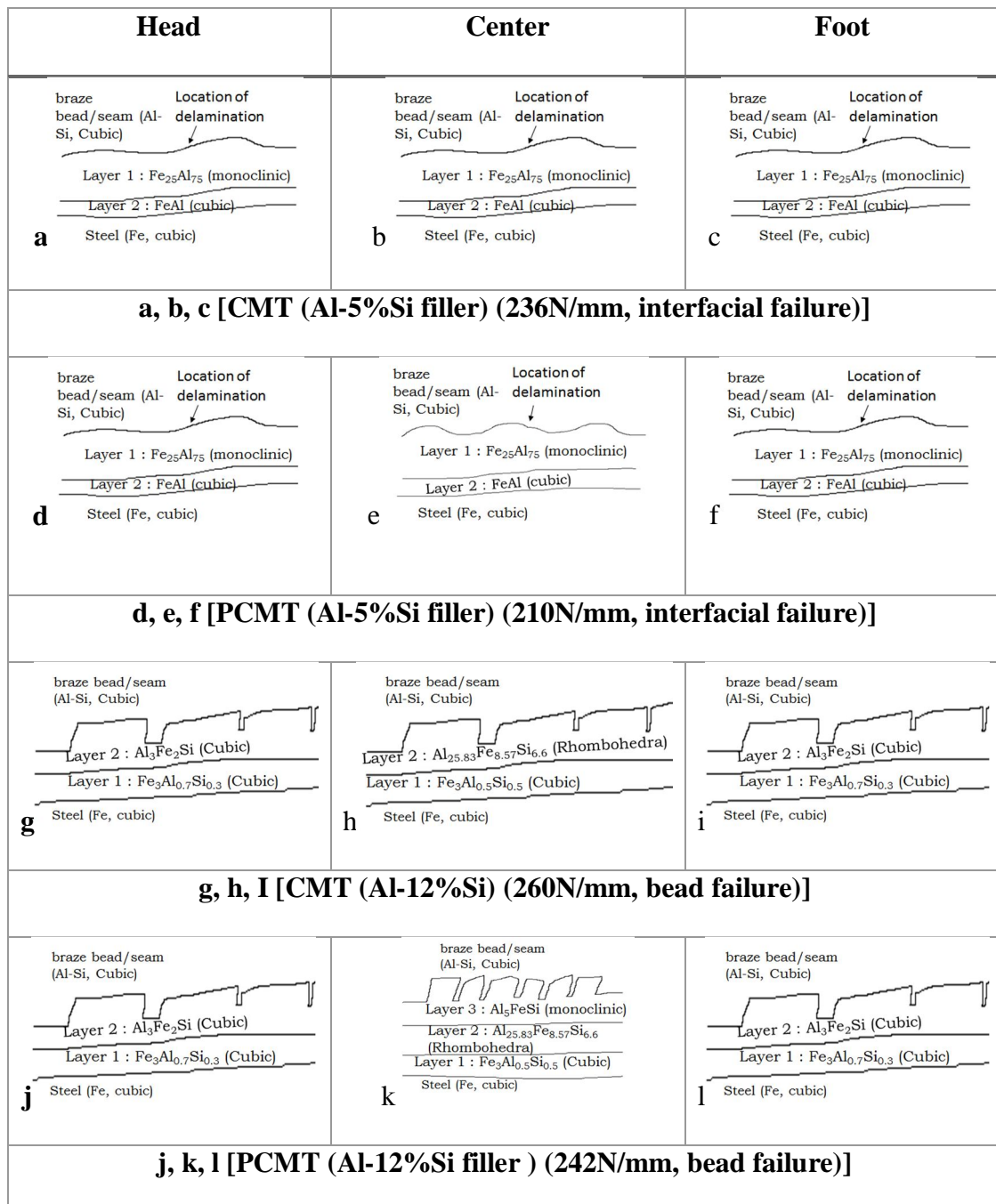


Figure 5.16 Schematic of bead/steel interface indicated with probable IMC compounds, fracture load and failure location a) head (CMT (Al-5%Si)) b) center (CMT (Al-5%Si)) c) foot (CMT(Al-5%Si)) d) head (P-CMT(Al-5%Si)) e) center (P-CMT(Al-5%Si)) f) foot (P-CMT(Al-5%Si)) g) head (CMT(Al-12%Si)) h) center (CMT(Al-12%Si)) i) foot (CMT(Al-12%Si)) j) head (P-CMT(Al-12%Si)) k) center (P-CMT(Al-12%Si)) l) foot (P-CMT(Al-12%Si)).

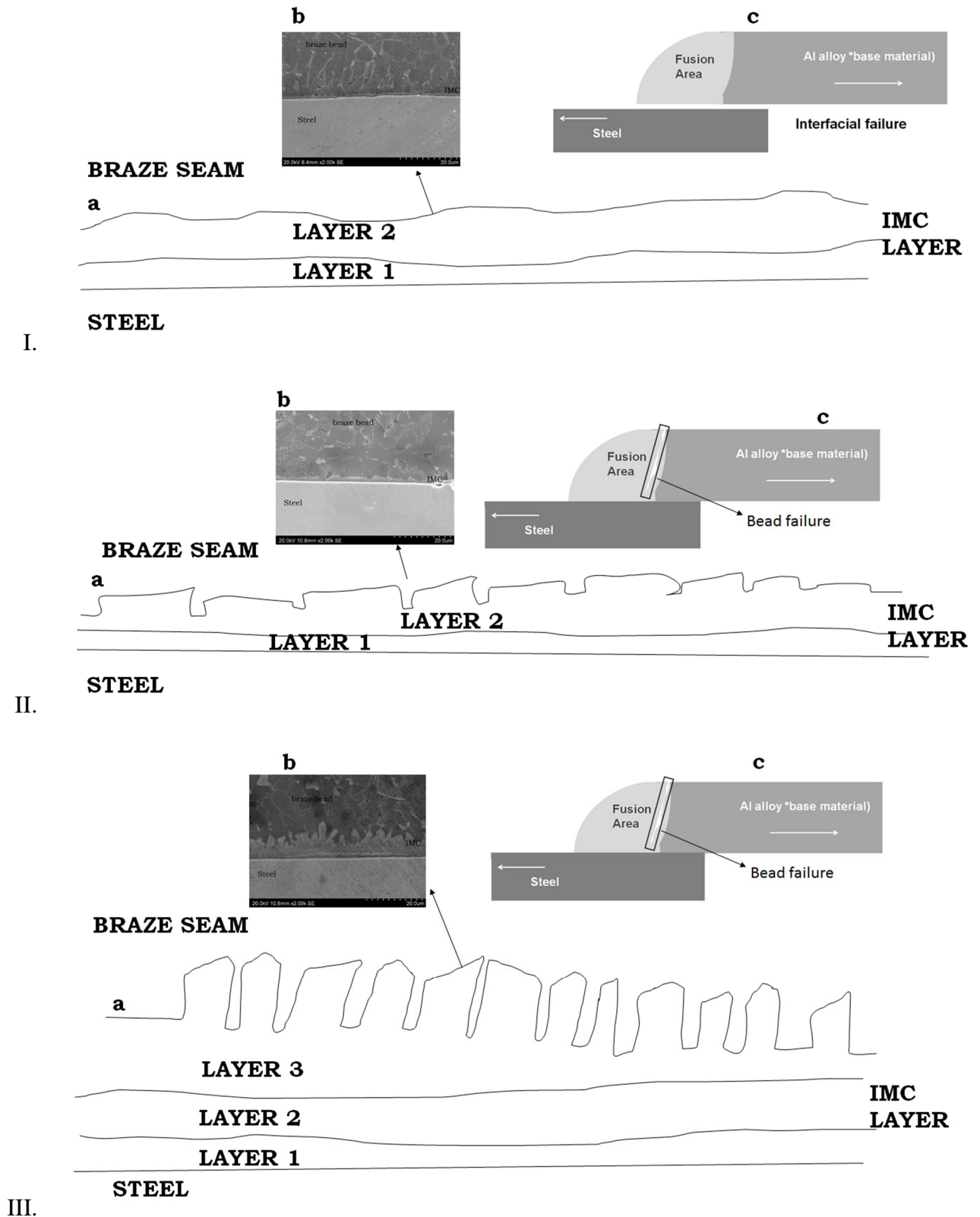


Figure 5.17 Various interfacial morphology I) wavy and curved type II) rectangular block type III) irregular blocks with flat surface.

Figs 5.16 & 5.17 show various interfacial morphologies corresponding to IMC compounds formed, strength and fracture location observed in CMT brazing of aluminium alloy and steel. In all the cases the steel/bead interface is always almost flat. During joining of aluminium alloy to steel the aluminium melt should wet the steel surface to form a sound and leak proof joint. During this operation, steel is in solid state and aluminium is in liquid state. The base material grains of steel acts as nucleating sites for melt. Therefore, the melt solidifies without altering the orientation of the grains on the base steel. This is found to be a planar solidification. Therefore the steel/IMC interface always shows a flat interface. The layer adjacent to steel is found to be of Fe rich cubic phase in all the cases which agrees with the planar solidification mode. Hence, the layer adjacent to steel is intact with steel. The variation in IMC/bead interface is observed to vary with processing conditions as shown in Fig 5.17. The type of interfaces like I) wavy and curvy II) rectangular block type III) irregular block with flat surface are observed. The wavy and curvy interface is evident in the joints made using Al-5%Si filler wire (Fig 5.8 a-e, Fig 5.16a-e). The interface is not flat and even delamination (Fig 5.17Ia) at IMC/bead interface was observed in these interfaces. The interfaces of joints made using Al-5%Si revealed the presence of binary Fe-Al based IMC phases. The CMT and P-CMT brazed joints made with Al-5%Si filler possesses $\text{Fe}_{25}\text{Al}_{75}$ (monoclinic) Al rich phase towards the bead side. Therefore there may be incoherency between the monoclinic structured IMC and cubic bead resulting in delamination at IMC/bead interface. Therefore in this case there is a strong steel/IMC interface and a weak IMC/bead interface. The delamination site is a weak zone and acts as crack leading to failure at IMC/bead interface. This is confirmed from the Lap shear test results. The samples possessing wavy and curvy type of interface failed at IMC/bead interface only as shown in Fig 5.17 Ic.

The second type of IMC/bead interface is rectangular block type (Fig 5.17 IIa). This type of interface is observed in the joints made using Al-12%Si. The x-ray diffraction study of the interface of joints made using Al-12%Si revealed the presence of Al-Fe-Si type ternary compounds. Delamination at IMC/bead interface is not observed as shown in Fig 5.17 Ib. The IMC layer is of rectangular block shape with flat top surface (Fig 5.17IIb). This type of morphology dominates the bead/steel interface of CMT brazed joints made with Al-12%Si filler wire. In this case it is observed that both the layers towards steel and bead side are of cubic structure. Therefore here both the steel/IMC interface and IMC/bead interfaces are strong without delamination or gaps. Hence due to strong interface the failure moved to bead resulting in higher load bearing capacity. This type of interfaces recorded high fracture loads in lap shear test results.

The third type of IMC/bead interface is of irregular blocks with flat surfaces as shown in Fig 5.17III. This type of interface reports three layered IMC layer as shown in Fig 5.17 IIIb and is more likely to occur at high heat input conditions with Al-12%Si filler wire. In this case also the steel/IMC interface is flat. Layer 1 is towards the steel side, layer 2 is next to layer 1 and layer 3 is towards bead side. In this, layer 3 is made up of irregular block shaped morphology with flat surfaces. In this, the protrusions towards the bead possess triangle shaped sharp and flat surface (Fig 5.17IIIb). In this case, the interlock between the layer 3 and bead is strong without any delamination. It is observed that layer 1 is of Fe rich cubic phase followed by medium Al rich rhombohedral phase followed by Al rich monoclinic phase. Therefore in this case also the steel/IMC interface and IMC/bead interface are strong resulting in failure in the bead, but at lower loads than the above mentioned rectangular block morphology. Therefore out of the three, rectangular block interfacial morphology (Fig 5.17II) records high fracture loads with failure in the bead. Therefore, type II and III interfacial morphologies don't have interfacial failures and among the two type II IMC morphology gives higher joint strength.

5.6 Summary

- The morphology, type of intermetallic layer at Al-steel interface formation is affected by filler wire composition and pulsing (additional heat input).
- Pulsed-CMT process results in higher IMC layer thickness due to higher heat input.
- The use of Al-5%Si filler wire favours the formation of Fe-Al based binary IMC compounds whereas the use of Al-12%Si filler wire favours the formation of Al-Fe-Si based IMC compounds at bead/steel interface.
- Three types of morphology of IMC layer are observed at the bead/steel interface a) Type I (curvy and wavy type), b) Type II (rectangular block type) and c) Type III (irregular blocks with flat surface). Type II IMC layer morphology yields the best strength among the three due to favourable crystal structure of the compounds.

5.7 Conclusions

- Under similar brazing conditions the peak temperature recorded in CMT process is less compared to P-GMAW process. CMT process shows faster cooling rate compared to P-GMAW process.
- Under similar brazing conditions the peak temperature and cooling rates of P-CMT is similar to P-GMAW process.
- Among the three CMT, P-CMT and P-GMAW, CMT brazed joints showed superior properties with less IMC layer thickness.
- The CMT process can restrict the growth of interfacial IMC layer thickness to less than 4 μm .

- The joint interface made with Al-5%Si filler wire showed the presence of binary Fe-Al based intermetallic phases whereas the joint interface made with Al-12%Si filler showed the presence of ternary Al-Fe-Si based intermetallic phases.
- The morphology and type of interfacial phases are found to affect the joint properties and failure mode. The presence of binary IMC is found to decrease the joint strength and led to interfacial failure whereas the presence of ternary phases has favoured bead failure at high failure loads. The presence of cubic structure at the bead/IMC interface has favoured high joint strengths whereas complex crystal structures like monoclinic are found to diminish the joint strength.
- Therefore CMT brazing process is successful and superior compared to P-GMAW process in all aspects.

References

- [1] M. Kang, C. Kim, *Materials & Design*, 81 (2015) 95-103.
- [2] H.T. Zhang, J.C. Feng, P. He, *Materials Science and Technology*, 24 (2008) 1346-1349.
- [3] H.T. Zhang, J.C. Feng, P. He, H. Hackl, *Materials Characterization*, 58 (2007) 588-592.
- [4] S. Yang, J. Zhang, J. Lian, Y. Lei, *Materials & Design*, 49 (2013) 602-612.
- [5] L.A. Jacome, S. Weber, A. Leitner, E. Arenholz, J. Bruckner, H. Hackl, A.R. Pyzalla, *Advanced Engineering Materials*, 11 (2009) 350-358.
- [6] P. Peyre, L. Berthe, X. Scherpereel, R. Fabbro, *Journal of Materials Science*, 33 (1998) 1421-1429.
- [7] G. Ghosh, Ternary Alloys, *A Comprehensive Compendium of Evalu-* 52. B. Sundman, B. Jansson, and J.-O. Andersson: CALPHAD, 1985, vol. ated Constitutional Data and Phase Diagrams, VCH Publishers, New York, 1992.
- [8] V. Raghavan, *Journal of Phase Equilibria*, 15 (1994) 414-416.

CHAPTER 6 LASER BRAZING

6.1 Introduction

In laser brazing of aluminium alloy to steel, the joints made without flux were failed during metallographic polishing. All the joint details reported in this chapter are made using flux. The use of flux aids in cleaning the surface of the steel and exposing the fresh surface of steel to the molten aluminium pool. There are reports defining the use of flux helping in improved wetting and spreading action [1-3].

6.2 Macrostructure

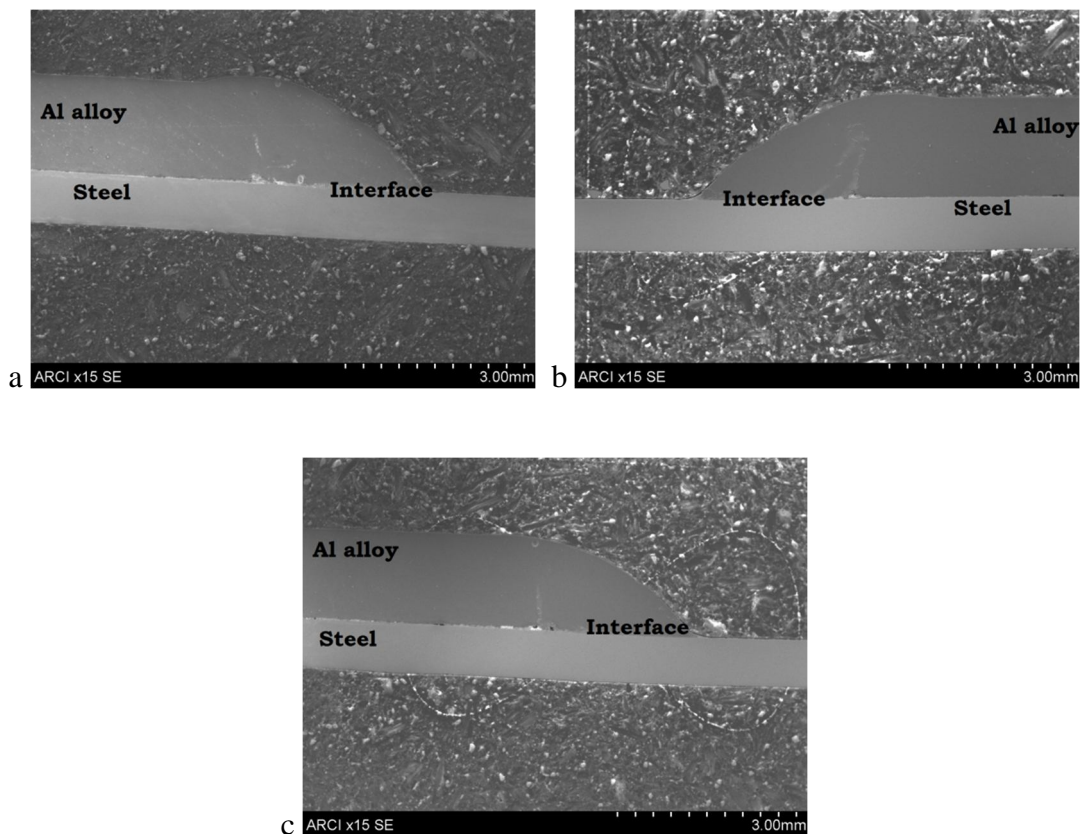


Figure 6.1 SEM transverse cross section macrostructures of laser brazed specimens.

Fig 6.1 shows the SEM transverse cross-sectional macrostructure of Al-steel laser brazed joints at 16X magnification. The bead geometry measurements are given in Table 6.1. It is

observed that with increase in heat input there is an increase in bead width, height and wetting angle (Fig 6.1a, c). The increased metal deposition resulting from increased heat input may probably result in increased bead measurements. It is observed that under similar heat input conditions the use of dynamic beam shaping technique aided in improving wetting behaviour (Fig 6.1 a, b). This is confirmed from the bead geometry measurements as shown in Table 6.1. In case of dynamic beam shaping the beam is scanned at a particular amplitude and frequency for a given spot size. This in turn increases the spot size of the laser beam, therefore increases the area being covered by the laser beam. Therefore it heats up the surrounding area of the base materials resulting in improved wetting of the aluminium melt on steel surface. Hence, use of dynamic beam shaping helps in improved wetting and spreading, in turn improves the joint properties.

Table 6.1: Bead geometry measurements of laser brazed specimens

Bead geometry measurements	Specimen id		
	S1	S2	S3
Bead width (mm)	2.2-2.3	2.45-2.55	2.6-2.7
Bead height (mm)	1.56-1.55	1.4-1.5	1.4-1.5
Wetting angle (°)	42-44	41-43	45-47

As reported in previous chapters Al/bead interface, braze bead and bead/steel interface are the three regions of microstructural interest of aluminium/steel joint. The SEM micrograph of braze bead is shown in Fig 6.2. A very fine grains are observed in braze bead. Laser brazing being a splat quenching process resulted in formation of fine grain structure as shown in Fig 6.2.

6.3 Microstructure

Fig 6.3 shows the bead/steel interfacial microstructures at various locations. It is observed that in all the cases the IMC layer thickness is restricted to less than $1.2\text{ }\mu\text{m}$. In laser brazing process the laser spot is focused on the filler wire tip. The stream of drops of melted filler wets the base materials to form a joint. Therefore, the effect of laser beam is less on base aluminium and steel materials. Hence, there will be minimal dilution between aluminium and steel base materials and the IMC layer growth is restricted. Unlike arc brazed joints, the interface of laser brazed joints is of uniform thickness along the cross-section (Fig 6.3 a-i). The maximum heat from laser source is spent in melting of the filler wire. Therefore, the heat transfer to the base material is possible only through molten drop of filler. Hence, there is no variation in heat intensity experienced by the base materials resulting in uniform diffusion rate along the seam. This may be the probable reason for uniformity in IMC layer thickness across the seam. The bead/steel interface is comprised of two layers, one is a pale white region towards the steel side and needle protruding into the Al melt. These two regions are observed in almost all the cases (Fig 6.3a-i).

The EDS analysis of the pale white region towards the steel side showed the presence of 12-20 at. % Al, 70-80 at. % Fe, 4-6 at % Si and 0.5-1 at. % Zn whereas the needles towards the Al melt showed the presence of 60-65 at. % Al, 8-10 at.%Fe, 24-27 at. % Si and 2-3 at. % Zn in almost all the cases. Therefore the interface is the combination of Al, Fe, Si and Zn. Therefore the layer towards the steel side is rich in Fe and the layer towards the bead side is rich in Al and Si. Unlike arc brazing process the presence of Zn at interface is observed. The low heat input experienced by the base materials restricted the vaporisation of Zn and fast cooling rates trapped Zn at the interface. Also white chunks were observed in the braze bead near to the bead/steel interface. These white chunks are made up of the flux material which is

also confirmed from the EDS analysis. The flux used in the process got settled near the interface.

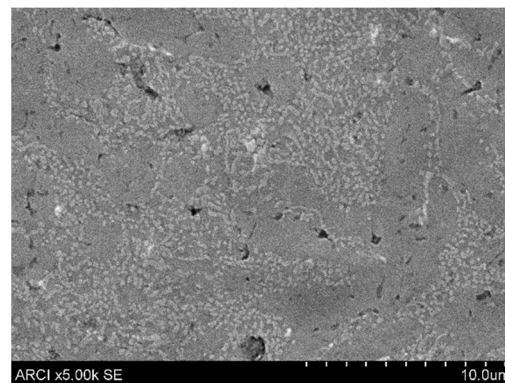


Figure 6.2 SEM micrograph of various braze bead of laser brazed specimen.

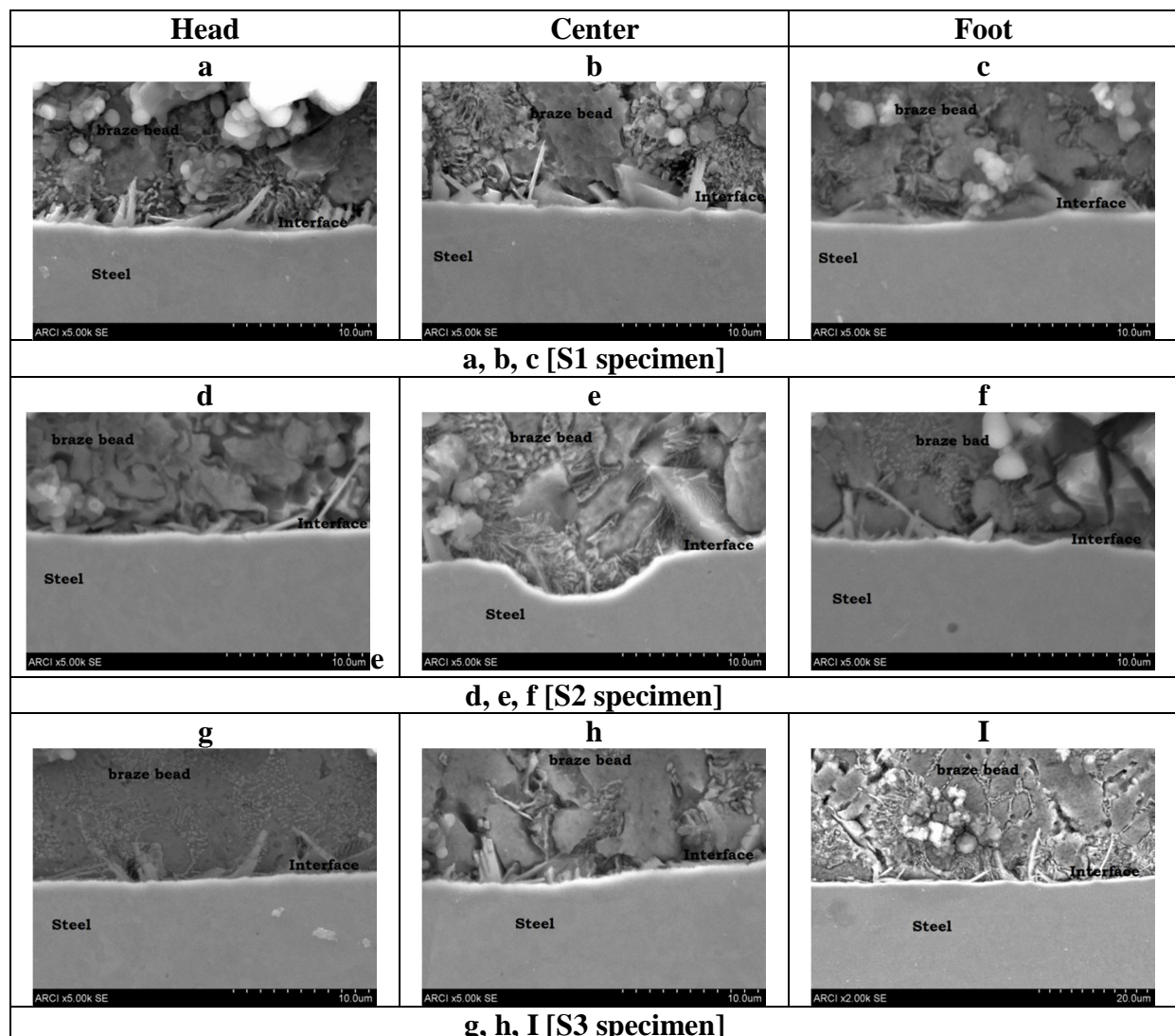


Figure 6.3 seam/steel interface of laser brazed joints under various processing conditions.

6.4 Lap shear test

Table 6.2 shows the fracture load and failure location for the laser brazed joints. The joint strength is in the range of 275-299 N/mm with failure in the bead can be achieved. It is observed that the specimens made using beam scanning technique showed better performance. There is a slight improvement in joint strength observed with increase in heat input. The improved wetting and spreading behaviour with increase in heat input may be the probable reason for improved mechanical properties of the joint.

Table 6.2 Lap shear test results

Samples	Fracture load (N/mm)/failure location		
	S1	S2	S3
Specimen 1	277±5 (bead)	296±5 (bead)	282±5 (bead)
Specimen 2	273±5 (bead)	299±5 (bead)	285±5 (bead)
Specimen 3	275±5 (bead)	294±5 (bead)	280±5 (bead)

6.5 Conclusions

- The interfacial IMC layer could be restricted to less than 1.2 μm using laser brazing technique.
- Joint strength in the range of 280-300 N/mm can be achieved with failure in the bead.
- The beam scanning technique aids in improving wetting and spreading action.

CHAPTER 7 SUMMARY AND CONCLUSIONS

Investigations were carried out on fusion joining of aluminium alloy 6061-T6 to IF steel in different surface conditions. Two reduced energy arc welding processes - Pulsed-GMAW and Cold Metal Transfer (CMT); and a low heat input and precision beam process - Laser brazing have been used.

The joints are accomplished through the arc/laser heat input creating an aluminium alloy melt pool which will wet the steel surface and form a brazing-like joint. As one of the base metals also melts in the process it is called as weld-brazing. Since it is a braze-like joint, that too of dissimilar materials combination, interface is expected to influence the mechanical strength of the joint. The wetting behaviour and formation of brittle intermetallic compound layers at the interfaces would govern the mechanical behaviour of the joints formed. The following process related and materials related parameters have been investigated in detail in order to fully understand the joint formation, interface metallurgical behaviour and consequent mechanical properties:

Process related

- a. welding torch orientation and position
- b. heat input variation through wire feed rate
- c. Al-steel interface gap
- d. use of flux in laser brazing

Materials related

- e. surface chemistry of the steel
- f. filler wire composition

The major contribution of this work is extensive evaluation of the interface morphology and chemistry of the intermetallic layer forming at the interface of the joints made by three

different fusion welding processes. Comparison of the interface metallurgy resulting from three different processes and filler wires gave a deep insight into the formation of various intermetallic phases under different heat input and chemical composition conditions. Use of micro-area XRD for this purpose is reported for the first time through this report. The following are the findings/observations of the present work:

a) Joint formation

- The fusion joining processes like arc and laser brazing techniques are found to be successful in joining Aluminium alloy to Steel with consistent results.
- The geometry of the weld/braze bead (bead width, contact angle and bead height) is influencing the joint strength and failure location.
- The bead formation and its geometry is found to be affected by wire feed rate, processing speed, steel surface, interface gap between the plates, filler wire composition and the joining process.
- The parameters like tilting of work-piece assembly, torch orientation showed positive effect on wetting and spreading resulting in enhanced the mechanical performance of the joint.
 - The increase in angle of tilt from 0-12° increased the joint strength by 15%
 - Changing the torch orientation from 0 to 60° to the welding direction aided in better wetting, thereby enabling use of reduced heat input by 32-35%.
- The wetting and spreading of Al melt on Steel is found to be affected by Steel surface, filler composition. The presence of elemental Zn on steel surface and increased Si content in the filler found to significantly increase the wetting and

spreading action. However, the Zn vapour emitted during the process seems to get entrapped in the weld bead resulting in porosity and crevice formation.

- The interface gap between the plates aided in minimising the Zn entrapment and improved the joint strength. The increase of gap from $<50\text{ }\mu\text{m}$ to $300\text{ }\mu\text{m}$ improved the joint strength by 22-25%.
- The increase in Si content of filler wire from 5 to 12% enhanced the joint strength by 17-20%. Joints made with Al-12%Si filler wire showed better strength.
- Among the arc brazed joints, the CMT brazed joints exhibited better joint strength than P-GMAW brazed joints.
- Pulsing in a CMT process is found to affect the bead formation and IMC layer formation.
- Laser brazed joints recorded slightly better properties than arc brazed joints. But, use of flux seemed necessary. Brazing speeds of up to 5 m/min could be achieved.

b) Intermetallic compound layer at the interface

- *Thickness and number of layers*
 - The thickness of the IMC layer can be restricted to $< 9\text{ }\mu\text{m}$ in P-GMAW process, $< 5\text{ }\mu\text{m}$ in CMT process and $< 1.2\text{ }\mu\text{m}$ in laser brazing process.
 - The IMC morphology and thickness is found to vary across the bead width in P-GMAW and CMT process whereas it is uniform in laser brazed joints.

- Among arc brazing processes, the P-GMAW brazed joints showed a three layered IMC layer at the centre whereas CMT brazed joint showed only two layered region.

○ *Phases and morphology*

- The type of IMC layer formed at the interface is dependent on the filler material and joining process adopted. Fe-Al based binary intermetallic compounds formed in arc brazed joints made with 4043 (Al-5%Si) filler wire whereas Al-Fe-Si based ternary IMC phases are evident in arc brazed joints made with 4047 (Al-12%Si) filler. The interfaces of laser brazed joints are comprised of Al, Fe, Si and Zn quaternary combination.
- The P-GMAW brazed joint made with Al-5%Si filler showed the presence of FeAl, FeAl₃ phases at head and foot regions, FeAl, FeAl₃, and Fe₂Al₅ at the center region. The CMT brazed joint interface showed FeAl, FeAl₃ all through the interface.
- The P-GMAW brazed joint made with 4047 (Al-12%Si) filler wire is comprised of Fe₃Al_{0.7}Si_{0.3}, Al₅FeSi at head and foot regions, Fe₃Al_{0.5}Si_{0.5}, Al₅FeSi, Al_{25.83}Fe_{8.57}Si_{6.6} along with trace amounts of Al₃Fe₂Si at central region whereas the CMT brazed specimen is comprised of Al₃Fe₂Si, Fe₃Al_{0.7}Si_{0.3} at head and foot regions whereas Al_{25.93}Fe_{8.57}Si_{6.6}, Fe₃Al_{0.5}Si_{0.5} at central region.
- The P-CMT brazed joints made with 4043 (Al-5%Si) filler wire is comprised of FeAl, FeAl₃ IMC phases all through the interface whereas the joints made with 4047 (Al-12%Si) filler wire showed the presence of Fe₃Al_{0.7}Si_{0.3}, Al₃Fe₂Si, at head and foot regions,

$\text{Fe}_3\text{Al}_{0.5}\text{Si}_{0.5}$, Al_5FeSi , $\text{Al}_{25.83}\text{Fe}_{8.57}\text{Si}_{6.6}$ along with the traces of Al_3FeSi_2 at central region.

○ *Nature of IMC layer and mechanical strength*

- The joint strength and failure location are varied with type of IMC phases and their crystal structure. The joint interface comprising binary Fe-Al compounds recorded interfacial failure whereas the joints having Al-Fe-Si ternary IMC phases facilitated bead failure. Especially the presence of cubic structured IMC phase at the joint interface favours maximum load bearing capacity.
- The above interfacial study once again proved that, the presence of Al rich IMC phases is deleterious to mechanical performance of the joint.

Overall, the joint formation and the interface are found to be very sensitive to the process parameters, and it is necessary to optimise the process parameters carefully to obtain a good and consistent joint.

CHAPTER 8 SCOPE FOR FUTURE WORK


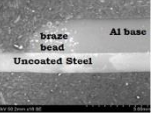
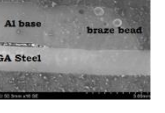
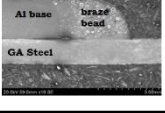
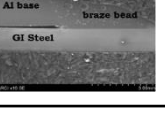
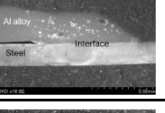
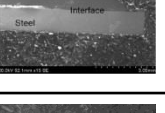
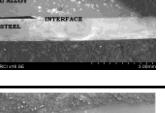
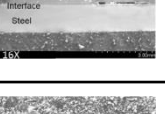

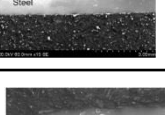
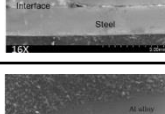
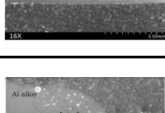
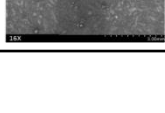
- Study on CMT brazing of various combinations of Aluminium and Steel and joint configurations
- Effect of various filler materials like Zn based filler on wetting behaviour and mechanical performance of the joint.
- Study on the effect of various processing parameters of a laser brazing technique on joint performance. For example effect of laser beam tailoring on the wetting behaviour and mechanical performance of the joint.
- Study of interfacial IMC layer using EBSD and TEM.

ARC BRAZING PROCESS (EFFECT OF PARAMETERS ON JOINT PROPERTIES)

EFFECT OF VARIOUS PARAMETERS

Processing parameter	Process related parameters								Material related parameters	
	Angle of tilt of lapped sheet assembly (°)	Torch orientation with respect to processing direction (°)	Gap between the plates (mm)	Wire feed rate (m/min)	Processing speed (m/min)	Arc position /position of filler wire tip	Gas flow rate (l/min)	Stand off distance (mm)	Surface chemistry of steel	Filler wire composition
Level of effect on joint properties	✓	✓	✓	✓	✓	✓	No significance	No significance	✓	✓

PARAMETERS VS JOINT PROPERTIES

S. No	Process	Materials used			Processing parameters				IMC layer thickness (µm)	Bead geometry	Joint strength (N/mm ²)	Failure location
		Al alloy (thickness : 2 mm)	Steel (various surface chemistry) (thickness : 1.2 mm)	Filler wire (diameter: 1.2 mm)	Angle of tilt of lapped assembly (°)	Torch orientation with respect to welding direction (°)	Wire Feed Rate (m/min)	Gap between the plates (µm)				
1	P-GMAW	6061-T6	Galvannealed IF	4043	0	0	5.2	50	10-12		105	interface
2		6061-T6	Uncoated-IF	4043	0	60	3.5	50	3.2-3.8		110	Interface
3		6061-T6	Galvannealed IF	4043	12	0	5.2	50	15-16		126	Interface
4		6061-T6	Galvannealed IF	4043	0	60	3.5	50	3-3.4		127	Interface
5		6061-T6	Galvanized IF	4043	0	60	3.5	50	2.8-3.5		180	Reduced region
6		6061-T6	Galvanized IF	4043	0	60	3.5	200	2.7-3.5		197	Interface
7		6061-T6	Galvanized IF	4043	0	60	3.5	500	2.8-3.4		198	interface
8		6061-T6	Galvanized IF	4043	0	60	4	300	3.2-3.8		212	Interface
9		6061-T6	Galvanized IF	4043	0	60	3.5	300	2.9-3.5		222	Interface
10		6061-T6	Galvanized IF	4047	0	60	3.5	300	9-20		245	Bead
11	P-CMT	6061-T6	Galvanized IF	4043	0	0	4	300	1.4-1.7		210	Interface
12	CMT	6061-T6	Galvanized IF	4043	0	0	4	300	2.7-3.2		236	Interface
13	P-CMT	6061-T6	Galvanized IF	4047	0	0	4	300	8-9		242	Bead
14	CMT	6061-T6	Galvanized IF	4047	0	0	4	300	3.3-3.6		260	Bead